Dynamics and Synchronization of Electromechanical Devices with a Duffing Linearity

René Yamapi

The University of Abomey-Calavi, Bénin

The abdus Salam International Centre for Theoretical Physics (ICTP), Italy.

Institut de Mathématiques et de Sciences Physiques (IMSP)

Order n^{0} : 0025/2003

Dissertation submitted to the IMSP and the University of Abomey-Calavi of the requierement for the Degree of

Doctorat es-Sciences

Option: *Theoretical Physics*

Speciality: *Nonlinear Vibrations and Chaotic Dynamics*

by

René YAMAPI

on November 05^{th}, 2003

Title :

DYNAMICS AND SYNCHRONIZATION OF ELECTROMECHANICAL DEVICES WITH A DUFFING NONLINEARITY

Jury :

President	:	**Prof. N. M. Hounkonnou** (Institut de Mathématiques et de Sciences Physiques, Université d'Abomey-Calavi, Bénin)
Referees	:	**Prof. Anaclet Somethe** (Ecole Nationale Supérieure Polytechnique, Université de Yaoundé I, Cameroun)
	:	**Prof. T. C. Kofané** (Laboratory of Mechanics, University of Yaoundé I, Cameroon)
	:	**Prof. Paul Woafo** (Laboratory of Mechanics, University of Yaoundé I, Cameroon)
	:	**Prof. J. B. Chabi Orou** (Institut de Mathématiques et de Sciences Physiques, Université d'Abomey-Calavi, Bénin)
Examiners	:	**Prof. Moussiliou Gbadamassi** (Faculté des Sciences et Techniques, Université d'Abomey-Calavi, Bénin)
	:	**Prof. Félix Hontinfindé** (Faculté des Sciences et Techniques, Université d'Abomey-Calavi, Bénin)

Supervisors:

Prof. Paul Woafo *and* **Prof. J. B. Chabi Orou**

*Supported by the Abdus Salam International Centre for Theoretical Physics (ICTP), Italy.

Email for author: ryamapi@yahoo.fr

DYNAMICS AND SYNCHRONIZATION OF ELECTROMECHANICAL DEVICES WITH A DUFFING NONLINEARITY

René YAMAPI
Institut de Mathématiques et de Sciences Physiques
Porto-Novo, Bénin
Email address: ryamapi@yahoo.fr

Dedications

Dedications

To my late father **Moukam René, 1918-1989.**
For the job you've done and the nature deprive you to enjoy the fruits. Your life is still for us an inexhaustible source of inspiration. Are we be able to fill the gap you've leave in our life? May your soul rest in peace.

To my two children, **Kevin Faride and Frank Loic.**
May this work constitute a constructives mirror for your future.

To my wife, born **Jeanne Siakam Tientcheu.**
Whose discrete and patient love has been my great support on the way of perseverance during my training. I especially appreciate my wife's encourragement and patience as i completed the research.

To my mother **Ngako Micheline**, *my uncle* **Neuko Michel**, *and my entire family, your moral and financial supports have permitted me to look forward despite the numerous around.*

To all my younger brothers and systers: **Tchouatou Marguerite, Djutu Guy Alexandre, Pedji Odette, Moukam Jean Michel, Tcheuffa Bernard and Duplex.**

Acknowledgements

Acknowledgements

The author wishes to thank those who helped him along the way to arrive at this research.

I would like to thank Professor **Jean Pierre Ezin**, *Director of IMSP and the technical staff of the institute for ensuring a smooth evolution of this work.*

I am highly indebted to Professor **Paul Woafo** *of the University of Yaoundé I (Cameroon) and to Professor* **J. B. Chabi Orou** *of the University of Abomey Calavi (Benin) for accepting to co-supervise this work. I will never forget their appreciated support and advice, without which it would have been difficult to achieve this personal challenge.*

Thanks to Professor **Joel Tossa**, *Doctors* **J. T. Hounsou** *and* **Kouagou Yebeni** *of the Institut de Mathématiques et de Sciences Physiques (IMSP) for their help in solving some of my computational problems and helpful for putting this work in final form.*

I would also like to thank the Abdus Salam International Centre for Theoretical Physics (ICTP) Italy, for their financial support via the IMSP Collaboration.

I would like to express my gratitude to all those, who have contributed directly or indirectly for the achievement of this work, and during my long period of education.

I wish to thank the **Chabi** *family for his friendly and fatherly loves during my stay in Porto-Novo (Benin).*

I cannot forget the warm hospitality of the entire Laboratory of Mechanics of the University of Yaoundé I during my four moon stay.

Table of contents

Contents

List of Figures

List of Figures

Abstract

Abstract

This thesis is concerned with the study of the dynamics and synchronization of electromechanical devices consisting of an electrical **Duffing** oscillator coupled magnetically and parametrically to linear mechanical oscillators. The interest devoted to such electromechanical devices is due to the fact that the model is widely encountered in various branches of electromechanical engineering.

Chapter 1 presents some sources of nonlinear components and electromechanical systems whose dynamics can be described by two coupled oscillators with **Duffing** nonlinearity.

In chapter 2, we study analytically and numerically the dynamics of forced and parametric electromechanical devices. Resonance, antiresonance and hysteresis phenomena are observed. The stability boundaries of the harmonic oscillations are derived and these boundaries are confirmed by a direct numerical simulation of the equations of motion. The characteristics of sub- and superharmonic oscillations are also derived. It is observed that chaos appears in the model for high value of the amplitude of the external excitation. The canonical feedback controllers algorithm is used to drive the model from chaos to a regular orbit. The effects of the parametric coupling on the dynamics and stability boundary of the harmonic oscillations are also analyzed.

Chapter 3 deals with the dynamics of an electromechanical device with multiple functions. We consider models with double and a large number of functions in series and in parallel, and derive the amplitudes of the harmonic oscillatory states and their stability, the time-delay, sub- and superharmonic oscillations which occur in the model. We discuss on the effects of the number of mechanical oscillators on the dynamics of the electromechanical systems.

In chapter 4, we consider the problem of synchronizing electromechanical devices both in their regular and chaotic states with and without delay. We derive the stability criteria, the optimal coupling strength of the synchronization process and the critical values K_{cr} under which, for a given precision, no synchonization is possible. Comparison of the analytical and numerical results shows an interesting agreement.

Résumé

Résumé

L'objectif de cette thèse est d'étudier la dynamique et la synchronisation des dispositifs électromécaniques décrits par le système couplé constitué d'un oscillateur électrique de **Duffing** couplé magnétiquement et paramètriquement aux oscillateurs mécaniques linéaires. L'intérêt porté sur ces dispositifs électromécaniques est dû à la présence de ce modèle dans plusieurs branches de l'électromécanique.

Le premier chapitre présente quelques sources de composantes non linéaires et les systèmes électromécaniques où la dynamique peut être décrite par deux oscillateurs couplés, avec la nonlinéarité de **Duffing**.

Dans le second chapitre, nous étudions analytiquement et numériquement la dynamique des systèmes électromécaniques avec des sources d'excitation forcée et paramètrique. Les phénomènes de résonance, d'antirésonance et d'hysteresis sont observés. Les frontières de stabilité des oscillations harmoniques sont déterminées en utilisant les études analytiques et la simulation numérique des équations du mouvement. Les caractéristiques des oscillations "sub-" et "superharmoniques" sont aussi déterminées. Il apparait à travers nos études numériques que le chaos apparait dans notre modèle pour une valeur très grande de l'amplitude de l'excitation extérieure. L'algorithme du contrôle rétroactif est utilisé pour orienter le modèle du chaos vers une orbite périodique ciblée. Les effets du couplage paramètrique sur la dynamique et sur la frontière des oscillations harmoniques sont analysés.

Le chapitre 3 est consacré à la dynamique des dispositifs électromécaniques avec des fonctions multiples. Nous considérons le modèle avec double et un nombre élevé de fonctions en série et en parallèle, et nous déterminons les amplitudes des états d'oscillations harmoniques et leur stabilité, la différence de phase, les oscillations "sub-" et supeharmoniques qui apparaissent dans ces modèles. Nous discutons les effets du nombre d'oscillateurs mécaniques sur la dynamique du système électromécanique.

Nous considérons dans le chapitre 4 le problème de synchronisation des états réguliers et chaotiques des dispositifs électromécaniques avec ou sans delay. Nous déterminons le critère de stabilité, le coefficient de couplage optimal du processus de la synchronisation, et les valeurs critiques K_{cr} sous lesquelles, pour une précision donnée, on n'a aucune possibilité de synchonisation. La compatibilité entre les résultats analytiques et numériques est assez bonne.

General introduction and statement of the problem

General introduction and statement of the problem

0.1 Brief history of nonlinear oscillations and chaos

The nonlinear electrical, mechanical and electromechanical oscillators are those in which the electrical and mechanical components have nonlinear characteristics. Among these nonlinear components, those which are currently used are diodes, resistances, capacitances, inductances and springs. Two classes of nonlinear oscillators have been considered.

The first class is consisted of the self-excited oscillators described by an electrical circuit with nonlinear resistance. The **Van der Pol** oscillator serves as a prototype of the self-excited oscillator with stable amplitude and frequency. Since its discovery in 1920 by the electrical engineer **Balthazar Van der Pol** [O1], extensive studies devoted to the **Van der Pol** oscillator have shown that it possesses a rich dynamical behavior. Notably in the absence of external excitation, it generates a limit cycle wave in sinusoidal form, quasi-periodic or relaxative oscillations with the fixed amplitude, giving rise to self-excited character of the oscillator. Submitted to sinusoidal excitation [O2], the **Van der Pol** oscillator leads to various phenomena: frequency entrainement [O3], devil's staircases phenomena and chaotic behavior with period-doubling cascades [O3, O4]. Recently, **Kaiser** proposed in ref.[05] another self-excited model consisting of a **Van der Pol** oscillator with a nonlinear damping function of higher polynomial order, which described certain specific processes in biophysical systems and multi-stable limit-cycle solution in the unforced case [O6]. In biology, this model is used to describe the coexistence of two stable oscillatory states. This situation can be found in some enzyme reactions [O7], to explain the existence of multiple frequency and intensity windows in the reaction of biological systems when they are irradiated with very weak electromagnetic fields [O8-O11]. We note that the superharmonic resonance structure [O12], symmetry-breaking crisis and intermittency [O13] have also been analyzed in such model.

In the second class, the oscillations are induced by the external excitation applied in the electrical circuit. A typical example is the **Duffing** oscillator whose electrical equivalent can be obtained with nonlinear capacitance or nonlinear inductance. With the external sinusoidal excitation, the **Duffing** oscillator shows various phenomena: harmonic, subharmonic and superharmonic oscillations, multistability and transitions to chaos [O14]. Indeed, the **Duffing** oscillator is used in microwave communication as parametric amplifier, HF converter, mixer, low power and electronic accordability device.

Another phenomenon resulting to the presence of nonlinear components in science is chaos which is a name for any order that produces confusion in our minds or effectively unpredictable long time behavior arising in a deterministic dynamical system because of sensitivity to initial conditions. The first true experimenter in chaos was a meteorologist named **Edward N. Lorenz** [O15]. The interest devoted to chaos by many scientist is due

to the fact that this new phenomenon appears in various fields, from mathematics, physics, biology, and chemestry, to engineering, economics and medecine. Consequently, there are many opportunities for application of chaos. For example, in physics chaos has been used to refine the understanding of planetory orbits, to reconceptualize quantum level processes, and to forecast the intensity of solar activity. In engineering, chaos has been used in the building of better digital filters, and to model the structural dynamics in such structures as buckling columns. In medecine, it has been used to study cardiac arrhythmias and patterns of disease communication. In psychology, it has been used to study mood fluctuations, the operation of the olfactory lobe during perception, and patterns of innovation in organizations. In economics it is being used to find patterns and develop new types of econometric model for the stack market to variations in coton prices. There are also many opportunities for exploitation of chaos: synchronized chaos, mixing with chaos, encoding information with chaos, anti-control of chaos, tracking of chaos and targetting of chaos.

The study of the nonlinearity effects in coupled nonlinear oscillators including **Duffing** and **Van der Pol** oscillators is an interesting subject. Recent studies on these systems have shown various types of behavior [O16-O20]. As concerns the coupling between two **Duffing** oscillators or between the **Duffing** oscillator and other types of oscillators, some interesting results have been obtained recently. **Kozlowski** et al. [O21] have analyzed various bifurcations of two coupled periodically driven **Duffing** oscillators. They are showed that the global pattern of bifurcation curves in the parameter space consists of repeated subpatterns similar to the superstructure observed for single, periodically driven, strictly dissipative oscillators. For the coupling between **Duffing** oscillator and self-sustained oscillators, the problem was considered in ref.[O18] by investigating the dynamics of a system constisting of a **Van der Pol** oscillator coupled dissipatively and elastically to a **Duffing** oscillator. Using the multiple time scales method, the oscillatory states were analyzed both in the resonant and non-resonant cases. Chaos was also found using the **Shilnikov** theorem.

0.2 Statement of the problem

The main purpose of our work is to consider electromechanical devices with **Duffing** nonlinearity which are widely encountered in various branches of electromechanical engineering as it is described in chapter 1. Indeed, because of the recent advances in the theory of nonlinear phenomena, it is interesting to consider such electrodynamic system containing one or various nonlinear components, or in the state where one or various of its components react nonlinearly. We consider the dynamics and synchronization of electromechanical devices with a **Duffing** nonlinearity.

The following points are considered:

• The derivation of the amplitudes and stability boundaries of harmonic behavior in the electromechanical devices using analytical and numerical investigations.

• The numerical simulation of the chaotic behavior of such devices.

• The continuous feedback control of the devices in the chaotic states.

•The synchronization of electromechanical devices in the regular and chaotic states.

0.3 Outline of this dissertation

This work consists of four chapters.

In chapter 1, which serves as preliminairies to this work, we present generalities on

electromechanical systems. A short description of the nonlinearity sources and some electromechanical systems are presented.

Chapter 2 deals essentially with the dynamics of forced and parametric electromechanical devices described by a coupled differential equation consisting of an electrical **Duffing** oscillator coupled magnetically with a linear mechanical oscillator.

Chapter 3 is devoted to the dynamics of electromechanical devices with multiple functions. We first consider the model with double and a large number of functions in series. Secondly, the dynamics of the model with double functions in parallel is considered.

In chapter 4, we consider the problem of synchronizing electromechanical devices both in their regular and chaotic states with and without delay. Our study uses the continuous feedback scheme of **Pyragas**. We use the **Floquet** theory to derive the stability criteria and the optimal coupling strength of the synchronization process. We derive the critical values K_{cr} under which, for a given precision, no synchonization is possible. Numerical simulations are used to complement our analytical results.

We end with a conclusion of our work containing a summary of our results and the outline of other points of interests to be solved in the future.

Bibliography

[O1] **Van der Pol B.,** Phil., Mag. **43**, 700 (1922).

[O2] **Van der Pol B.,** Phil., Mag. 7-3, 65 (1927).

[O3] **Hayashi, C.,** "Nonlinear Oscillations in Physical Systems," Mc-Graw-Hill, New-York. (1964).

[O4] **Parlitz U.** and **Lauterborn W.**, Phys. Rev. A**36**, 1428 (1987).

[05] **Kaiser F.**, "Coherent Excitations in Biological Systems: Specific Effects in Externally driven Self-Sustained Oscillating Biophysical Systems," Springer-Verlag, Berlin Heidelberg, (1983).

[O6] **Kaiser F.**, "Coherent Excitations in Biological Systems: Specific Effects in Externally driven Self-Sustained Oscillating Biophysical Systems," Springer-Verlag, Berlin Heidelberg, (1983).

[O7] **Li. Y-X** and **Goldberter. A.**, J. Theor. Biol. **138**, 149 (1989).

[08] **Kaiser F.,** "Coherent Oscillations in Biological Systems: Interaction with extremely low frequency fields," Radio Science 17 (5S), 17S.

[O9] **Kaiser F.,** "Theory of Resonant Effects of RF and MW Energy," in Biological Effects of an Dosimetry of Nonionizing Radiation, ed. Grandolfo, M., Michaelson, S. M. and Rindi, A.(Plenum Press, New York) 251 (1983).

[O10] **Kaiser F.,** "The role of chaos in Biological Systems," in Energy Transfer Dynamics, ed. Barret, T.W. and Pohl, H.A (Springer, Berlin) 224 (1987).

[O11] **Kaiser F.,** "Nichtlineare resonane and chaos. Ihre relevanz für biologische funktion," Kleinheubacher Berichte **32**, 395 (1989).

[O12] **Szemplińska-Stupnicka** and **Jerzy Rudowski**, Phys. Lett. A**192**, 201 (1994).

[O13] **Kaiser F.** and **Eichwald C.,** Int. J. Bif. and Chaos 1 **2**, 485 (1991).

[O14] **Nayfeh A. H.** and **Mook D. T.**, Nonlinear Oscillations, Wiley-Interscience, New York (1979).

[O15] **Gleick J.,** in"La théorie du chaos", Nouveaux horizons, New York (1987).

[O16] **Kapitaniak T.,** Phys. Rev. E 50, 1642 (1994).

[O17] **Woafo P.**, **Chedjou J. C.** and **Fotsin H. B.**, Phys. Rev. E **54**, 5929 (1996).

[O18] **Woafo P.**, **Fotsin H. B.** and **Chedjou J. C.,** Physica scripta **57**, 195, (1998).

[O19] **Asfar K. R.** and **Masoud K. K.**, Int. J. of Non-linear Mech. **29**, 421 (1994).

[O20] **Asfar K. R.,** J. of Vibrations and Acoustics, stress and reliability in Design, **111**, 130, (1989).

[O21] **Kozlowski J., Parlitz U.** and **Lauterborn W.,** Phys. Rev. E **51**, 1861 (1995).

Chapter 1 : **Generalities on the electromechanical systems**

Chapter 1

Generalities on the electromechanical systems

1.1 Introduction

In this first chapter, we deal with generalities on electromechanical systems and give some informations for their interaction with electromechanical engineering. We present in section 1.2 the sources of nonlinear components which appear in such electromechanical systems. Section 1.3 is devoted to the description of the electromechanical systems studied in this thesis. The resulting equations of motion are derived using the **Newton** second laws of dynamics and the **Kirchhoff** law for the voltage. The technological applications of the device and the useful of nonlinearity are discussed. In section 1.4, a short description of the piezoelectric and electrostatic transducers is presented. The last section is devoted to the conclusion.

1.2 Nonlinearity in electromechanical systems

Electromechanical system focusses on all the devices which make electrical and mechanical systems work together. The electrical components (like diodes, resistances, capacitors and inductances) will be able to have nonlinear characteristics introduced in the electrical part by the user, while in the mechanical part, the nonlinear components are connected to the functioning of the device. Our aim in this section is to give some details on the above two categories of nonlinear components encountered in the electromechanical systems.

1.2.1 Functioning inherent nonlinearity

This type of nonlinearity generally appears in the components of the mechanical part, particulary to a spring. For hardening spring effect in mechanical problems, it is found experimentally that the stiffness is not constant but increases with the received constraint. It is approximately defined by the relation:

$$K(x) = K_o + K_1 x^2, \tag{1.1}$$

where K_o is the stiffness for small stretching, x the elongation and K_1 a coefficient of nonlinearity. An example of an electromechanical device with a nonlinear spring has been studied recently by **Chedjou** et al. in ref.[I1, I2] and **Chembo** et al. in ref.[I3]. Let us note that other forms of $K(x)$ can be found such as that of the soft spring.

1.2.2 Introduced nonlinearities

In this case, the sources of nonlinearity can be introduced in three ways: Firstly, the voltage of the capacitor is a nonlinear function of the instantaneous electrical charge q [I4] given for instance by

$$V_c(q) = \frac{1}{C_o}q + a_2q^2 + a_3q^3 + ..., \tag{1.2}$$

where C_o is the linear value of C and a_i are the nonlinear coefficients depending on the type of the capacitor in use. This is typical of nonlinear reactance components such as varactor diodes widely used in many areas of electrical engineering to design for instance parametric amplifiers, up-converters, mixers, low-power microwave oscillators, etc [I5].

Secondly, the nonlinear sources can also be obtained by using a resistor with non-linear character so that the I-V curve is given as

$$V_R = R_o i_o \left[-\left(\frac{i}{i_o}\right) + \frac{1}{3}\left(\frac{i}{i_o}\right)^3 \right], \tag{1.3}$$

where R_o and i_o are respectively the normalization resistance and current, i is the value of current corresponding for the limit resistor voltage. In this case, the model have the property to exhibit self-excited oscillations. This is due to the presence of the nonlinear resistor whose current-voltage charateristic curve shows a negative slope and the fact that the model incorporate through its nonlinear resistance a dissipative mechanism to damp oscillations that grow too large and a source of energy to pump up those that become small. Because of this particular behavior, we can qualify our physical system with nonlinear resistor as a self-sustained oscillator. The nonlinear resistor can be realized using a block consisting of two transistors [I1, I2]. This type of nonlinear resistance with a negative slope was used recently in ref.[I1] for the dynamics of self-sustained electromechanical transducer.

Thirdly, we also consider an electrical circuit in which the nonlinear oscillation takes place owing to the presence of a saturable-core coil of inductance L. So that, an inductor L have a saturable stone, and the saturation law of the magnet can be explained as follows

$$ni = a_1\phi + a_3\phi^3 + ..., \tag{1.4}$$

where the coefficients a_i are constants, depend of the stone caracteristic, ϕ the magnetic flux in the core and n a number of turns of the coil. This is known as the hysteresis effects in the inductance. The dynamical behavior of various electrical circuits with nonlinear inductance are analyzed in ref.[I6] by **Hayashi**.

1.2.3 Useful and unfavorable effects of nonlinearity

The presence of nonlinearity in science can have positive interests and negative effects. So why the nonlinearity appears to be merely negative? In fact, nonlinear systems exhibit surprising and complex effects that would never be anticipated by a scientist trained only in linear techniques. Prominent examples of these are bifurcation, chaos and solitons. Nonlinearity has its most profound effects on dynamical systems and we currently not have general techniques (and very few special ones) for telling whether a particular nonlinear system will exhibit the complexity of chaos, or the simplicity of order. However, nonlinear science has

applications to a wide variety of fields, ranging from mathematics, physics, biology, and chemistry, to engineering, economics, and medecine. This is one of its most exciting aspects that brings reseachers from many disciplines together with a common language. For instance, we note that undesired phenomena such as chaos are now applied to problems in many fields of science and engineering. For example, in physics, chaos has been used to refine the understanding of planetary orbits, to reconceptualize quantum level processes, and to forecast the intensity of solar activity. In engineering, chaos has been used in the building of better digital filters, and to model the structural dynamics in such structures as buckling columns. In medecine it has been used to study cardiac arrhythmias and patterns of disease communication. In psychology it has been used to study mood fluctuations, the operation of the olfactory lobe during perception, and patterns of innovation in organizations. In economics it is being used to find patterns and develop new types of econometric models from the stock markets to variations in good prices.

Other interesting phenomena resulting of the presence of non-linear components in science is the multistability, which is understand like a coexistence between stability and instability phenomena encounter in various branches of science, it is usually described by discussing the possible steady-state solutions of some non-linear process having a single variable and one or more control or bifurcation parameters. In this case, the system presents the well-known hysteresis phenomena with two stable harmonic oscillations with different amplitudes, resulting generaly to the presence of the cubic nonlinearity.

1.3 The electrodynamical transducer

1.3.1 Description of the model and equations of motion

The electromechanical device shown in Figure 1.1 is an electromechanical transducer. It is composed of an electrical part coupled magnetically with a mechanical part. The coupling between both parts is realized through the electromagnetic force due to a permanent magnet which creates a **Laplace** force in the mechanical part and the Lenz electromotive voltage in the electrical part. The electrical part of the system consists of a resistor R, an inductor L, a condenser C and a sinusoidal voltage source $e(\tau') = v_o \cos \Omega\tau'$ (v_o and Ω being respectively the amplitude and frequency, and τ' the time), all connected in series. The mechanical part is composed of a mobile beam which can move along the $\vec{z}$ axis on both sides. The rod T which has the similar motion is bound to a mobile beam with a spring.

In our electromechanical model, the nonlinear term is introduced by considering only the nonlinear character of the condenser. Assuming that the quadratic term of $V_c(q)$ is negligible (i.e $a_2 = 0$), we have

$$V_c(q) = \frac{1}{C_o} q + a_3 q^3. \tag{1.5}$$

This is typical of nonlinear reactance components such as varactor diodes widely used in many areas of electrical engineering to design for instance parametric amplifiers, up-converters, mixers, low-power microwave oscillators, etc [I4]. Applying the **Newton** second law of dynamics and the **Kirchhoff** law for the voltage in the electromechanical transducer and taken into account the contributions of the **Laplace** force ($\vec{f} = \vec{l}(\vec{I} \wedge \vec{B})$) and the **Lenz** electromotive voltage ($\vec{e} = -\vec{l}(\vec{B} \wedge \dot{\vec{z}})$), it is found that the system is described by the following set of differential equations

$$
\begin{aligned}
L\ddot{q} + R\dot{q} + \frac{q}{C_o} + a_3 q^3 + lB_m\dot{z} &= v_o \cos\Omega\tau', \\
m\ddot{z} + \lambda\dot{z} + kz - lB_m\dot{q} &= 0,
\end{aligned}
$$

where l is the length of the domain of the interaction between $\vec{B}_m$ and the two mobile rods supporting the beam. The dot over quantities denotes the time derivative. Let us use the dimensionless variables

$$
x = \frac{q}{Q_o}, \qquad y = \frac{z}{l}, \qquad t = w_e\tau',
$$

where Q_o is a reference charge of the condenser and

$$
w_e^2 = \frac{1}{LC_o}, \quad w_m^2 = \frac{k}{m}, \quad \gamma_1 = \frac{R}{Lw_e}, \quad \beta = \frac{a_3 Q_o^2}{Lw_e^2}, \quad \lambda_1 = \frac{l^2 B_m}{LQ_o w_e},
$$

$$
E_0 = \frac{v_o}{LQ_o w_e^2}, \quad w = \frac{\Omega}{w_e}, \quad \gamma_2 = \frac{\lambda}{mw_e}, \quad w_2 = \frac{w_m}{w_e}, \quad \lambda_2 = \frac{B_m Q_o}{mw_e}.
$$

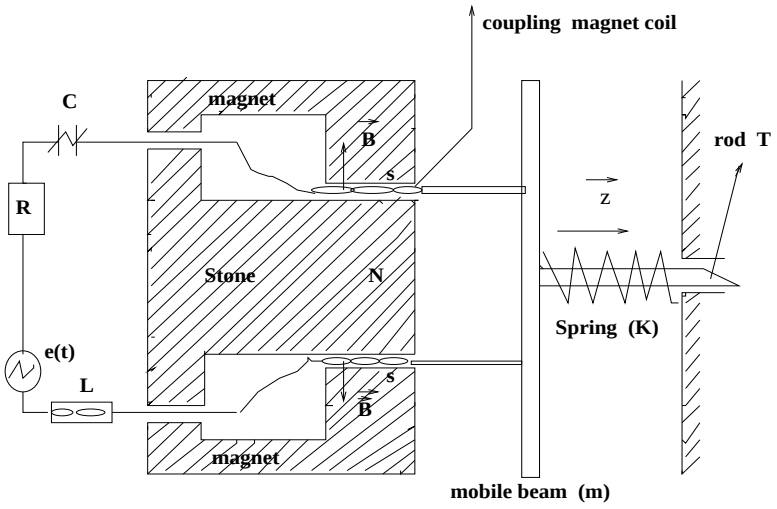

Figure 1.1: *Non-linear electromechanical transducer.*

Then the above two differential equations reduce to the following set of nondimensional differential equations:

$$
\begin{aligned}
\ddot{x} + \gamma_1\dot{x} + x + \beta x^3 + \lambda_1\dot{y} &= E_o \cos wt, \\
\ddot{y} + \gamma_2\dot{y} + w_2^2 y - \lambda_2\dot{x} &= 0.
\end{aligned} \tag{1.6}
$$

Let us note that in the absence of the coupling ($\lambda_i = 0$), the set of equations (1.6) reduces to a classical and well-studied **Duffing** oscillator [I7] and a linear oscillator. Submitted to an external sinusoidal excitation with one component, the **Duffing** oscillator leads to various interesting phenomena like hysteresis, subharmonic and superharmonic oscillations, multi-stability, and transitions to chaos. For the case of the external sinusoidal excitation with two

components (i.e $E(t) = K_1 \cos(w_1 t + \theta_1) + K_2 \cos(w_2 t + \theta_2)$), some interesting results have been obtained recently. **Nayfeh** and **Mook** analyzed the problem in ref.[I7] by investigating the dynamics of the **Duffing** oscillator submitted to two terms of the external excitation. Using the multiple time scales method, they showed that it is possible to obtain some resonant combinations leading to subharmonic and superharmonic resonances. Recently, **Fotsin** et al. [I8] used the multiple time scales method to obtain the behavior of the oscillator when it enters in resonance with one of the component of the external excitation. They used the **Melnikov** theorem to derive the condition for fractal basin boundary, a sign of a chaotic motion. Bifurcation diagrams showing transitions from regular to chaotic motion have also been drawn.

1.3.2 Technological applications and useful of nonlinearity on the device

The interest on such device is justified by the fact that the model is widely encountered in various branches of electromechanical engineering. In particular, in its linear version, it describes the well-known electrodynamic loudspeaker [I9]. In this case, the sinusoidal signal $e(t)$ represents an incoming pure message. Because of the recent advances in the theory of nonlinear phenomena, it is interesting to consider such an electromechanical system containing one or various nonlinear components or in the state where one or various of its components react nonlinearly. One such state occurs in the electrodynamic loudspeaker due to the nonlinear character of the diaphragm suspension system resulting in signal distorsion and subharmonics generation [I9]. Moreover, the model can serve as a servo-command mechanism which can be used for various applications. Here one would like to take advantage of nonlinear responses of the model in manufacturing processes.

Before we end with this subsection, let us note other technological applications of such device

• With the rod T, the device serves as perforator device, precision electrical saw or drill and sifter or sieve electromechanical device in industry.

• One can used the device like a mechanical vibration for uncrunching a tarred road in civil engineering.

• The model can also be used as an electromechanical vibration absorber [I10]. In this case, the electrical part represented an electrical absorber device with linear characteristic for the vibration of the mechanical part.

The presence of nonlinear components in our electromechanical device can also have positive effects. As in the case of **Duffing** oscillator, the electromechanical transducer with nonlinear components can also exhibits various complex behaviors like hysteresis phenomena, harmonic, subharmonic and superharmonic oscillations, quasiperiodicity, multiperiodicity and chaotic behaviors. Our aim is to look if the above mentioned nonlinear phenomena on the device are interesting for the technological exploitation of such device in electromechanical engineering.

For example, the hysteresis phenomena is interesting in nonlinear oscillations and generally manifests itself in any physical systems with cubic nonlinearity. The frequency-response curves in this case are multivalued while others are single valued. The multiplicity of the response has a significance from the physical point of view because it leads to hysteresis phenomena with two stable amplitudes. Consequently, the electromechanical transducer can vibrate in these domains with two stable different amplitudes of the harmonic oscillations depending to the initial conditions. With the quasiperiodic and chaotic behaviors, the electromechanical device vibrates with a large frequency band and can be interesting when the

model is used as a sifter or sieve electromechanical device in industry.

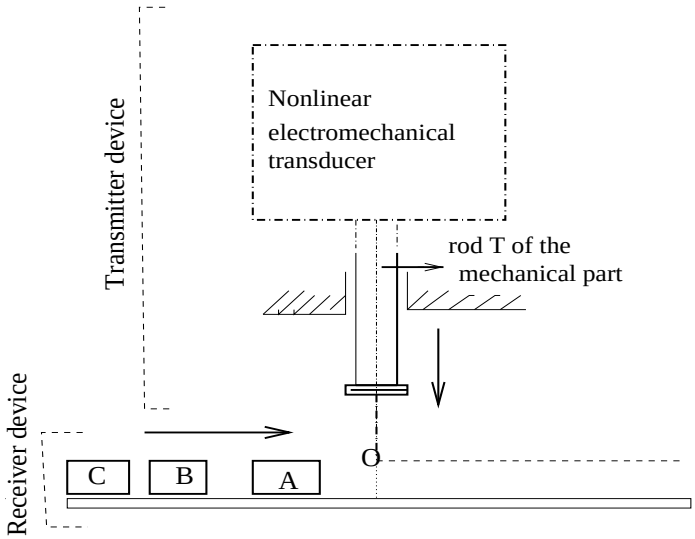

Figure 1.2: *Schematic diagram of the functioning electromechanical device.*

Concerning the use of the electromechanical device for the manufacturing process, the prototype schematic diagram of the functioning electromechanical device is shown in Figure 1.2. It is composed of two independently operating elements, transmitter and receiver devices. We note that the transmitter device is represented by the rod T of the mechanical part of the electromechanical device, while the receiver device stands for the manufacturing products. The transmitter device, excited by the sinusoidal voltage source of the electrical part of the electromechanical device, operates with the translatory motion in the vertical axis. In periodic regime and for any received oscillations of the electrical part, the device shown in figure 1.2 operates so that the extremity of the mobile beam of the mechanical part encounters the receiver device in O. It can be noticed that the role of the extremity of the mobile beam is to execute on any receiver device one single contact during any translatory motion. This requires the use of the linear or nonlinear periodic oscillations. However, for some practical or technological reasons, one can need to execute during any oscillation of the mobile beam more than one contact on any receiver device which passes in O. This also requires another type of oscillations: period-nT oscillations which appear only in the nonlinear regime. The generation of the period-nT oscillations in our device is one of the reasons to introduce nonlinear components in electromechanical transducer.

1.4 Other electromechanical systems

1.4.1 The piezoelectric transducer

Figure 1.3 shows an electromechanical device which converts electrical energy directly to mechanical energy and vice-versa through the use of the piezoelectric effect in which certain materials change dimension when an electrical charge is applied to them.

Electrical energy is supplied to the transducer by the generator. This electrical energy is applied to piezoelectric element(s) in the transducer which vibrate at the same frequency as that of the applied voltage of the generator. These vibrations are amplified by the resonant masses of the transducer. Early piezoelectric transducers used such piezoelectric materials as naturally occuring quartz crystals and barium titanate which were fragile and unstable.

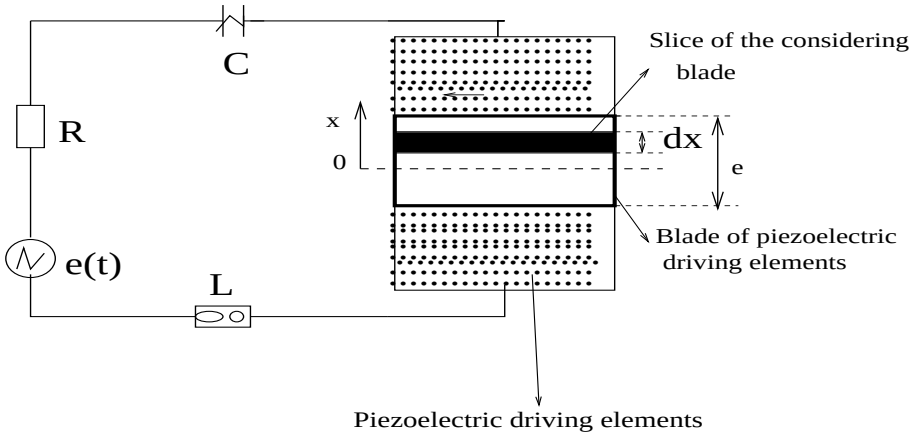

Figure 1.3: *Piezoelectric transducer*

Today's transducers incorporate stronger, more efficient and highly stable ceramic piezoelectric materials. A large number of transducers used today are based on the piezoelectric effects. Let us note that the electrical energy is obtained for a RLC circuit as described in the previous section.

To establish the governed equations of motion of the piezoelectric transducer, we consider a blade with thickness in the piezoelectric driving elements, and taken inside this blade a slice with small thickness dx. The stationary motion of the mechanical part is described by the displacement x of the considering slice of the blade. Using the electrical and mechanical laws, and taken into account the contributions of the mechanical force produced by the charge of the material and the electrical voltage produced by the displacement of the slice of the material induced by reverse piezoelectric effect, it is found that the piezoelectric transducer is described by the following set of non-linear coupled differential equations consisting of an electrical **Duffing** oscillator coupled to a linear oscillator as follows

$$\begin{aligned} L\ddot{q} + R\dot{q} + \frac{q}{C_o} + a_3 q^3 + \Gamma x &= v_o \cos\Omega\tau', \\ m\ddot{x} + w_o^2 x + \lambda\dot{x} - \Gamma q &= F_0 \cos\Omega_1\tau'. \end{aligned} \tag{1.7}$$

where Γ is a piezoelectric coupling coefficient, m is the mass of the slice, λ the damping coefficient, w_o the natural frequency of the slice, q denotes the instantaneous electrical charge of the condenser while x is the displacement of the slice of the piezoelectric element(s). We have also used a nonlinear component as in the case of electrodynamical transducer.

The piezoelectric transducers serve as transmitters and receivers in imaging systems for sonar, medical imaging and non-destructive evaluation applications, as well as in nonimaging applications like surface acoustic wave devices in signal processing [I11]. One of most technical applications is ultrasound (ultrasonic) medical imaging. Operational emphasis for imaging transducers is broadband (impulsive) rather than narrowband (continuous wave). Piezoelectric transducers are currently available for diagnostic imaging and Doppler velocity measurement [I12], as well as a host of speciality applications (intracavity, biospy, etc.) including disease treatment (lithotripsy, hyperthermia, tissue ablation) [I13].

1.4.2 The electrostatic transducer

Electrostatic transducers point out any type of device that converts an electrical signal into mechanical signals (as in loudspeakers) or converts a mechanical signals into an electrical signal (as in the microphone) through the variation of the capacitor of the condenser. This model is shown in Figure 1.4 and it is composed of a resistance R and inductor L in series with a high voltage source E_0 which polarizes a condenser C. This condenser is composed of two conducting plates, one fixed and the other mobile. This mobile plate is linked to the rest of the system by two conducting spring of constant k. The most popular form of this type of device is the electret condenser microphone, in which the plates are given a permanent electrical charge. The interest devoted to this type of transducer is due to the electromechanical coupling established by the variation of the capacitor of the condenser versus the electrical and mechanical external excitation.

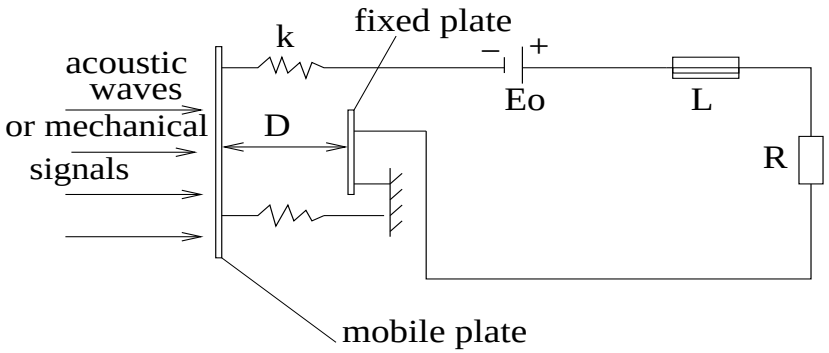

Figure 1.4: *Electrostatic transducer.*

Applying to the condenser C a continuous voltage of polarization, superimposed to an alternative voltage with small amplitude, the two plates are submitted to an attractive or repulsive force, the mobile plate vibrates giving rise to sound waves (as in electrostatic loudspeaker). Inversely, when the incident sound waves cause the charged diaphragm to vibrate, the voltage across the plates changes, creating a signal in the electrical part as one observes in microphones.

The interest on such devices is justified by the fact that with the revival of the electret old idea, electrostatic microphones are widely used for various types of technological applications such as monoscope tube for TV set signals, cassette recorders devices and evidently telephone devices [I14]. **Woafo** et al. had carried out a series of studies on this device taking into account the nonlinearities and applications in communication engineering [I3, I15, I16].

1.5 Conclusion

In this chapter, we have dealed with the generalities on electromechanical systems and their interactions with electromechanical engineering. Different types of sources of nonlinear components in the electromechanical systems have been presented. We have presented electromechanical, piezoelectric and electrostatic transducers, and given the resulting equations of motion. In the remaining of the thesis, we will consider only the electrodynamical system with a cubic nonlinearity in the V-q characteristics of the condenser.

Bibliography

[I1] **Chedjou J. C., Woafo P.** and **Domngang S.,** Journal of Vibrations and Acoustics, **123**, 170 (2001).

[I2] **Chedjou J. C.** , "Etude de la dynamique régulière et chaotique du système couplé oscillateur de Van der Pol-Oscillateur de Duffing" Thèse de Doctorat de 3^{eme} cycle, Laboratoire d'électronique, Université de Yaoundé I, Cameroun (1999).

[I3] **Chembo Kouomou Y.** and **Woafo P.**, Physica Scripta **62**, 255 (2000).

[I4] **Oksasoglou A.** and **Vavrim D.,** IEEE Trans. Circuits Syst, **41**, 669 (1994)

[I5] **Fotsin H.,** "Phénomene coherent et incoherent dans le microphone à condensateur et dans les circuits électroniques à Diode Varicap", Thèse de Doctorat de 3^{eme} cycle, Laboratoire d'électronique, Université de Yaoundé I, Cameroun (1999).

[I6] **Hayashi C.,** "Nonlinear Oscillations in Physical Systems," Mc-Graw-Hill, New-York (1964).

[I7] **Nayfeh A. H.** and **Mook D. T.**, "Nonlinear Oscillations", Wiley-Interscience, New York (1979).

[I8] **Fotsin H., Chedjou J.** and **Woafo P.**, Physica Scripta **54**, 545 (1996).

[I9] **Olson H. F.**, Acoustical Engineering, Van Nostrand, Princeton (1967).

[I10] **Korenev B. G.** and **Reznikov L. M.,** "Dynamics vibration absorbers", John-wiley, new york (1997).

[I11] **Lines M. E.,** and **Glass, A., M.,** "Principles and application of Ferroelectric related materials," Clarendon press, Oxford (1977).

[I12] **Kine G. S.,** Acoustic waves, Prentice-Hall Inc. (1987)

[I13] **Fish P.,** "Physics and Instrumentation of Diagnostic Medical Ultrasound", John wiley and sound, New York (1990)

[I14] **Sinclair I. R.,** in "Sensors and Transduscers" 2^{nd} edition Butterworth-Heinemann, (1992).

[I15] **Woafo P., Fotsin H. B.** and **Chedjou J. C.**, Physica Scripta **57**, 195 (1998)

[I16] **Woafo P.,** Phys. Lett A**267**, 31 (2000).

Chapter 2 :
Dynamics of a nonlinear electromechanical system

Chapter 2

Dynamics of a nonlinear electromechanical system

2.1 Introduction

This chapter deals with the dynamics of a forced and parametric nonlinear electromechanical system consisting of an electrical **Duffing** oscillator coupled magnetically with a linear mechanical oscillator as we have shown in the previous chapter (see equations (1.6)). Two main points are considered: the first point concerns the dynamics of the model with external excitation, while in the second point, the excitation also appears in the coupling coefficient. The chapter is organized as follows. In the next section, we concentrate on the dynamics of the forced nonlinear electromechanical system. We first consider the regular dynamics of the system using analytical method [II1]. We find and analyze the stability of harmonic oscillatory states using respectively the method of harmonic balance and the **Floquet** theory. The analytical results are then compared to the numerical ones. The numerical simulation of the equations of motion will use the fourth-order **Runge-kutta** algorithm. Secondly, we derive the characteristics of sub- and superharmonic oscillatory states in the model. We also analyze the types of transitions from regular behavior to chaos which appear in such device. The indicators used are the one-dimensional **Lyapunov** exponent and the bifurcation diagrams. Thirdly, the canonical feedback controllers algorithm [II2] is used to drive the electromechanical transducer from chaos to a regular target trajectory. In section 2.3, we extend our investigations by considering our model with parametric coupling. We analyze the effects of the parametric coupling on the dynamics and stability boundaries of the harmonic oscillations, and amplitudes of sub- and superharmonic oscillatory states. The last section devoted to the conclusion.

2.2 Forced electromechanical transducer

2.2.1 Harmonic oscillatory states

In this subsection, we aim to derive the harmonic oscillations of equations (1.6). It is assumed that the fundamental component of the solutions has the period of the sinusoidal voltage source. We use the harmonic balance method [II1]. For this purpose, we express x and y in the form

$$\begin{aligned} x &= a_1 \cos wt + a_2 \sin wt, \\ y &= b_1 \cos wt + b_2 \sin wt. \end{aligned} \tag{2.1}$$

Set $A^2 = a_1^2 + a_2^2$ and $B^2 = b_1^2 + b_2^2$. Inserting equations (2.1) in equations (1.6) and equating the coefficients of $\cos wt$ and $\sin wt$ separately to zero (assuming that the terms due to higher frequencies can be neglected), we obtain:

$$\begin{aligned}
(1 - w^2 + \frac{3}{4}\beta A^2)a_1 + \gamma_1 w a_2 + \lambda_1 w b_2 &= E_0, \\
-w\gamma_1 a_1 + (1 - w^2 + \frac{3}{4}\beta A^2)a_2 - \lambda_1 w b_1 &= 0, \\
(w_2^2 - w^2)b_1 + \gamma_2 w b_2 - \lambda_2 w a_2 &= 0, \\
-w\gamma_2 b_1 + (w_2^2 - w^2)b_2 + \lambda_2 w a_1 &= 0.
\end{aligned} \tag{2.2}$$

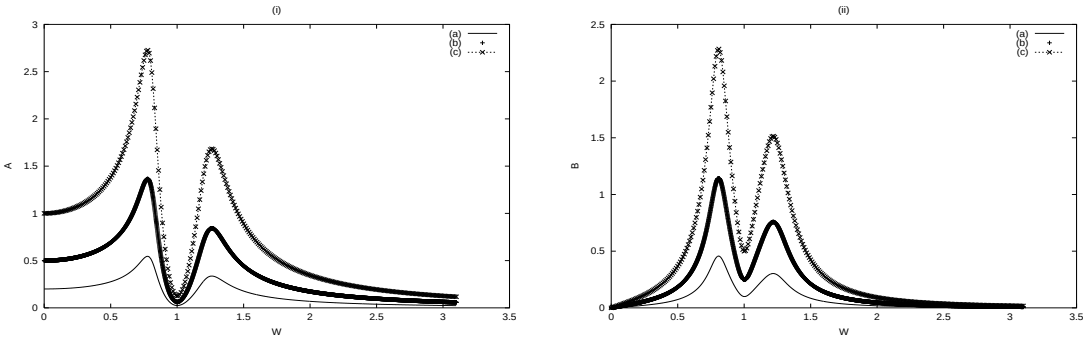

Figure 2.1: *Frequency-response curves in the linear oscillations. (i) for $A(w)$ and (ii) for $B(w)$ with $E_o = 0.2, \gamma_1 = 0.01, \gamma_2 = 0.1, \lambda_2 = 0.4, \lambda_1 = 0.2; w_2 = 1.0$; (a): $E_0 = 0.2, (b) : E_0 = 0.5$, $(c) : E_0 = 1.0$.*

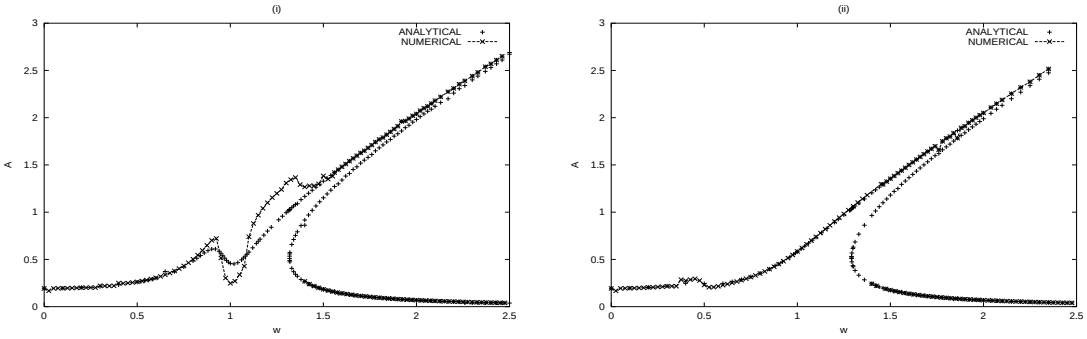

Figure 2.2: *Analytical and numerical frequency-response curves $A(w)$. The parameters are those of figure 2.1 and $E_0 = 0.2, \beta = 0.95$. $(i) : w_2 = 1.0; (ii) : w_2 = 0.5$.*

After some algebraic manipulations, it comes that the amplitudes A and B satisfy the following nonlinear algebraic equations

$$\begin{aligned}
&\frac{9}{16}\beta^2 A^6 + \frac{3}{2}\beta F_1 A^4 + (F_1^2 + G_1^2)A^2 - E_0^2 = 0, \\
&B = \frac{\lambda_2 w}{\sqrt{D}} A,
\end{aligned} \tag{2.3}$$

where

$$\begin{aligned}
D &= (w_2^2 - w^2)^2 + w^2\gamma_2^2, \\
F_1 &= 1 - w^2 - \frac{\lambda_1\lambda_2 w^2(w_2^2 - w^2)}{D}, \\
G_1 &= \gamma_1 w + \frac{\lambda_1\lambda_2\gamma_2 w^3}{D}.
\end{aligned}$$

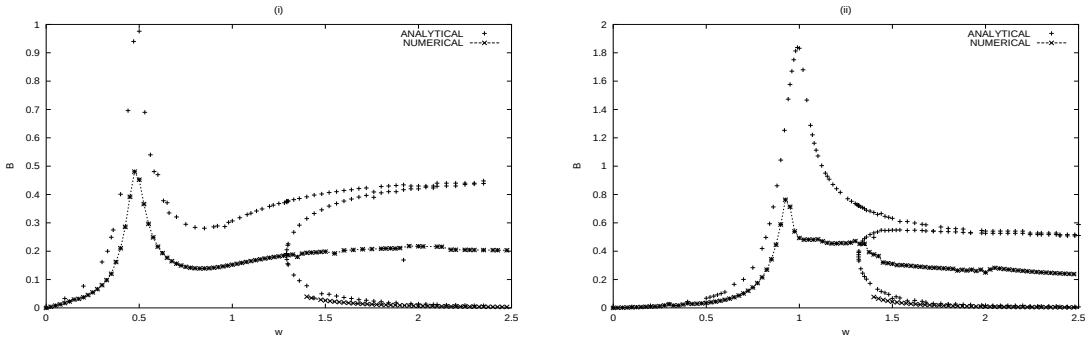

Figure 2.3: *Analytical and numerical frequency-response curves $B(w)$. (i): $w_2 = 1.0$; (ii): $w_2 = 0.5$ The other parameters are those of figure 2.1 and $E_0 = 0.2, \beta = 0.95$.*

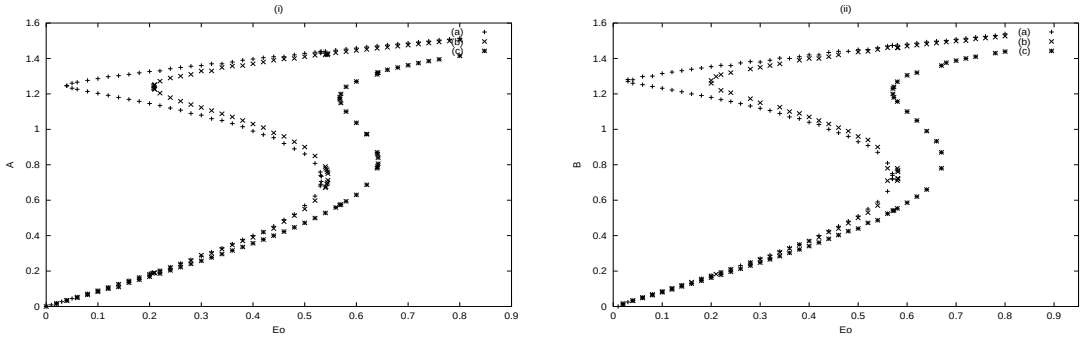

Figure 2.4: *Amplitude-response curves. The parameters are the same in figure 2.1 and (a): $\gamma_1 = 0.01, (b) : \gamma_1 = 0.1; (c) : \gamma_1 = 0.3$.*

We first consider the linear case ($\beta = 0$, the condenser C has the usual linear characteristic form). The frequency-response curves of the linear electromechanical model are represented in Figures 2.1(i) for A(w) and 2.1(ii) for B(w) for several values of the amplitude E_0 of the external excitation. The curves also show one peak of antiresonances and two peaks of resonances. Around the resonance peaks, the amplitude and the accumulate energies of the electromechanical transducer are very high than those received in any oscillation. In this case, the model can give more interesting applications in engineering, particulary when the model is used like a perforator electromechanical device, but the model with high energies is very dangerous since it can give rise to catastrophe damage. For the antiresonance peak, the electromechanical transducer vibrates with small amplitude and accumulate energies. This phenomenon is interesting when the model is used as an electromechanical vibration absorber [II3].

In the nonlinear case ($\beta \neq 0$), we use the **Newton-Raphson** algorithm to find the behavior of the amplitudes A and B when the frequency w is varied. The analytical and numerical frequency-response curves obtained are provided in Figure 2.2 for A(w) and in Figure 2.3 for B(w). The curves show antiresonance and resonance peaks besides the hysteresis domains. In Figure 2.4, we provide the amplitude-response curves of the model for three fixed values of the damping coefficient γ_1 in the resonant case. The curves show the well-known jump phenomena resulting from a cubic nonlinearity. We note that the curves are multivalued while others are single valued. The multivaluedness of the response due to cubic nonlinearity has a significance from the physical point of view because it leads to jump and hysteresis phenomena with two stable amplitudes. Consequently, the electromechanical transducer can vibrate in these domains with two stable different amplitudes of the harmonic oscillations depending on the initial conditions.

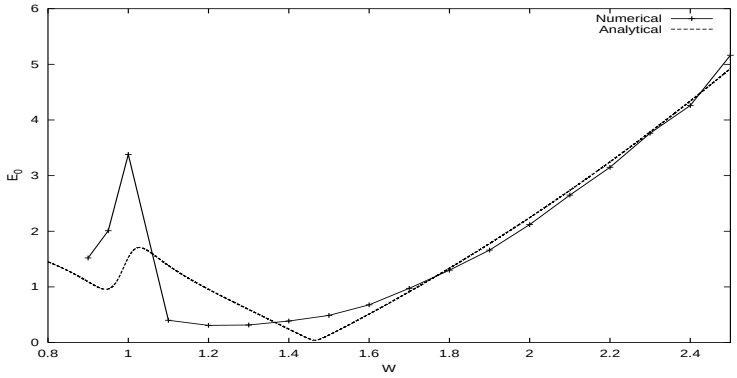

Figure 2.5: *Analytical and numerical stability domains in the (w, E_o) plane with the parameters of figure 2.1*

2.2.2 Stability of the harmonic oscillations

The electromechanical model shown in Figure 1.1 is physically interesting only so long as their vibrations described by equations (1.6) are stable. To study the stability of the harmonic oscillatory states, one considers the following variational equations of equations (1.6) around the harmonic oscillatory states given by equations (2.1)

$$\begin{aligned} \delta\ddot{x} + \gamma_1\delta\dot{x} + \delta x + 3\beta x_s^2\delta x + \lambda_1\delta\dot{y} &= 0, \\ \delta\ddot{y} + \gamma_2\delta\dot{y} + w_2^2\delta y - \lambda_2\delta\dot{x} &= 0, \end{aligned} \tag{2.4}$$

where x_s is the harmonic oscillatory state defined by equations (2.1). The harmonic oscillatory states (x_s, y_s) are stable if δx and δy remain bounded as the time goes up. The appropriate analytical tool to investigate the stability conditions of the harmonic oscillatory states is the **Floquet** theory [II1]. Let us then express δx and δy in the form

$$\begin{aligned} \delta x &= u\exp(-\epsilon_a\tau), \\ \delta y &= v\exp(-\epsilon_b\tau), \end{aligned} \tag{2.5}$$

where

$$\epsilon_a = \frac{\gamma_1}{w}, \qquad \epsilon_b = \frac{\gamma_2}{w}, \qquad \epsilon = \epsilon_b - \epsilon_a, \qquad t = \frac{2\tau}{w},$$

Inserting equations (2.5) into equations (2.4), we obtain the following coupled canonical **Mathieu** equations:

$$\begin{aligned} &\frac{d^2u}{d\tau^2} + [\delta_{11} + 2\epsilon_{11}\cos(4\tau - 2\phi)]u + \delta_{12}v\exp(-\epsilon\tau) + c_1\frac{dv}{d\tau}\exp(-\epsilon\tau) = 0, \\ &\frac{d^2v}{d\tau^2} + \delta_{21}u\exp(\epsilon\tau) + \delta_{22}v + c_2\frac{du}{d\tau}\exp(\epsilon\tau) = 0, \end{aligned} \tag{2.6}$$

where the new parameters δ_{ij}, c_i and ϵ_{11} are given by:

$$\begin{aligned} \delta_{11} &= -\epsilon_a^2 + \frac{4}{w^2} + \frac{3\beta A^2}{w^2}, \qquad \delta_{12} = \frac{-2\lambda_1\epsilon_b}{w}, \qquad \delta_{22} = -\epsilon_b^2 + \frac{4w_2^2}{w^2}, \\ \delta_{21} &= \frac{2\epsilon_a\lambda_2}{w}, \quad \epsilon_{11} = \frac{3\beta A^2}{2w^2}, \qquad c_1 = \frac{2\lambda_1}{w}, \quad c_2 = \frac{-2\lambda_2}{w}. \end{aligned}$$

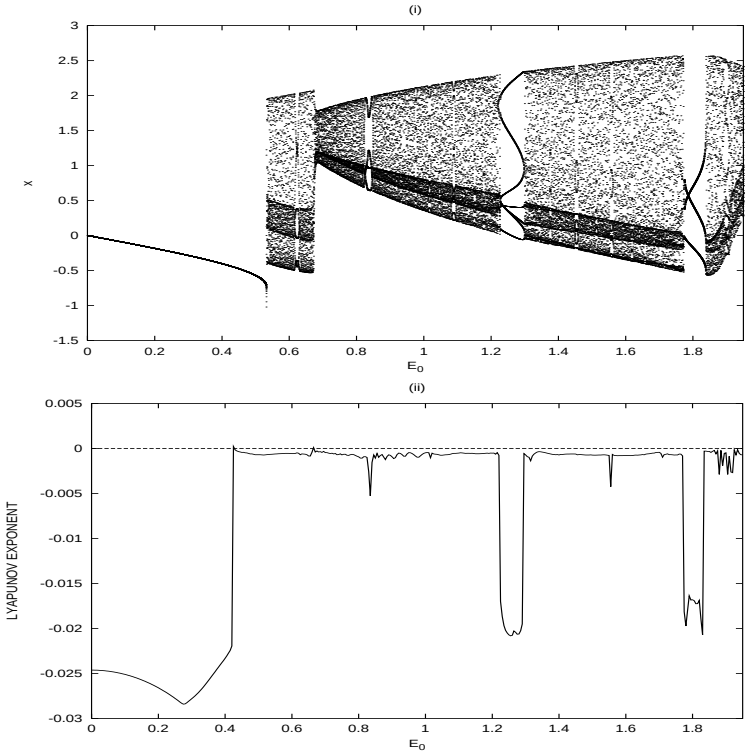

Figure 2.6: *Transition from the stability domain to the instability domain. The other parameters are those in figure 2.2 and* $w = 1.5$. *(i) Bifurcation diagram showing the coordinate* x *versus* E_0. *(ii) The variation of the corresponding Lyapunov exponent.*

According to the **Floquet** theory [II1], equations (2.6) has normal solutions given by

$$\begin{aligned} u &= \exp(a\tau)\alpha(\tau) = \sum_{n=-\infty}^{n=+\infty} \alpha_n \exp(a_n\tau), \\ v &= \exp(b\tau)\beta(\tau) = \sum_{n=-\infty}^{n=+\infty} \beta_n \exp(b_n\tau), \end{aligned} \tag{2.7}$$

where

$$a_n = a + 2in, \qquad b_n = b + 2in.$$

This means that

$$\begin{aligned} \delta x(\tau) &= \exp((a-\epsilon_a)\tau)\alpha(\tau), \\ \delta y(\tau) &= \exp((b-\epsilon_b)\tau)\beta(\tau). \end{aligned} \tag{2.8}$$

The functions $\alpha(\tau) = \alpha(\tau+\pi)$ and $\beta(\tau) = \beta(\tau+\pi)$ have been decomposed in **Fourier** series, a and b are two complex numbers, while α_n and β_n are constants. Substituting equations (2.7) into equations (2.6) yields

$$\sum_{n=-\infty}^{n=+\infty} (\delta_{11} + a_n^2)\alpha_n \exp(a_n\tau) + (\epsilon_{11}\exp(-2i\phi)) \sum_{n=-\infty}^{n=+\infty} \alpha_n \exp(a_{n+2}\tau) +$$

$$(\epsilon_{11}\exp(2i\phi)) \sum_{n=-\infty}^{n=+\infty} \alpha_n \exp(a_{n-2}\tau) + (\delta_{12} + c_1 b_n)\exp(-\epsilon\tau) \sum_{n=-\infty}^{n=+\infty} \beta_n \exp(b_n\tau) = 0,$$

$$\sum_{n=-\infty}^{n=+\infty} (\delta_{22} + b_n^2)\beta_n \exp(b_n\tau) + (\delta_{21}\exp(\epsilon\tau)) \sum_{n=-\infty}^{n=+\infty} \alpha_n \exp(a_n\tau) +$$

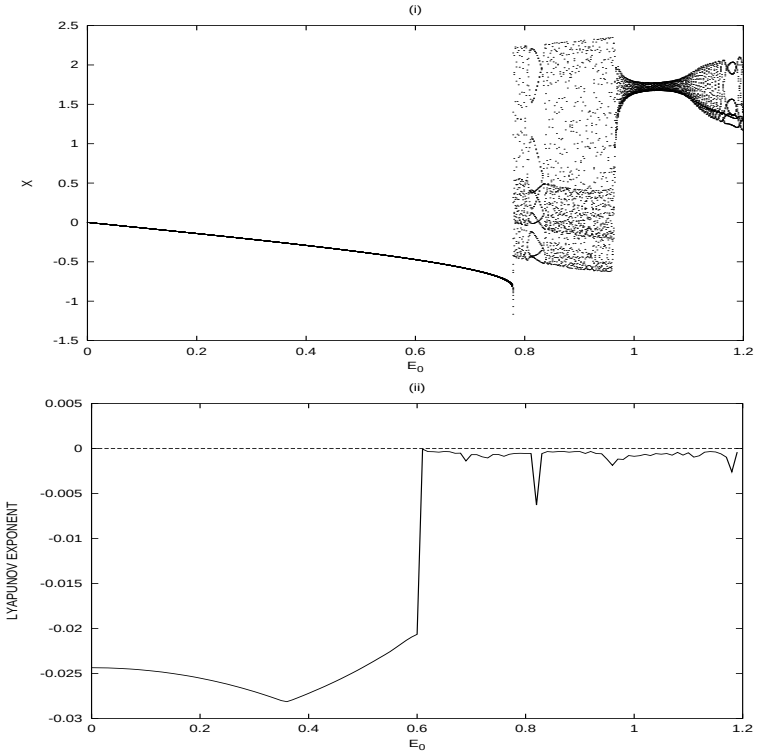

Figure 2.7: *Transition from the stability domain to the instability domain. The other parameters are those in figure 2.2 and* $w = 1.6$. *(i) Bifurcation diagram showing the coordinate* x *versus* E_0. *(ii) The variation of the corresponding Lyapunov exponent.*

$$(c_2 \exp(\epsilon\tau)) \sum_{n=-\infty}^{n=+\infty} a_n \alpha_n \exp(a_n \tau) = 0. \tag{2.9}$$

Equating each of the coefficients of the exponential functions to zero yields the following infinite set of linear, algebraic, homogeneous equations for the α_m and β_m

$$\begin{aligned}
&(\delta_{11} + a_m^2)\alpha_m + (\epsilon_{11} \exp(-2i\phi))\alpha_{m-2} + (\epsilon_{11} \exp(2i\phi))\alpha_{m+2} \\
&+(\delta_{12} + c_1 b_m) \exp(-\epsilon\tau)\beta_m = 0, \\
&(\delta_{22} + b_m^2)\beta_m + (\delta_{21} \exp(\epsilon\tau))\alpha_m + c_2 \exp(\epsilon\tau) a_m \alpha_m = 0.
\end{aligned} \tag{2.10}$$

For the nontrivial solutions the determinant of the matrix in equations (2.10) must vanish. Since the determinant is infinite, we divide the first and second expressions of equations (2.10) by $(\delta_{11} - 4m^2)$ and $(\delta_{22} - 4m^2)$ respectively for convergence considerations. Equating to zero the **Hill's** determinant [II1] and set $a = \epsilon_a$, $b = \epsilon_b$, we obtain the hypersurface which separates stability from instability domains. This hypersurface becomes a curve when two parameters of the system are varied. When the ϵ_{11} is small, approximate solutions can be obtained considering only the central rows and columns of the **Hill's** determinant. The small **Hill** determinant for this case is the sixth rows and columns given by

$$\begin{aligned}
\Delta(\epsilon_a, \epsilon_b) \;=\; & [(\delta_{11} + \epsilon_a^2)(\delta_{22} + \epsilon_b^2) - (\delta_{12} + c_1\epsilon_b)(\delta_{21} + c_2\epsilon_a)] \\
& \{-(\delta_{21} + c_2(\epsilon_a + 2i))(\delta_{12} + c_1(\epsilon_b - 2i)) \\
& \Big\{(\delta_{11} + (\epsilon_a - 2i)^2)(\delta_{22} + (\epsilon_b - 2i)^2) - \\
& (\delta_{12} + c_1(\epsilon_b - 2i))(\delta_{21} + c_2(\epsilon_a - 2i))\}
\end{aligned}$$

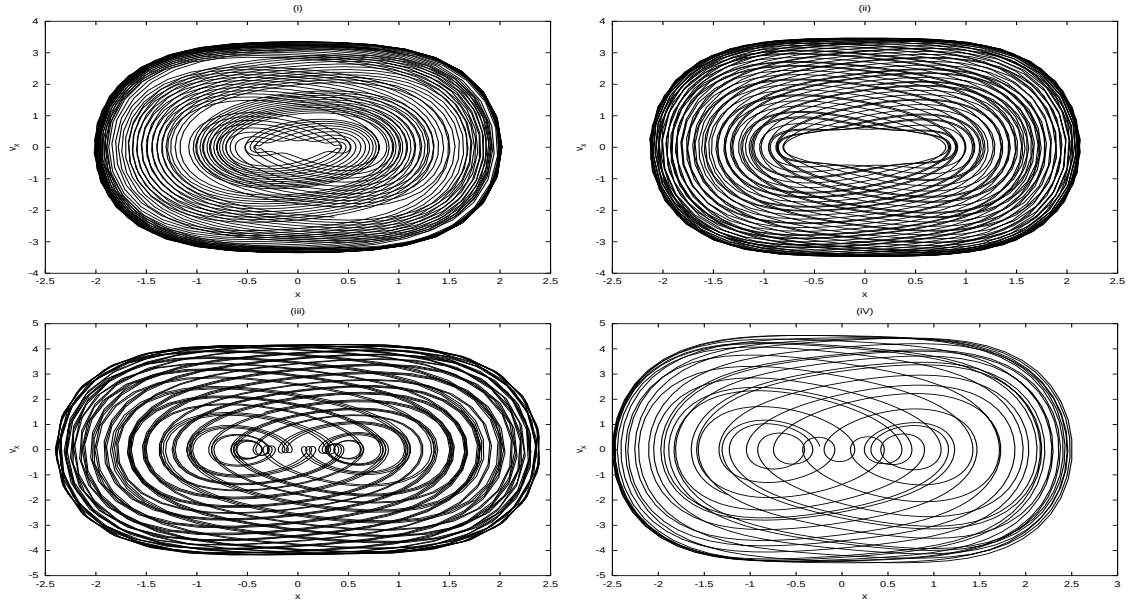

Figure 2.8: *Behavior of the model in the unstable domains with the parameters of figure 2.1 and (i): $E_0 = 0.6$; (ii) $E_0 = 1.0$; (iii) $E_0 = 1.4$ (iV) $E_0 = 1.9$.*

$$
\begin{aligned}
&-(\delta_{22} + (\epsilon_b + 2i)^2)(\delta_{11} + (\epsilon_a + 2i)^2) \\
&(\delta_{12} + c_1(\epsilon_b - 2i))(\delta_{21} + c_2(\epsilon_a + 2i)) + \\
&(\delta_{22} + (\epsilon_b - 2i)^2)(\delta_{22} + (\epsilon_b + 2i)^2) \\
&\Big\{(\delta_{11} + (\epsilon_a - 2i)^2)(\delta_{11} + (\epsilon_a + 2i)^2) - \epsilon_{11}^2\Big\}\Big\} = 0. \qquad (2.11)
\end{aligned}
$$

From this equation, A^2 can be extracted and then substituted in the equation satisfied by A from the harmonic balance method (see equations (2.3)). This gives the stability boundary as a function of the parameters of the electromechanical system. In Figure 2.5, we show a stability boundary in the (w, E_0) plane both from the analytical treatment (equation (2.11)) and for the direct numerical checking of the stability boundary from the differential equations. Good agreement is obtained between the analytical and the numerical results. We note that the domain of stable harmonic oscillations is the region below the curves. To look for what really appears to the instability domains, we have drawn bifurcation diagrams and the variation of the corresponding **Lyapunov** exponent as E_0 varies for $w = 1.5$ and $w = 1.6$. Our results are reported in Figures 2.6 and 2.7 and the following results are observed. As the amplitude E_0 increases, a period-1 orbit exist until $E_0 = 0.55$ and 0.78 respectively (critical value corresponding to the limit values of E_0 for the stability of the harmonic oscillations) where a transition from a period-1 orbit to a quasiperiodic behavior appears. Figure 2.8 presents in the $(x, \dot{x})$ plane the types of behavior the electromechanical model exhibits in the unstable domains, for $E_0 = 0.6; E_0 = 1.0; E_0 = 1.4; E_0 = 1.5$ with parameters of Figure 2.2 and $w = 1.5$.

2.2.3 Stability chart

In this subsection, we aim to derive the stability chart using the numerical simulations of the equations of motion (1.6). For identifying different steady states, the dynamical transitions are derived using the bifurcation diagram when the amplitude E_0 varies for a fixed frequency w. The resulting phase diagram in the E_0-w plane is shown in Figure 2.9 with the set of parameters defined in Figure 2.2. The diagram covers the transition threshold in the

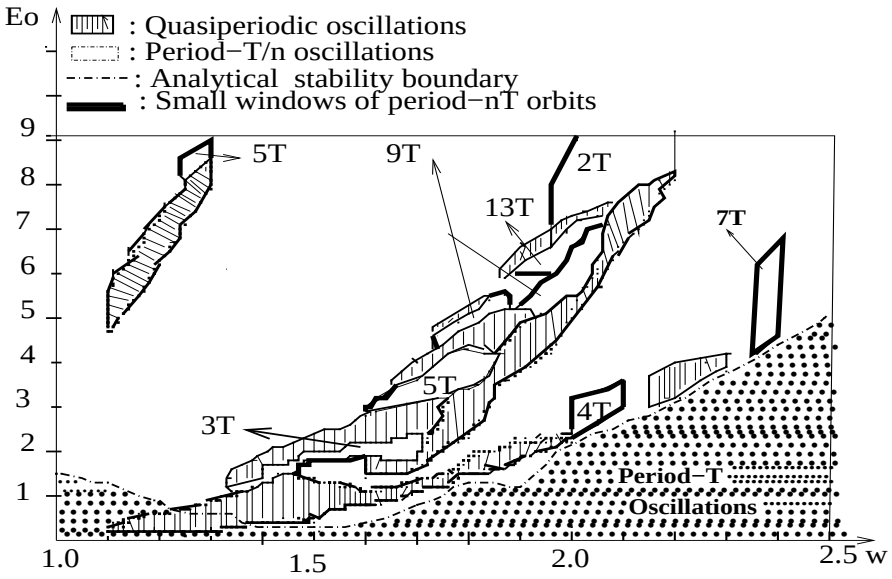

Figure 2.9: *Stability chart with the parameter of Figure 2.2.*

region of undesired solution $1 < w < 2.5$ and the amplitude lying in the region $0.0 < E_0 < 9$. The following results are observed. One observes that our electromechanical model exhibits periodic oscillations when the external excitation enters in resonance with the two oscillators ($w_2 = w = 1$). Consequently, the model could not exhibits undesired behavior in the region $w < 1$ (see the frequency-response curves of Figure 2.2). On increasing the frequency w further $w > 1$, the system exhibits quasiperiodic and multiperiodic oscillations between two regular motions, within a range of the frequency w. For example, at $w = 1.4$, quasiperiodic oscillations occur in the region $E_0 \in [0.36; 1.27]U[1.32; 1.44]$ while period-3T oscillations appear for $E_0 \in]1.27; 1.32[$. The other scenario is observed for another fixed values of w. We note that another types of period-nT oscillations appears in Figure 2.9 with $n \neq 3$. This types of behavior are predicted analytically in reference [II4] by **Hayashi** for electrical circuits described by cubic non-linear equation. Examples of period-nT oscillations of 3T and 5T oders are shown respectively in Figures 2.10 and 2.11. The regions of period-T/n are also presented in the stability chart.

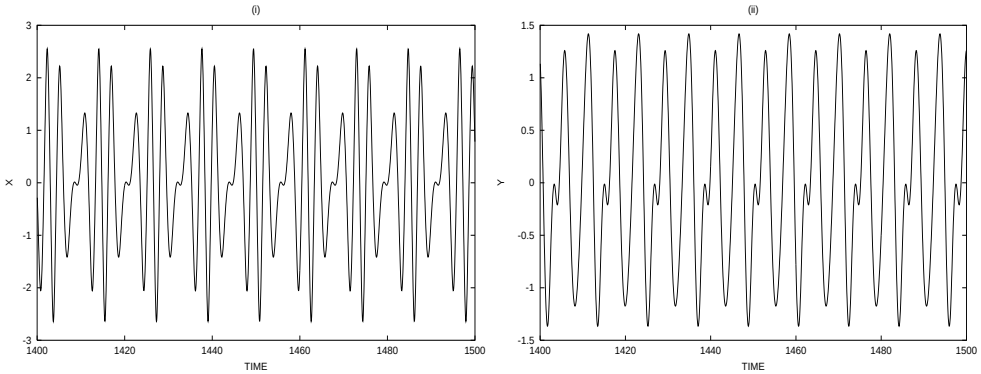

Figure 2.10: *Period-3T oscillations with the parameters of Figure 2.2 and* $w = 1.6; E = 2.0$.

2.2.4 Sub- and superharmonic oscillatory states

Technological exploitation of sub- and superharmonic oscillatory states are important in

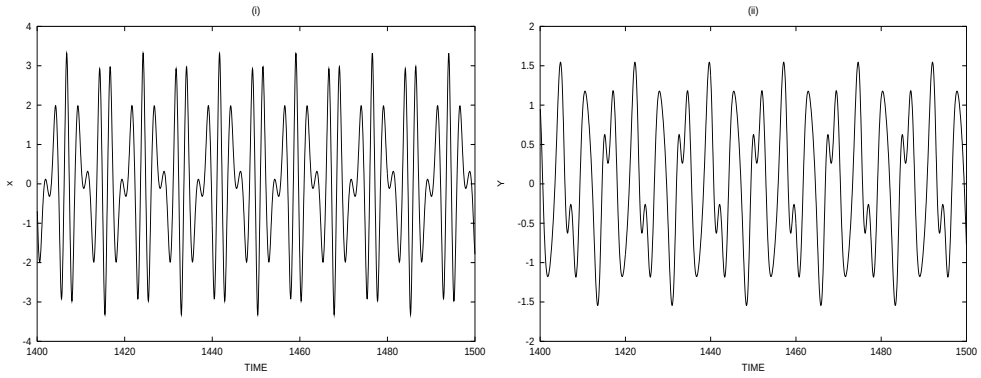

Figure 2.11: *Period-5T oscillations with the parameters of figure 2.2 and* $w = 1.8; E = 4.0$.

the field of nonlinear oscillations, and they frequently occur in various branches of electromechanical engineering and physical sciences [II5, II6]. As it appears in the frequency response curves, when the frequency of the voltage source is very large or very small as compare to the values of the natural frequencies of the oscillators, the effects of the excitation will be small unless the amplitude E_o is hard. This can be well established using the multiple time scales method (see ref.[II1]). When E_o is large, higher or superharmonic and subharmonic oscillations can be generated. To deal with such oscillations in our model, one can also use the harmonic balance method. But the calculations will be more difficult to handle. We prefer the multiple time scales method which is more indicated to find and establish the amplitudes of various orders of resonant states [II1]. For this method, we seek an asymptotic expansion of equations (1.6) in the form:

$$\begin{aligned} x &= \epsilon x_1(T_o, T_2) + \epsilon^3 x_3(T_o, T_2) + ... \\ y &= \epsilon y_1(T_o, T_2) + \epsilon^3 y_3(T_o, T_2) + ... \end{aligned} \tag{2.12}$$

where the independent variables or time scales T_o and T_2 are respectively the fast scale and the slow scale. ϵ is a small dimensioness parameter. We assumed that $\gamma_i = \epsilon^2 \gamma_{oi}$ and $\lambda_i = \epsilon^2 \lambda_{oi}$ (with i=1,2). The amplitude E_o is taken at the order $E_0 = \epsilon E$ to indicate that E_o is hard. Inserting these expansions in equations (1.6) and equating coefficients of like powers of ϵ, we obtain

Order ϵ,

$$\begin{aligned} D_o^2 x_1 + x_1 &= E \cos w T_o, \\ D_o^2 y_1 + w_2^2 y_1 &= 0, \end{aligned} \tag{2.13}$$

Order ϵ^3,

$$\begin{aligned} D_o^2 x_3 + x_3 &= -2 D_o D_2 x_1 - \gamma_{o1} D_o x_1 - \beta x_1^3 - \lambda_{o1} D_o y_1, \\ D_o^2 y_3 + w_2^2 y_3 &= -2 D_o D_2 y_1 - \gamma_{o2} D_o y_1 + \lambda_{o2} D_o x_1, \end{aligned} \tag{2.14}$$

where $D_o = \frac{\partial}{\partial T_o}$, $D_2 = \frac{\partial}{\partial T_2}$ and $T_n = \epsilon^n t, n = 0, 1, 2....$ The solutions of equations (2.13) can be expressed as:

$$\begin{aligned} x_1 &= A_1(T_2) \exp(jT_o) + \Lambda \exp(jwT_o) + \bar{A}_1(T_2) \exp(-jT_o) + \Lambda \exp(-jwT_o), \\ y_1 &= A_2(T_2) \exp(jw_2 T_o) + \bar{A}_2(T_2) \exp(-jw_2 T_o), \end{aligned} \tag{2.15}$$

where the over-bar represents the complex conjugate, $j^2 = -1$ and

$$\Lambda = \frac{1}{2} \frac{E}{1 - w^2}.$$

Substituting x_1 and y_1 into equations (2.14), we obtain

$$\begin{aligned}
D_o^2 x_3 + x_3 &= -(2jA_1' + j\gamma_{o1}A_1 + 3\beta A_1^2\bar{A}_1 + 6\Lambda^2 A_1)\exp(jT_o) \\
&\quad +(j\gamma_{o1}w\Lambda + 4\beta\Lambda A_1\bar{A}_1 + 3\Lambda^3\beta)\exp(jwT_o) \\
&\quad -\beta A_1^3\exp(3jT_o) - 3\beta A_1^2\Lambda\exp(j(2+w)T_o) \\
&\quad -3\beta A_1\Lambda^2\exp(j(2w+1)T_o) - 3\beta\Lambda^2 A_1\exp(j(1-2w)T_o) \\
&\quad -3\beta\Lambda A_1^2\exp(j(2-w)T_o) - \Lambda^3\beta\exp(3jwT_o) \\
&\quad -jw_2\lambda_{o1}A_2\exp(jw_2T_o) + C.C, \\
D_o^2 y_3 + w_2^2 y_3 &= -jw_2(2A_2' + \gamma_{o2}A_2)\exp(jw_2T_o) + j\lambda_{o2}A_1\exp(jT_o) \\
&\quad +jw\lambda_{o2}\Lambda\exp(jwT_o) + C.C,
\end{aligned} \tag{2.16}$$

where the prime (on A_i, i=1,2) denotes the differentiation with respect to T_2 and C.C stands for the complex conjugate of the previous terms. From equations (2.16), it comes two interesting resonant structures: the first one is the superharmonic state $w_2 = 1$ and $3w = 1$, and the second one corresponds to the subharmonic state $w = 3$ with $w_2 = 1$. Therefore, we restrict our attention in this section to the case of sub- and superharmonic resonances.

- **Superharmonic resonances**
  We consider the case where the nonlinear oscillator enters in superharmonic resonance with the external excitation, that is $3w = 1 + \epsilon^2\sigma_1$. We also assume that:

$$w_2 = 1 + \epsilon^2\sigma_2, \tag{2.17}$$

  where σ_1 and σ_2 are the detuning parameters indicating the accuracy of the resonances. The secular producing terms in equations (2.16) must be eliminated. Hence, the solvability conditions are defined as

$$\begin{aligned}
2jA_1' + j\gamma_{o1}A_1 + 6\Lambda^2 A_1 + 3\beta A_1^2\bar{A}_1 \\
+jw_2\lambda_{o1}A_2\exp(j\sigma_2T_2) + \Lambda^3\beta\exp(j\sigma_1T_2) = 0, \\
-w_2(2A_2' + \gamma_{o2}A_2)\exp(j\sigma_2T_2) + \lambda_{o2}A_1 = 0.
\end{aligned} \tag{2.18}$$

  We express $A_i(T_2)$, (i=1,2) in the polar form:

$$A_i(T_2) = \frac{1}{2}a_i(T_2)\exp(jb_i(T_2)), \tag{2.19}$$

  where a_i and b_i are respectively the amplitudes and the phases of the oscillators. Substituting equation (2.19) into equations (2.18), we obtain after separating real and imaginary parts the following set of first order differential equations

$$\begin{aligned}
\frac{3}{8}\beta a_1^3 - a_1b_1' + 3\Lambda^2 a_1 + \beta\Lambda^3\cos\delta_1 - \frac{1}{2}w_2\lambda_{o1}a_2\sin\delta_2 &= 0, \\
\frac{1}{2}\gamma_{o1}a_1 + a_1' + \beta\Lambda^3\sin\delta_1 + \frac{1}{2}w_2\lambda_{o1}a_2\cos\delta_2 &= 0, \\
w_2a_2b_2'\cos\delta_2 + w_2(a_2' + \frac{1}{2}\gamma_{o2}a_2)\sin\delta_2 &= 0, \\
-w_2(a_2' + \frac{1}{2}\gamma_{o2}a_2)\cos\delta_2 + w_2b_2'a_2\sin\delta_2 - \frac{1}{2}\lambda_{o2}a_1 &= 0,
\end{aligned} \tag{2.20}$$

  where $\delta_1 = \sigma_1T_2 - b_1$ and $\delta_2 = \sigma_2T_2 + b_2 - b_1$. For the steady-state responses, we must have $a_i' = 0$ and $\delta_i' = 0$. Thus $b_1' = \sigma_1$ and $b_2' = \sigma_1 - \sigma_2$. Eliminating δ_i from equations

(2.20), we obtain the following set of nonlinear equations:

$$\frac{9}{64}\beta^2 a_1^6 + \frac{3}{2}\beta M_1 a_1^4 + N_1 a_1^2 - \beta^2 \Lambda^6 = 0,$$
$$a_2 = \frac{\lambda_2 a_1}{w_2\sqrt{Z}}, \tag{2.21}$$

where

$$\begin{aligned} Z &= 4(\sigma_1 - \sigma_2)^2 + \gamma_{o2}^2, \\ M_1 &= 3\Lambda^2 - \sigma_1 + \frac{\lambda_{o1}\lambda_{o2}(\sigma_1 - \sigma_2)}{4(\sigma_1 - \sigma_2)^2 + \gamma_{o2}^2}, \\ N_1 &= \frac{1}{4}\left\{\gamma_{o1} + \frac{\lambda_{o1}\lambda_{o2}\gamma_{o2}}{4(\sigma_1 - \sigma_2)^2 + \gamma_{o2}^2}\right\}^2 + M_1^2. \end{aligned}$$

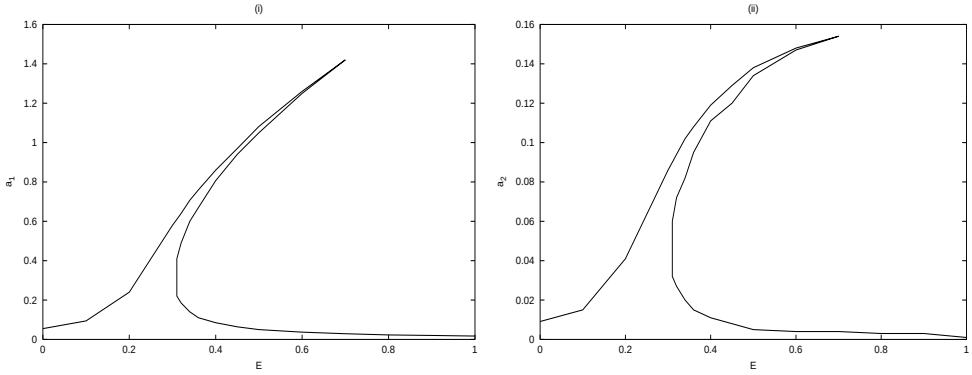

Figure 2.12: *Superharmonic frequency-response curves. (i) corresponding for $a_1(\sigma_1)$ and (ii) for $a_2(\sigma_1)$ with the parameters $E = 0.5, \gamma_{o1} = 0.01, \gamma_{o2} = 1.2, \lambda_{o1} = 0.12, \lambda_{o2} = 0.2$, $\beta = 0.6, \sigma_2 = 0$.*

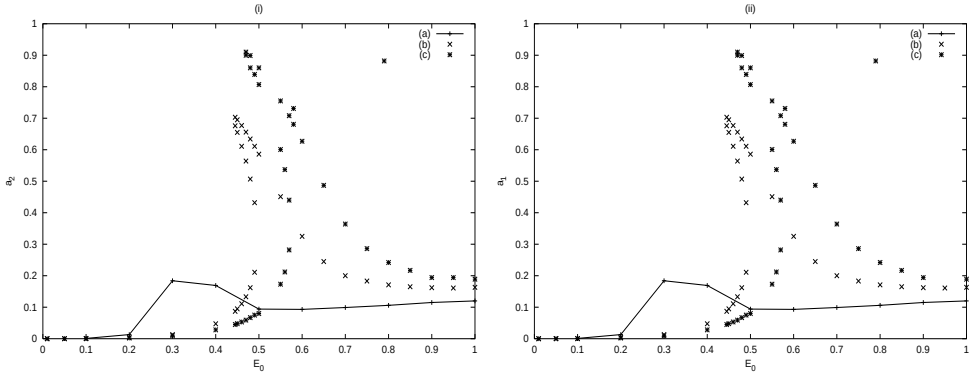

Figure 2.13: *Superharmonic amplitude-response curves . (i) corresponding for $a_1(E_0)$ and (ii) for $a_2(E_0)$ with the parameters of Figure 2.6 and (a): $\sigma_1 = 0.1, (b) : \sigma_1 = 0.3; (c) : \sigma_1 = 0.4$.*

Thus, in the case of superharmonic resonances, the motion of the two oscillators are coupled and described by:

$$\begin{aligned} x(t) &= \epsilon a_1 \cos(3wt + \delta_1) + \epsilon\Lambda \cos wt + 0(\epsilon^3), \\ y(t) &= \epsilon a_2 \cos(3wt + \delta_2 - \delta_1) + 0(\epsilon^3). \end{aligned} \tag{2.22}$$

Using the **Newton-Raphson** algorithm, we find the amplitudes a_1 and a_2 when the detuning parameter σ_1 is varied. In the exact internal resonance ($\sigma_2 = 0$), the superharmonic frequency-response curves obtained for a given set of parameters are provided in Figure 2.12(i) for $a_1(\sigma_1)$ and in Figure 2.12(ii) for $a_2(\sigma_1)$. The behavior of the frequency-response curves in the superharmonic resonances show the well-known hysteresis phenomena. In Figure 2.13, we provide the superharmonic amplitude-response curves $a_i(E_0)$ (i=1,2) obtained for three fixed values of the detuning parameter σ_1. The curves of figure 2.13 show the jump phenomena for $\sigma_1 = 0.4$ and $\sigma_1 = 0.3$. It appears that for $\sigma_1 = 0.2$, the hysteresis domain disappears. Our investigations show that, when $\sigma_1 > 0.3$, the curves show the hysteresis phenomena.

- **Subharmonic resonances**

To analyze these subharmonic resonances, we set $w = 3 + \epsilon^2\sigma_o$. σ_o is another detuning parameter indicating the accuracy of the subharmonic resonances. Eliminating the terms in equations (2.23) that produce secular terms in x_3, y_3 and considering the expressions given by equations (2.17), we have:

$$\begin{aligned} 2jA_1' + (j\gamma_{o1} + 6\Lambda^2)A_1 + 3\beta A_1^2\bar{A}_1 + \\ jw_2\lambda_{o1}A_2\exp(j\sigma_2 T_2) + 3\Lambda\beta\bar{A}_1^2\exp(j\sigma_4 T_2) = 0, \\ -w_2(2A_2' + \gamma_{o2}A_2)\exp(j\sigma_2 T_2) + \lambda_{o2}A_1 = 0. \end{aligned} \tag{2.23}$$

Again, introducing the polar notations (2.19) for $A_i (i = 1, 2)$ and separating real and imaginary parts yields after some algebraic manipulations

$$\begin{aligned} \frac{3}{8}\beta a_1^3 - a_1 b_1' + 3\Lambda^2 a_1 + \frac{3}{4}\beta\Lambda a_1^2\cos\delta_4 - \frac{1}{2}w_2\lambda_{o1}a_2\sin\delta_2 &= 0, \\ \frac{1}{2}\gamma_{o1}a_1 + a_1' + \frac{3}{4}\beta\Lambda a_1^2\sin\delta_4 + \frac{1}{2}w_2\lambda_{o1}a_2\cos\delta_2 &= 0, \\ a_2 b_2'\cos\delta_2 + w_2(a_2' + \frac{1}{2}\gamma_{o2}a_2)\sin\delta_2 &= 0, \\ w_2(a_2' + \frac{1}{2}\gamma_{o2}a_2)\cos\delta_2 - w_2 b_2' a_2\sin\delta_2 - \frac{1}{2}\lambda_{o2}a_1 &= 0, \end{aligned} \tag{2.24}$$

where $\delta_4 = \sigma_o - 3b_1$, and $\delta_2 = \sigma_2 T_2 + b_2 - b_1$. For the steady-state responses, we must have $a_i' = 0$ and $\delta_i' = 0$. Thus $b_1' = \frac{\sigma_o}{3}$ and $b_2' = \frac{\sigma_o}{3} - \sigma_2$. Eliminating δ_i from equations (2.24), we obtain the following set of nonlinear equations:

$$\begin{aligned} \frac{9}{64}\beta^2 a_1^6 + \frac{3}{4}P_1 a_1^4 + Q_1 a_1^2 = 0, \\ a_2 = \frac{\lambda_2 a_1}{w_2\sqrt{M}}, \end{aligned} \tag{2.25}$$

where

$$\begin{aligned} M &= \gamma_{o2}^2 + 4(\frac{\sigma_o}{3} - \sigma_2)^2, \\ P_1 &= 3\Lambda^2 - \frac{\sigma_o}{3} - \frac{3}{2}\beta\Lambda^2 + \frac{\lambda_{o1}\lambda_{o2}(\frac{\sigma_o}{3} - \sigma_2)}{\gamma_{o2}^2 + 4(\frac{\sigma_o}{3} - \sigma_2)^2}, \\ Q_1 &= \frac{1}{4}\left\{\gamma_{o1} + \frac{\lambda_{o1}\lambda_{o2}\gamma_{o2}}{\gamma_{o2}^2 + 4(\frac{\sigma_o}{3} - \sigma_2)^2}\right\}^2 + P_1^2. \end{aligned}$$

Equations (2.25) show that either $a_1 = 0$ or

$$\frac{9}{64}\beta^2 a_1^4 + P_1 a_1^2 + Q_1 = 0, \tag{2.26}$$

which is quadratic in a_1^2. Its solutions are

$$a_1^2 = p \pm \sqrt{p^2 - q}, \tag{2.27}$$

where

$$p = \frac{-8P_1}{3\beta^2}, \qquad\qquad q = \frac{64Q_1}{9\beta^2}.$$

We note that q is always positive, and thus nontrivial oscillation amplitudes occur only when $p^2 \geq q$. These conditions demand that:

$$[(3 - \frac{3}{4}\beta)^2 - 9]\Lambda^4 - \frac{3}{2}\beta(U_1 - \frac{\sigma_o}{3})\Lambda^2 + \frac{1}{4}(\gamma_1 + V_1)^2 \geq 0, \tag{2.28}$$

where

$$U_1 = \frac{\lambda_{o1}\lambda_{o2}(\frac{\sigma_o}{3} - \sigma_2)}{4(\frac{\sigma_o}{3} - \sigma_2)^2 + \gamma_{o2}^2}, \qquad V_1 = \frac{\lambda_{o1}\lambda_{o2}\gamma_{o2}}{4(\frac{\sigma_o}{3} - \sigma_2)^2 + \gamma_{o2}^2}.$$

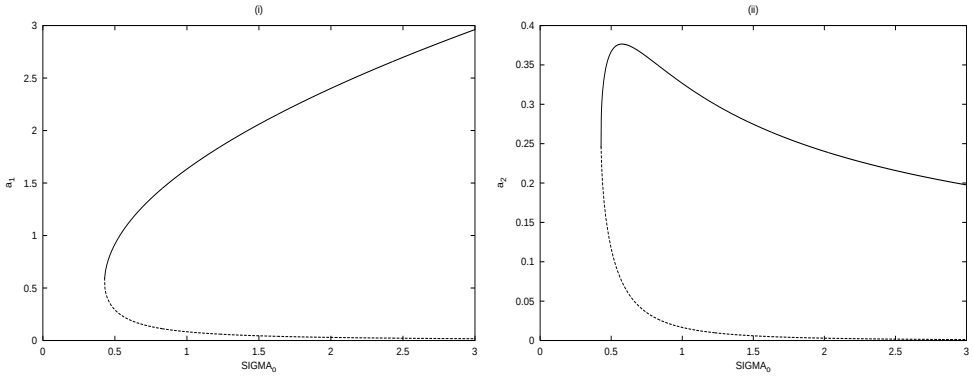

Figure 2.14: *Subharmonic frequency-response curves. (i) corresponding for* $a_1(\sigma_4)$ *and (ii) for* $a_2(\sigma_4)$ *with the parameters* $\gamma_{o1} = 0.01; \lambda_{o1} = 0.2; \lambda_{o2} = 0.4; \beta = 0.6; \sigma_2 = 2.0$ *and (a):* $E = 0.5, (b) : E = 1.0$.

It follows from equations (2.28) that, for a given σ_o, nontrivial solutions can exist only if

$$p_1 - \sqrt{p_1^2 + q_1} \leq \Lambda^2 \leq p_1 + \sqrt{p_1^2 + q_1},$$

where

$$p_1 = \frac{3\beta(U_1 - \frac{\sigma_o}{3})}{4(\frac{\sigma_o}{3} - \sigma_2)^2 + \gamma_{o2}^2}, \qquad q_1 = \frac{(\gamma_{o1} + V_1)^2}{4(\frac{\sigma_o}{3} - \sigma_2)^2 + \gamma_{o2}^2}.$$

In the $\Lambda\sigma_4$-plane, the boundary of the region where nontrivial solutions can exist is given by:

$$\Lambda^2 = p_1 \pm \sqrt{p_1^2 + q_1}. \tag{2.29}$$

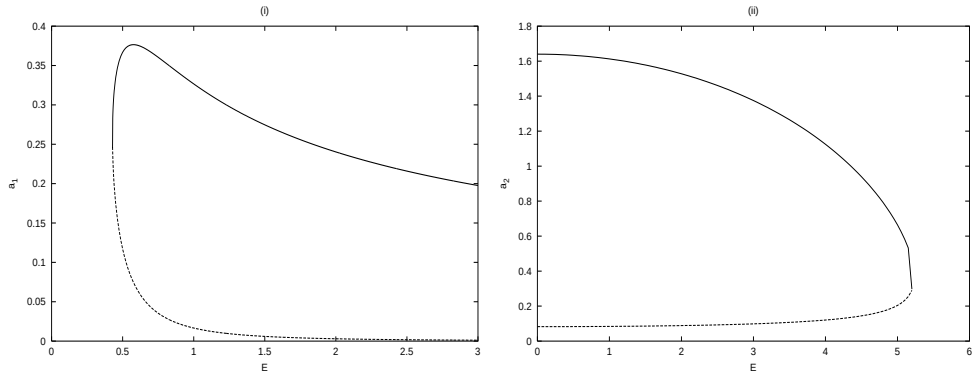

Figure 2.15: *Subharmonic amplitude-response curves. (i) corresponding for* $a_1(\sigma_4)$ *and (ii) for* $a_2(\sigma_4)$ *with the parameters of Fig.2.8 and (a):* $\sigma_1 = 2.0, (b) : \sigma_1 = 4.0$;

In the subharmonic resonance, the motion of the two oscillators are described by:

$$\begin{aligned} x(t) &= \epsilon a_1 \cos(\frac{1}{3}wt + \delta_o) + \epsilon\Lambda \cos wt + 0(\epsilon^3), \\ y(t) &= \epsilon a_2 \cos(\frac{1}{3}wt + \delta_2 - \delta_o) + 0(\epsilon^3), \end{aligned}$$

We find the amplitudes a_1 and a_2 when the detuning parameter σ_o is varied. The subharmonic frequency-response curves obtained for a given set of parameters are provided in Figure 2.14(i) for $a_1(\sigma_o)$ and in Figure 2.14(ii) for $a_2(\sigma_o)$. The amplitude-response curves are reported in Figure 2.15.

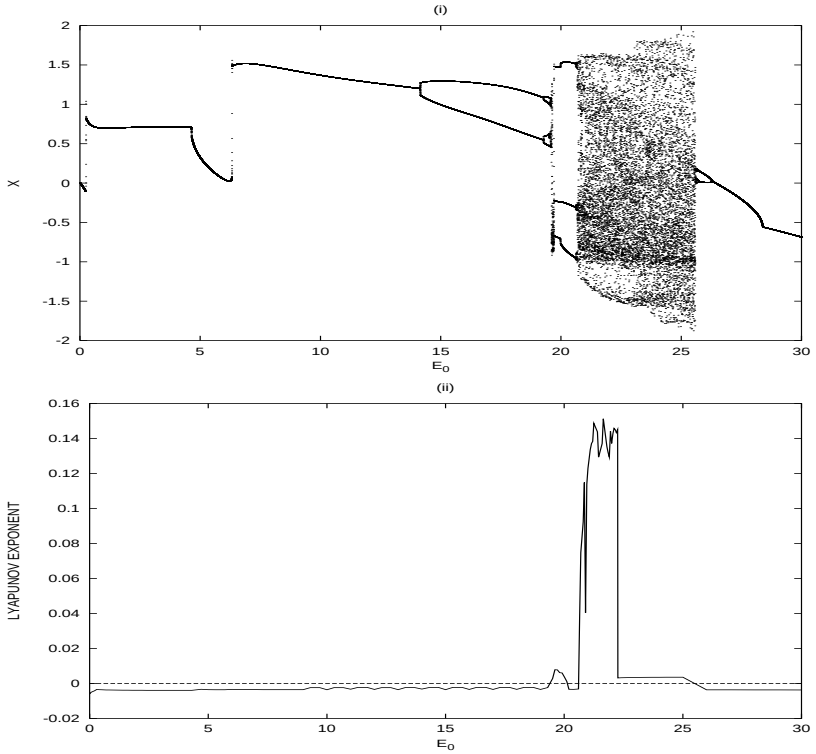

Figure 2.16: *Bifurcation diagram (i) and variation of Lyapunov exponent (ii) when* E_o *vary with the parameters* $\gamma_1 = 0.1; \gamma_2 = 0.3; \lambda_1 = 0.01; \lambda_2 = 0.06; w_2 = 1.2; w = 1.3; \beta = 1.32$.

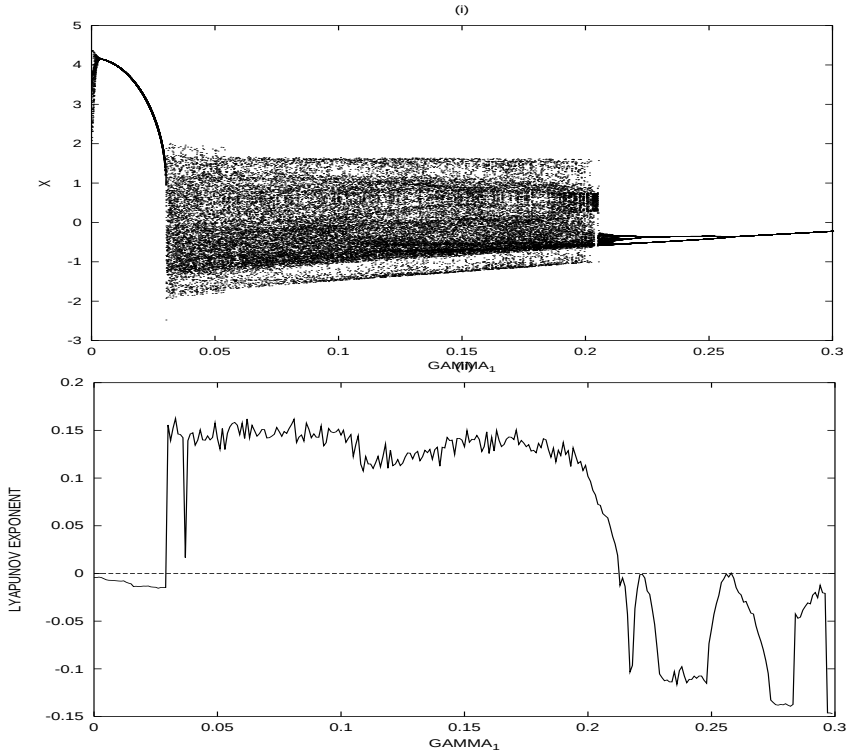

Figure 2.17: *Bifurcation diagram (i) and Lyapunov exponent (ii) when γ_1 vary with the parameters of Figure 2.16 and $E_0 = 22.0$.*

2.2.5 Bifurcations and transitions to chaos

We first consider the behavior of the model as the amplitude E_0 of the external excitation $e(t)$ varies. As in the case of the hard **Duffing** equation [II7], we have found that chaos appears in the model only for large value of E_0. Figure 2.16 shows a representive bifurcation diagram and the variation of the corresponding **Lyapunov** exponent. Both curves are obtained by solving numerically, using the four-order formulas of the **Runge-Kutta** algorithm with the PASCAL code, equations (1.6) and the corresponding variational equations, the **Lyapunov** exponent being defined by:

$$\mathbf{Lya} = \lim_{t\to\infty} \frac{\mathbf{ln}(d(t))}{t}, \tag{2.30}$$

with

$$d(t) = \sqrt{dx^2 + dv_x^2 + dy^2 + dv_y^2},$$

where dx, dv_x, dy and dv_y are the variations of $x, \dot{x}, y$ and $\dot{y}$ respectively. That is a measure of the rate of divergence between initially closed trajectories in the four dimensional phase space $(x, dx/dt, y, dy/dt)$. As it appears, different types of bifurcations take place before the onset of chaos. As E_0 increases from zero, the amplitude of the symmetrical periodic oscillations increases until $E_0 = 4.67$ where the symmetrical behavior bifurcates into an asymmetrical oscillatory states. Then at $E_0 = 6.15$, a tiny multiperiodic transition appears and the system passes into another periodic state. As E_0 increases further, a period doubling transition takes place at $E_0 = 13.76$. At $E_0 = 19.17$, the period-2 orbit bifurcates to a period-4 orbit and the period doubling cascade continues leading to a small chaotic window. This window suddenly bifurcates into a period-3 orbit. Another set of period doubling sequences leads to a more larger chaotic domain for $E_0 = 20.65$ to $E_0 = 25$. But let us note that for $E_0 = 22.6$ to $E_0 = 25$, the system shows a weak or transient chaos characterized by a sort of fractal nature

of the basin of attraction. In fact, in this domain, it is found that chaos appears only for some initial conditions. This behavior manifests itself in Figure 2.16(ii) by small values of the **Lyapunov** exponent and in Figure 2.16(i) by a sudden expansion of the bifurcation diagram. This type of behavior is characteristic of the hard **Duffing** equation as reported by **Pezeshki** and **Dowell** in ref.[II6]. At the other side of the chaotic domain, a reverse period doubling sequence takes place leading to a period-1 orbit (harmonic oscillations).

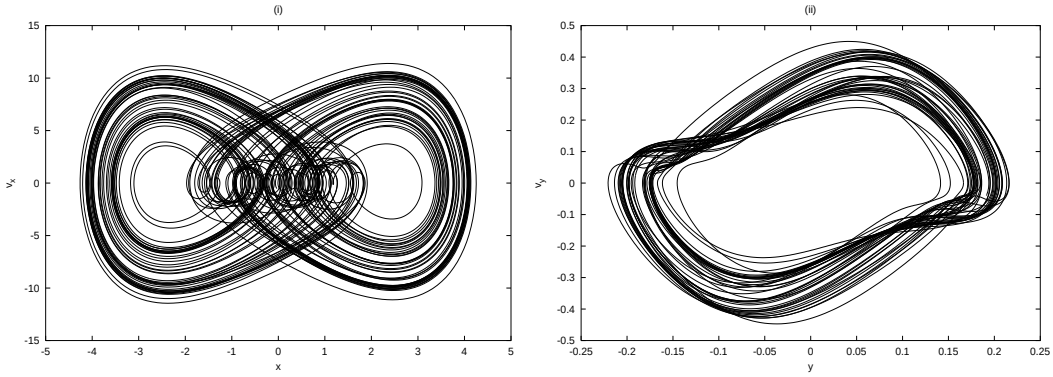

Figure 2.18: *Phase portrait of the chaotic electromechanical model with the parameters of Figure 2.16 and* $E_0 = 22$.

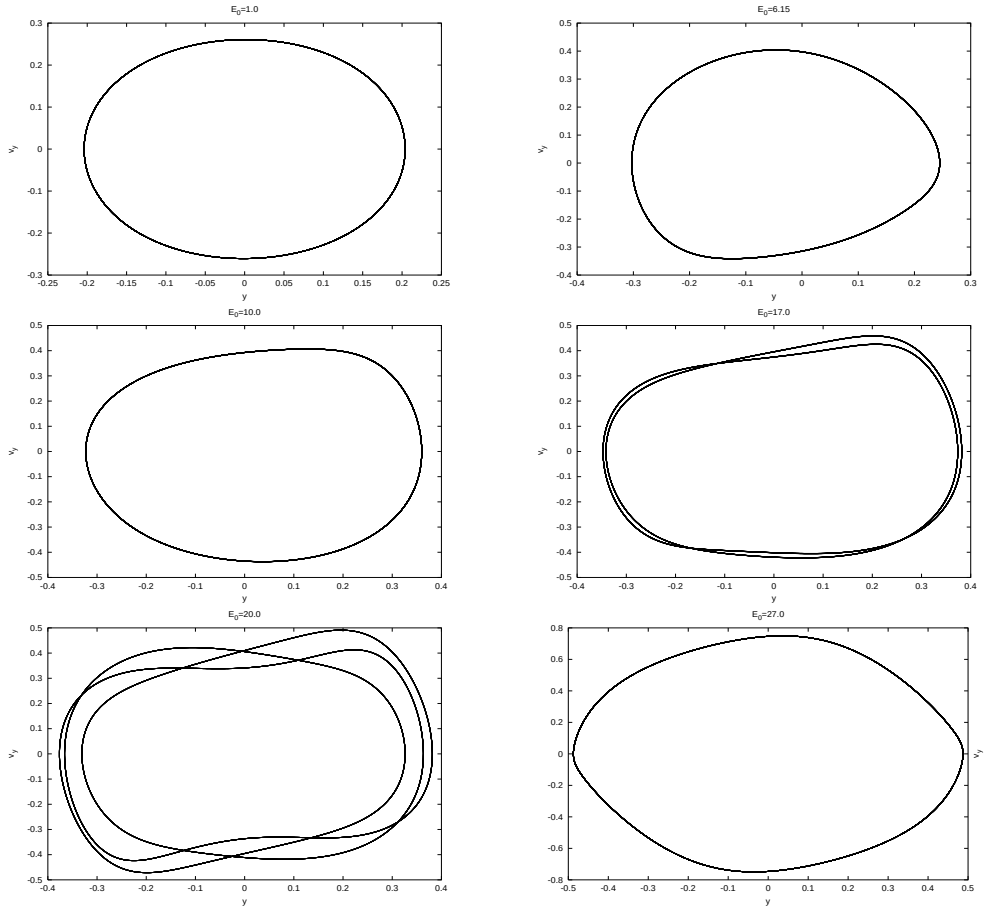

Figure 2.19: *Phase portrait of the linear mechanical oscillator in the regular motion with the parameters of Figure 2.16 for several values of* E_0.

In Figure 2.17, the control parameter is the damping coefficient γ_1. As γ_1 increases from zero, we have the periodic oscillations until $\gamma_1 = 0.025$ where the chaotic motions take place. At the otherside of the chaotic domain, a reverse period doubling sequence takes place at

$\gamma_1 = 0.2625$ leading to a period-1 orbit. We present in Figure 2.18 the phase portrait of the electromechanical device in the chaotic states while in Figure 2.19, the behavior of the mechanical oscillator is presented in the regular regime with several values of the control parameter E_0 and the set of parameters defined in Figure 2.16.

From the above results, we can resort the following comments. Firstly, the presence of chaos in our model can be considered as a positive or negative issue. In fact, in many situations, chaos is undesirable since it leads to irregular performance and possible catastrophic failures. In this case, it should be suppressed or controlled. But in some other cases, chaos appears to be a beneficial feature such as in mechanical heat and transport phenomena [II9]. Serious progress in the way of using chaos to secure communication [II10] has also been made recently. Moreover, intensive research is carried out to discuss the wide variety of applications of chaos in various fields ranging from natural, physical, engineering and social sciences. For example, in engineering, chaos has been used in the building of better digital filters, and to model the structural dynamics in such structures as buckling columns. It is in this spirit that we expect that the presence of chaos in an electromechanical transducer can be useful both in its irregular structure or in a regular structure obtained after the control. Let us note that chaos is considered here on our electromechanical device as a positive issue when the device is used for sifter or sieve device. Secondly, from the nature of the regular behavior of the mechanical oscillator, particulary for $E_0 = 17.0$ and $E_0 = 20$, we have respectively the period-2 and period-3 oscillations. In this case, the mechanical oscillator vibrates respectively with two and three modes of mechanical vibrations.

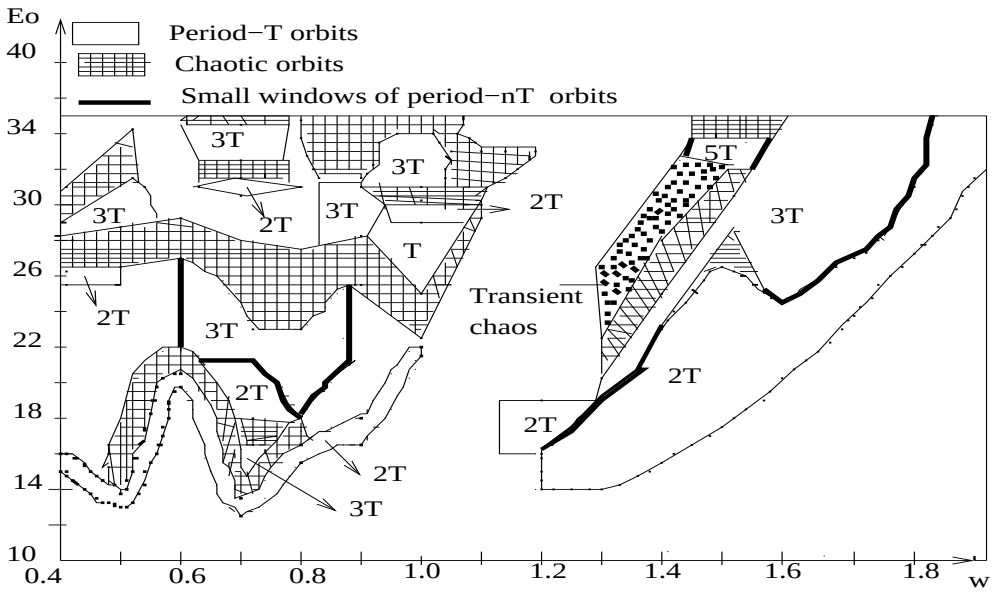

Figure 2.20: *Stability chart with the parameters of figure 2.13*

To identify different steady-states, we use the procedure presented before to derive the stability chart with the set of parameters of Figure 2.16. The resulting phase diagram in the $E_0 - w$ plane is shown in Figure 2.20. The diagram covers the transition threshold in the region of undesired solution $0.4 \leq w \leq 1.9$ and the amplitude lying in the region $10 \leq E_0 \leq 35$. The following results are observed. On increasing the frequency w further $w > 0.4$ and amplitude of the external excitation, the electromechanical transducer exhibits various multiperiodic, chaotic and transient chaotic orbit which depend on the values of E_0 and w.

2.2.6 Chaos control

Due to the presence of chaos in our electromechanical system, one would like to suppress it or take avantage of the flexibility and the various infinite number of different unstable orbits embedded in the chaotic attractor to tune the system to a desired target regular orbit. This subsection is devoted to this task. We follow the procedure of **Chen** and **Dong** [II2]. This has also been used recently in ref.[II8] for chaos control in electrostatic transducers. Let us introduce the new variables $x_1 = x, x_2 = \dot{x}, x_3 = y, x_4 = \dot{y}$, equations (1.6) can then be rewritten as

$$\dot{x}_i = g_i(t, x_1, x_2, x_3, x_4). \tag{2.31}$$

We let $(\bar{x}_1, \bar{x}_2, \bar{x}_3, \bar{x}_4)$ be the periodic orbit that we are targetting, in the sense that for any given $\epsilon > 0$, there exists a time $T_\epsilon > 0$ such that $|x_i(t) - \bar{x}_i(t)| \leq \epsilon$ for all $t \geq T_\epsilon$.

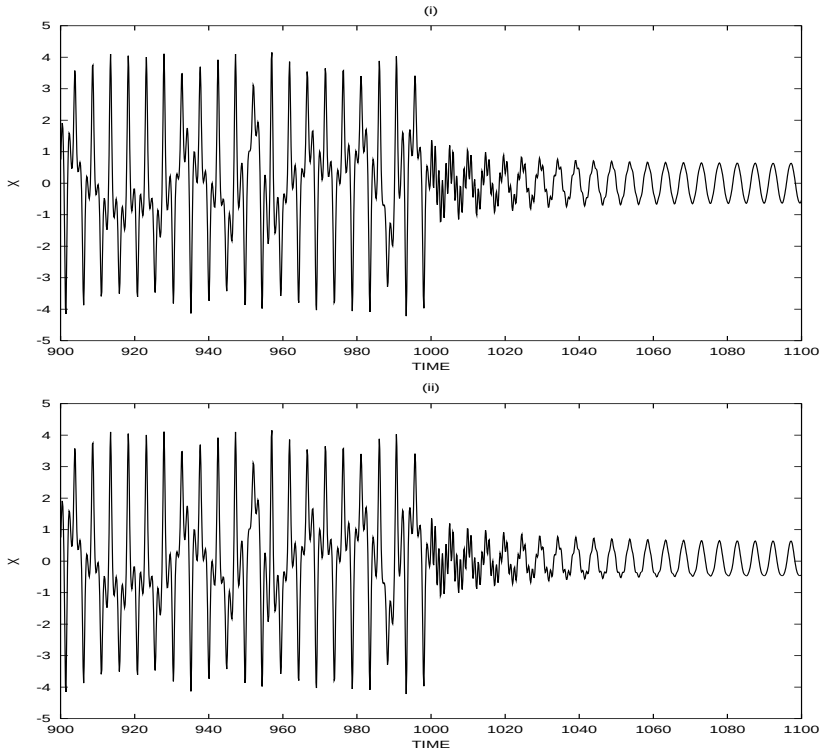

Figure 2.21: *Control to a period-T orbit (i) and to period-T/2 orbit (ii) with the parameters of Figure 2.16*

For this purpose, we use the conventional feedback controllers method to convert the system into:

$$\dot{x}_i = g_i(t, x_1, x_2, x_3, x_4) - \sum_{j=1}^{4} K_{ij}(x_j - \bar{x}_j), \tag{2.32}$$

where the K_{ij} are the feedback gain matrix elements. We restrict ourselves to the case where all $K_{ij} = 0$ except, K_{21} and K_{43} which are assumed to be strictly positive. Then equation (2.32) becomes:

$$\begin{aligned}
\dot{x}_1 &= x_2, \\
\dot{x}_2 &= -\gamma_1 x_2 - x_1 - \beta x_1^3 - \lambda_1 x_4 - K_{21}(x_1 - \bar{x}_1) + E_o \cos wt, \\
\dot{x}_3 &= x_4, \\
\dot{x}_4 &= -\gamma_2 x_4 - w_2^2 x_3 + \lambda_2 x_2 - K_{43}(x_3 - \bar{x}_3).
\end{aligned} \tag{2.33}$$

The control should not introduce additional instability in the system. It is therefore required that all the roots of the characteristic equation derived from the Jacobian of equations (2.33) have their real part less than zero. Using the **Routh-Hurwitz** criterium, it comes the following condition:

$$w_2^2 K_{21} + K_{21}K_{43} + w_2^2(1 + 3\beta\bar{x}_{max}^2) + K_{43}(1 + 3\beta\bar{x}_{max}^2) > 0, \tag{2.34}$$

where $\bar{x}_{max}$ is the amplitude of the targetting orbit of the first oscillator.

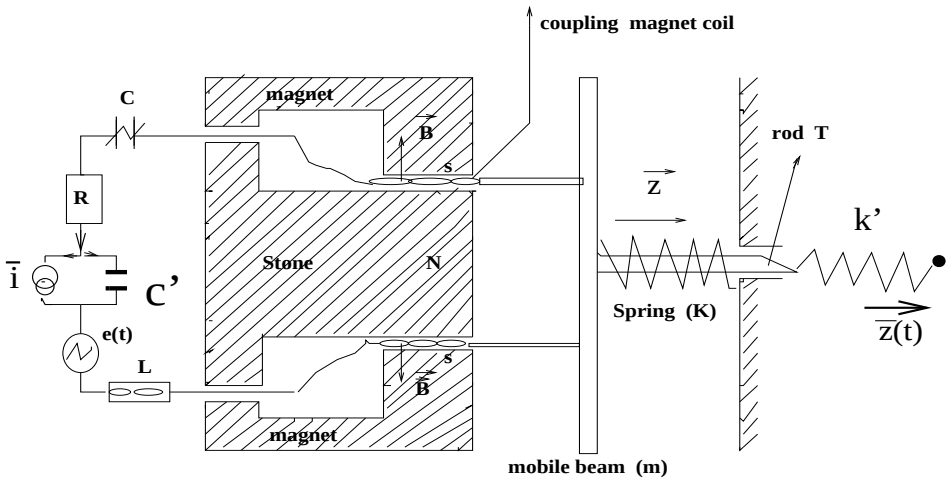

Figure 2.22: *Controlled electromechanical transducer*

In view of applying the control strategy, we consider the system with the parameters of Figure 2.16. In this state, the system has a chaotic behavior as it appears in the phase portrait of Figure 2.18. Two sets of target trajectories have been considered. The first one has the same frequency as the external excitation (period-1 targetting orbit) and is defined as:

$$(\bar{x_1}, \bar{x_2}, \bar{x_3}, \bar{x_4}) = (0.08\cos wt, -0.08w\sin wt, 0.08\cos wt, -0.08w\sin wt).$$

The second set defined by:

$$(\bar{x_1}, \bar{x_2}, \bar{x_3}, \bar{x_4}) = (0.08\cos w't, -0.08w'\sin w't, 0.08\cos w't, -0.08w\sin w't),$$

has the frequency $w' = 2w$. The feedback matrix elements are $K_{21} = 40$ and $K_{43} = 10$. The results of the control strategy are implemented in Figure 2.21 and show the efficiency of the control strategy.

With the previous results, the interesting question is how to launch the control at a given time in electromechanical engineering. Practically, the control of the electromechanical transducer can be realized as follows: in the mechanical part, the rod T is coupled with a spring of constant k' where the instantaneous displacement of it extremity is $\bar{y}$, while in the electrical part, we insert in the electrical circuit a courent source $(\bar{i})$ in parallel with a condenser (C'). With this consideration, we have in the electrical part a new additional voltage $V_{c'} = \frac{1}{c'}(q - \bar{q}_o^o\cos wt)$ and in the mechanical part a new external force $f_o = k'(z - \bar{z}_o\cos wt)$. So that the feedback gain matrix elements K_{21} and K_{43} are respectively proportional to

$\frac{1}{c'}$ and k'. The controlled electromechanical model is represented in Figure 2.22, and the resulting equations of motion are established in the appendix Ap-1. Our investigation leads to the following comments. Better chaos control ensures greater values of the coefficients K_{21} and K_{43}, this requires greater energy inputs. It can be practically interesting to find a suitable balance between the quality of control and the quantity of energy available for the realization.

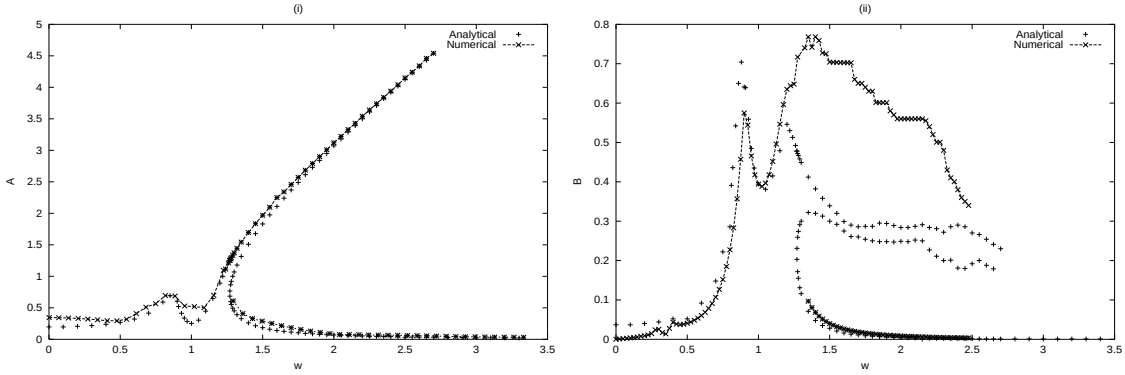

Figure 2.23: *Comparison of analytical and numerical frequency-responce curves in the case* $w_2 = 1$. *(i) corresponding for* $A(w)$ *and (ii) for* $B(w)$. *with* $\gamma_2 = 0.2, \lambda_1 = 0.4, \lambda_2 = 0.25, \beta = 0.4, \gamma_1 = 0.01, E_o = 0.2, \epsilon_1 = 0.5$.

2.3 Parametric electromechanical transducer

In some applications depending on the way the coupling is ensured or voluntary for the engineering purposes, parametric variations of the coupling parameters may occur, leading to another type of dynamical behavior. In certain circumstances, some parameters of the electromechanical device can vary with time because of the functioning constraints. This is particulary the case for the parameters of the electromagnetic coupling: i.e time variations of the magnetic field $\vec{B}_m$ and the region of electromagnetic action. The time variation can also be ordered voluntarily: for the control purposes. We assume that the time variation is periodic with frequency $2w$, so that in non-dimensional units, the parametric electromechanical system is described by the following coupled nonlinear differential equations:

$$\begin{aligned} \ddot{x} + \gamma_1 \dot{x} + x + \beta x^3 + \lambda_1 (1 + \epsilon_1 \cos 2wt)\dot{y} &= E_o \cos wt, \\ \ddot{y} + \gamma_2 \dot{y} + w_2^2 y - \lambda_2 (1 + \epsilon_1 \cos 2wt)\dot{x} &= 0, \end{aligned} \tag{2.35}$$

where ϵ_1 is the amplitude of the parametric coupling with $0 \leq \epsilon_1 < 1$. Our aim in this section is mainly to analyze the effects of the parametric coupling on the dynamics, stability, and bifurcation sequences of the nonlinear electromechanical system.

2.3.1 Harmonic oscillatory states

As we have mentioned in the above section, the harmonic oscillatory solutions of equations (2.35) can be approximated by the expressions defined by equations (2.1). By a procedure like that used before, it comes that the amplitudes A and B satisfy the following nonlinear equations:

$$\frac{81}{256}\beta^4 A^{10} + \frac{27}{16}\beta^3 F A^8 + [\frac{27}{8}\beta^2 F^2 + \frac{9}{8}\beta^2 NM]A^6, +[3\beta F^3 + 3\beta FNM - \frac{9}{16}\beta^2 E_o^2]A^4$$
$$+[(F^2+NM)^2 - \frac{3}{2}\beta F E_o^2]A^2 - (F^2+M^2)E_o^2 = 0,$$
$$B^2 = \frac{\lambda_2^2 w^2 E_o^2[(1+\frac{\epsilon_1}{2})^2 M^2 + (1-\frac{\epsilon_1}{2})^2 (F+\frac{3}{4}\beta A^2)^2]}{[(w_2^2-w^2)^2+\gamma_2^2 w^2][(F+\frac{3}{4}\beta A^2)^2+NM]^2}. \tag{2.36}$$

where

$$\begin{aligned} F &= 1 - w^2 - \frac{\lambda_1\lambda_2 w^2(1-\frac{\epsilon_1^2}{4})(w_2^2-w^2)}{(w_2^2-w^2)^2+\gamma_2^2 w^2}, \\ M &= \gamma_1 w + \frac{\lambda_1\lambda_2\gamma_2 w^3(1-\frac{\epsilon_1}{2})^2}{(w_2^2-w^2)^2+\gamma_2^2 w^2}, \\ N &= \gamma_1 w + \frac{\lambda_1\lambda_2\gamma_2 w^3(1+\frac{\epsilon_1}{2})^2}{(w_2^2-w^2)^2+\gamma_2^2 w^2}. \end{aligned}$$

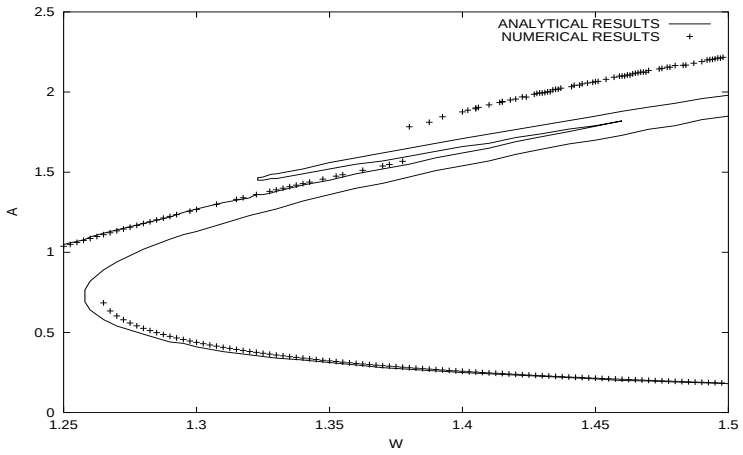

Figure 2.24: *Analytical and numerical frequency-responce curves when* $\epsilon_1 = 0.8$. $A(w)$ *with the parameters of Figure 2.23.*

Using again the **Newton-Raphson** algorithm, we find the amplitudes A and B when the frequency w is varied. Comparison between analytical and numerical frequency-response curves is provided in Figure 2.23. The curves show antiresonance and resonance peaks, hysteresis phenomenon. Analyzing the effects of ϵ_1 on the response curves, we find two ranges as ϵ_1 varies. The first range leads to the well-known hysteresis phenomena with two stable and one unstable values of the amplitudes A and B as it appears in Figure 2.23. In the second range, we have five values of A (and B) with three values corresponding to stable harmonic oscillations. This is shown in Figure 2.24 with the parameters of Figure 2.23 (the boundaries of two ranges occurs at $\epsilon_1 = 0.64$ with this set of parameters). Consequently, the electromechanical transducer with parametric coupling can vibrate in these domains with three stable different amplitudes for $\epsilon_1 > 0.64$ and two stable different amplitudes for $\epsilon_1 < 0.64$ of the harmonic oscillations depending to the initial conditions.

In the linear case, the frequency-response curves are represented in Figure 2.25. As ϵ_1 increases, the values of the amplitudes A and B decrease. The same is observed in the

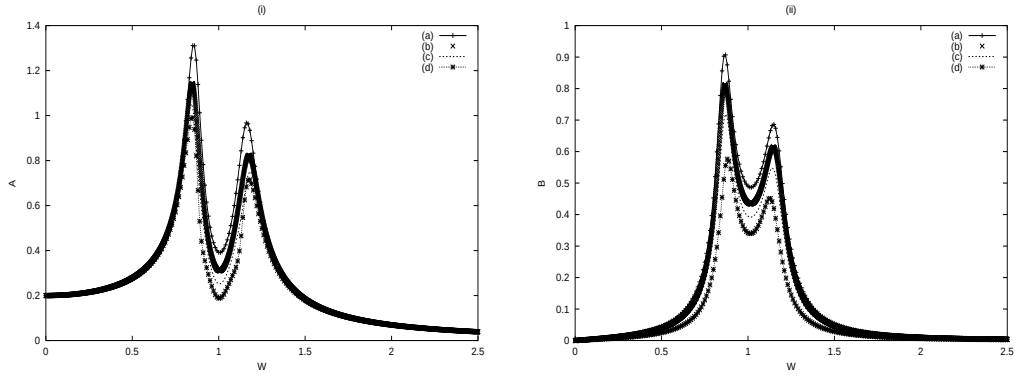

Figure 2.25: *Effects of the amplitude ϵ_1 on the frequency-responce curves $A(w)$ for (i) and $B(w)$ for (ii) in the linear system: $(a) : \epsilon_1 = 0, (b) : \epsilon_1 = 0.25, (c) : \epsilon_1 = 0.5, (d) : \epsilon = 0.9$. The other parameters are those of figure 2.23.*

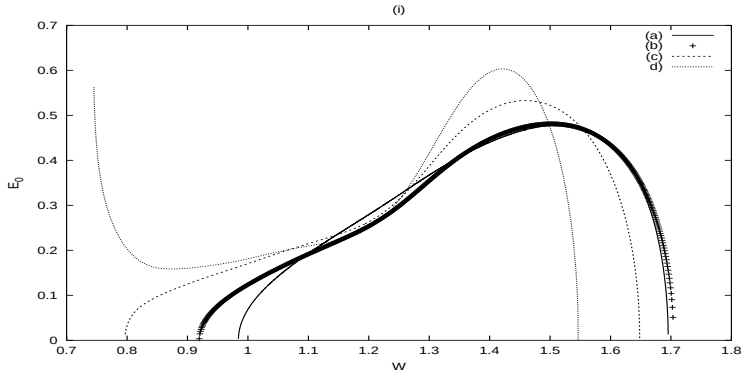

Figure 2.26: *Effects of the amplitude ϵ_1 on the stability boundaries in the (w, E_o) plane, (i) corresponding for the case $w_2 = 1$ and (ii) for $w_2 = 0.5$. The parameters are those of figure 2.23 and (a): $\epsilon_1 = 0.0$: (b): $\epsilon_1 = 0.25$: (c): $\epsilon_1 = 0.5$: (d): $\epsilon_1 = 0.9$.*

nonlinear limit where the antiresonant peak (see Figure 2.23) decreases as ϵ_1 increases. This behavior is interesting when the model is used as an electromechanical vibration absorber [II3].

2.3.2 Stability of the parametric harmonic oscillations

To study the stability of the harmonic oscillatory states, one considers the following variational equations of equations (2.35) around the harmonic oscillatory states given by equations (2.1) as follows:

$$\begin{aligned} &\delta\ddot{x} + \gamma_1\delta\dot{x} + \delta x + 3\beta x_s^2\delta x + \lambda_1(1 + \epsilon_1\cos 2wt)\delta\dot{y} = 0, \\ &\delta\ddot{y} + \gamma_2\delta\dot{y} + w_2^2\delta y - \lambda_2(1 + \epsilon_1\cos 2wt)\delta\dot{x} = 0. \end{aligned} \tag{2.37}$$

Let us then express δx and δy as defined by the expressions (2.5). Inserting equations (2.5) into equations (2.37), we obtain:

$$\begin{aligned} &\frac{d^2u}{d\tau^2} + [\delta_{11} + 2\epsilon_{11}\cos(4\tau - 2\phi)]u + \delta_{12}\exp(-\epsilon\tau))v + c_1\exp(-\epsilon\tau)\frac{dv}{d\tau} \\ &+2c_1\epsilon_1\cos(4\tau)\exp(-\epsilon\tau)\frac{dv}{d\tau} + 2c_3\epsilon_1\cos(4\tau)\exp(-\epsilon\tau)v = 0, \\ &\frac{d^2v}{d\tau^2} + \delta_{21}\exp(\epsilon\tau)u + \delta_{22}v + c_2\exp(\epsilon\tau)\frac{du}{d\tau} \end{aligned}$$

$$+2c_2\epsilon_1\cos(4\tau)\exp(-\epsilon\tau)\frac{du}{d\tau}+2c_4\epsilon_1\cos(4\tau)\exp(-\epsilon\tau)u=0, \tag{2.38}$$

where the new parameters c_3 and c_4 are given by

$$c_3=c_4=\frac{-2\lambda_2\epsilon_a}{w}.$$

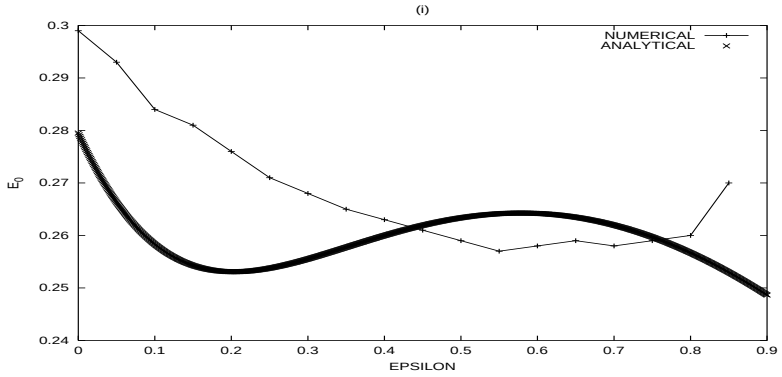

Figure 2.27: *Stability domains (below the curves) in the* (ϵ_1, E_o) *plane. The parameters are those of Figure 2.24 and* $w = 1.2$.

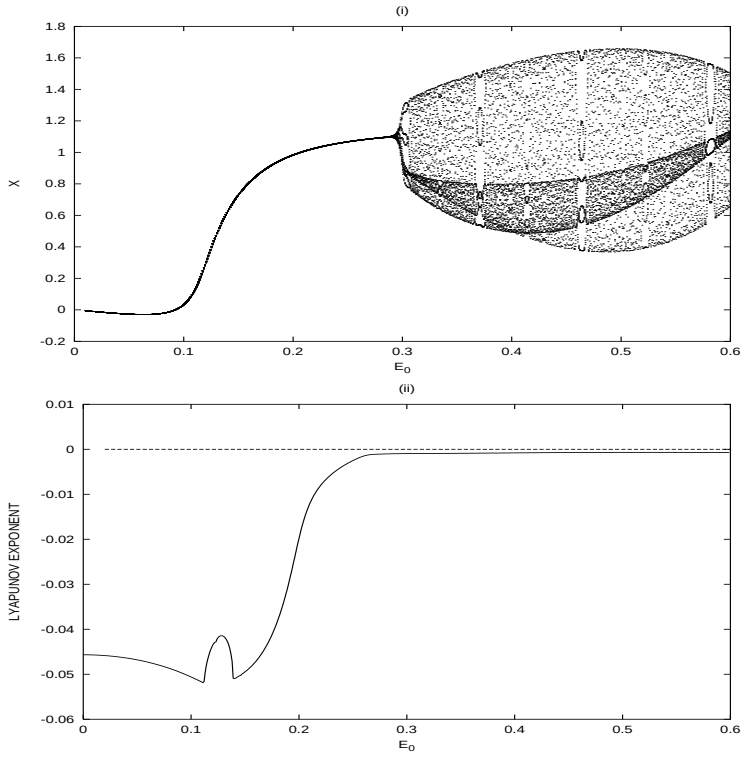

Figure 2.28: *Transition from the stability domain to the instability domain. The parameters are those of Figure 2.19. (i) Bifurcation diagram showing the coordinate x versus* E_0. *(ii) The variation of the corresponding Lyapunov exponent.*

Following the **Floquet** theory [II1], the small **Hill** determinant gives the following equation:

$$\Delta(\epsilon_a,\epsilon_b) \;=\; \Delta_{11}\Delta_{63}\Delta_{36}\Delta_{44}(\delta_{22}+\epsilon_b^2)(\delta_{11}+\epsilon_a^2)+\Delta_{11}\Delta_{66}(\delta_{22}+\epsilon_b^2)(\delta_{11}+\epsilon_a^2)$$

$$
\begin{aligned}
&(\Delta_{33}\Delta_{44} - \Delta_{43}\Delta_{34}) + \epsilon_{11}e^{2i\phi}\Delta_{16}(\delta_{22}+\epsilon_b^2)(\delta_{11}+\epsilon_a^2)\Delta_{36}\Delta_{44} - \\
&\epsilon_{11}e^{2i\phi}\Delta_{66}(\delta_{22}+\epsilon_b^2)(\delta_{11}+\epsilon_a^2)(\epsilon_{11}e^{-2i\phi}\Delta_{44} - \Delta_{43}\Delta_{14}) + \\
&\Delta_{52}\Delta_{25}\epsilon_{11}e^{2i\phi}\Delta_{16}\Delta_{44}\Delta_{63} + \Delta_{52}\Delta_{25}\Delta_{66}\epsilon_{11}e^{2i\phi}(\epsilon_{11}e^{-2i\phi}\Delta_{44} - \Delta_{43}\Delta_{14}) \\
&+[\Delta_{41}(\delta_{22}+\epsilon_b^2)(\delta_{11}+\epsilon_a^2) - \Delta_{41}\Delta_{52}\Delta_{25}][\Delta_{63}(\Delta_{14}\Delta_{36} - \Delta_{34}\Delta_{16}) + \\
&\Delta_{66}(\epsilon_{11}e^{-2i\phi}\Delta_{34} - \Delta_{33}\Delta_{14})] - [\Delta_{61}\Delta_{43}(\delta_{22}+\epsilon_b^2)(\delta_{11}+\epsilon_a^2) + \Delta_{61}\Delta_{52}\Delta_{25}] \\
&(\Delta_{14}\Delta_{36} - \Delta_{34}\Delta_{16}) + [\Delta_{61}\Delta_{44}(\delta_{22}+\epsilon_b^2)(\delta_{11}+\epsilon_a^2) + \Delta_{61}\Delta_{52}\Delta_{25}] \\
&(\Delta_{36}\epsilon_{11}e^{-2i\phi} - \Delta_{33}\Delta_{16}) - \Delta_{11}\Delta_{25}\Delta_{52}\Delta_{66}(\Delta_{33}\Delta_{44} - \Delta_{43}\Delta_{34}) + \\
&\Delta_{11}\Delta_{52}\Delta_{25}\Delta_{63}\Delta_{36}\Delta_{44} \\
= \;& 0, \qquad (2.39)
\end{aligned}
$$

where

$$
\begin{aligned}
\Delta_{44} &= \delta_{22} + (\epsilon_b - 2i)^2, & \Delta_{11} &= \delta_{11} + (\epsilon_a - 2i)^2, \\
\Delta_{14} &= (\delta_{12} + c_1(\epsilon_b - 2i)), & \Delta_{25} &= (\delta_{12} + c_1\epsilon_b), \\
\Delta_{36} &= (\delta_{12} + c_1(\epsilon_b + 2i)), & \Delta_{41} &= (\delta_{21} + c_2(\epsilon_b - 2i)), \\
\Delta_{52} &= (\delta_{21} + c_2\epsilon_a), & \Delta_{63} &= (\delta_{21} + c_2(\epsilon_a + 2i)), \\
\Delta_{34} &= (c_3 + c_1(\epsilon_b + 2i)^2)\epsilon_1, & \Delta_{43} &= (c_4 + c_2(\epsilon_a - 2i)^2)\epsilon_1, \\
\Delta_{61} &= (c_4 + c_2(\epsilon_a + 2i)^2)\epsilon_1, & \Delta_{33} &= \delta_{11} + (\epsilon_a + 2i)^2, \\
\Delta_{16} &= (c_3 + c_1(\epsilon_b - 2i)^2)\epsilon_1, & \Delta_{66} &= \delta_{22} + (\epsilon_b + 2i)^2.
\end{aligned}
$$

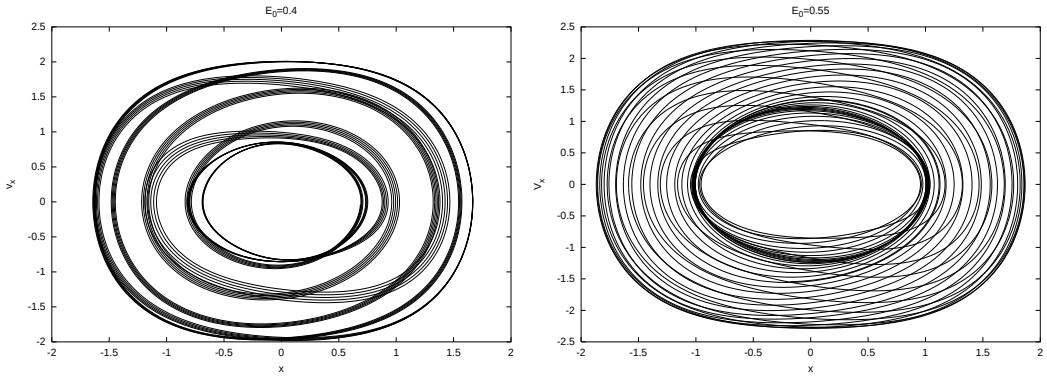

Figure 2.29: *Behavior of the parametric model in the unstable region with the parameters of Figure 2.23.*

In Figure 2.26, we have drawn the stability boundary of the harmonic oscillations in the (w, E_o) plane with the parameters of Figure 2.23 for several different values of the amplitude ϵ_1. The domain of stable harmonic oscillations is the region below the curves. In comparison to the case $\epsilon_1 = 0$ (constant coupling), it is found that as ϵ_1 varies, they are ranges of ϵ_1 where the stability domain is large and other ranges where the stability domain is small. This is also shown in Figure 2.27 where boundary limit is plotted in the (ϵ_1, E_0) plane. In this Figure, we have also plotted the stability boundary obtained from the numerical simulations of equations (2.35). For $\epsilon_1 \geq 0.45$, the numerical and analytical curves show opposite behavior. This can be explained by the fact that the analytical curve is obtained from a truncation of the **Hill** determinant which can be poor for large ϵ_1.

Let us consider the particular frequency $w = 1.2$ and $\epsilon_1 = 0.5$, it appears from Figure 2.27 that the stability domains are comprised in the interval $E_0 \in [0.0; 0.2633]$. To verify our analytical results, we have drawn, after solving numerically equations (2.35), a bifurcation

diagram and the variation of the corresponding **Lyapunov** exponent as E_0 varies. Our results are reported in Figure 2.28. where it is seen that a period-1 orbit exist for $E < 0.29$. After this critical value corresponding to the limit value of E_0 for the stability of the harmonic oscillations, a transition from period-1 orbit to a quasiperiodic behavior appears. Figure 2.29 shows the behavior of the electromechanical transducer for two values of the amplitude E_0 in the instability region.

Figure 2.30 presents the stability chart of the parametric model in the $E_0 - w$ plane with the set of parameter defined in Figure 2.23. One observes that our electromechanical system with parametric coupling exhibits periodic oscillations when $w = 1.0$ and quasiperiodic, period-3T and period-5T oscillations for increasing w.

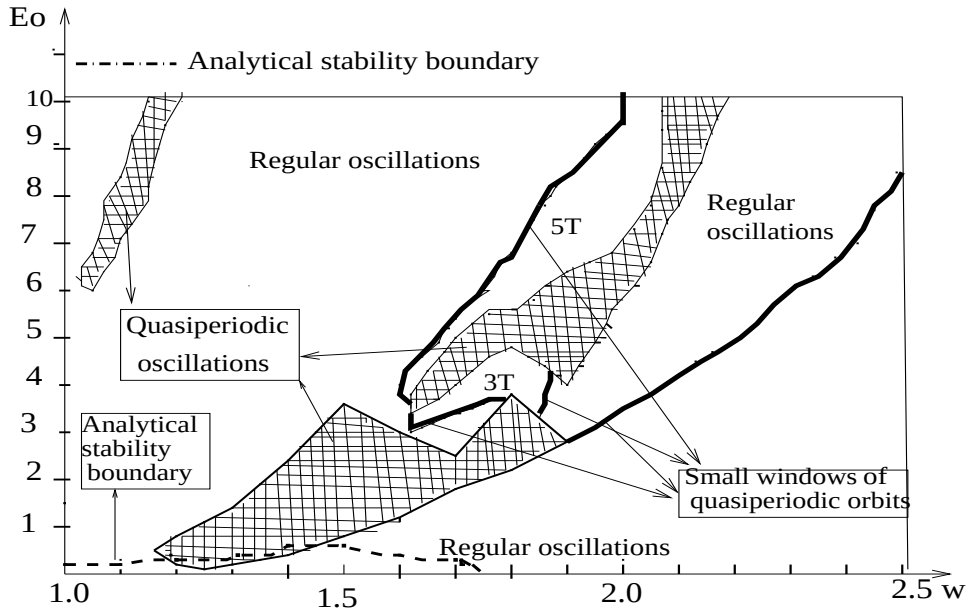

Figure 2.30: *Stability chart with the parameters of Figure 2.23*

2.3.3 Sub- and superharmonic oscillations

With the parametric coupling, the sub- and superharmonic oscillations can be established in the same manner as in the case of constant coupling. Following the above manipulations, equations (2.16) take the form:

$$
\begin{aligned}
D_o^2 x_3 + x_3 &= -(2jA_1' + j\gamma_{10}A_1 + 3\beta A_1^2\bar{A}_1 + 6\Lambda^2 A_1)\exp(jT_o) + (j\gamma_{10}w\Lambda + 4\beta\Lambda A_1\bar{A}_1 + \\
&\quad 3\Lambda^3\beta)\exp(jwT_o) - \beta A_1^3\exp(3jT_o) - 3\beta A_1^2\Lambda\exp(j(2+w)T_o) - \\
&\quad jw_2\lambda_{10}A_2\exp(jw_2T_o) - 3\beta A_1\Lambda^2\exp(j(2w+1)T_o) - \Lambda^3\beta\exp(3jwT_o) \\
&\quad -3\beta\Lambda^2 A_1\exp(j(1-2w)T_o) - 3\beta\Lambda A_1^2\exp(j(2-w)T_o) \\
&\quad -\frac{1}{2}jw_2\lambda_{10}\epsilon_1 A_2\exp(2w+w_2)T_o) - \frac{1}{2}jw_2\lambda_{10}\epsilon_1 A_2\exp(w_2-2w)T_o) + C.C, \\
D_o^2 y_3 + w_2^2 y_3 &= -jw_2(2A_2' + \gamma_{20}A_2)\exp(jw_2T_o) + j\lambda_{20}A_1\exp(jT_o) + jw\lambda_{20}\Lambda\exp(jwT_o) \\
&\quad +\frac{1}{2}j\lambda_{20}\epsilon_1 A_1\exp(j(2w+1)T_o) + \frac{1}{2}j\lambda_{20}\epsilon_1 A_1\exp(j(-2w+1)T_o) \\
&\quad +\frac{1}{2}jw\lambda_{20}\epsilon_1\Lambda\exp(3jwT_o) - \frac{1}{2}jw\lambda_{20}\epsilon_1\Lambda\exp(jwT_o) + C.C. \qquad (2.40)
\end{aligned}
$$

Equations (2.40) show that there exist superharmonic resonances ($w = 1/3$ and $w_2 = 1$) and subharmonic resonances (when $w = 3$ and $w_2 = 1$) as analyzed below. Therefore, we restrict our investigation to the case of sub- and superharmonic resonances.

- **Superharmonic resonances.**
  In the parametric electromechanical system, the secular producing terms in the equations (2.40) must be eliminated. Hence, the solvability conditions are the following:

$$\begin{aligned} 2jA_1' + j\gamma_{10}A_1 + 6\Lambda^2 A_1 + 3\beta A_1^2 \bar{A}_1 + \\ jw_2\lambda_{10}A_2 \exp(j\sigma_2 T_2) + \Lambda^3 \beta \exp(j\sigma_1 T_2) = 0, \\ -w_2(2A_2' + \gamma_{20}A_2)\exp(j\sigma_2 T_2) + \lambda_{20}A_1 + \frac{1}{2}w\lambda_{10}\epsilon_1 \Lambda \exp(j\sigma_1 T_o) = 0, \end{aligned} \tag{2.41}$$

  We express $A_i(T_2)$, (i=1,2) in the polar form (2.19), and obtain after separating real and imaginary parts the following set of first order differential equations:

$$\begin{aligned} \frac{3}{8}\beta a_1^3 - a_1 b_1' + 3\Lambda^2 a_1 + \beta\Lambda^3 \cos\delta_1 - \frac{1}{2}w_2\lambda_{10}a_2 \sin\delta_2 &= 0, \\ \frac{1}{2}\gamma_{10}a_1 + a_1' + \beta\Lambda^3 \sin\delta_1 + \frac{1}{2}w_2\lambda_{10}a_2\cos\delta_2 &= 0, \\ w_2 a_2 b_2' \cos\delta_2 + w_2(a_2' + \frac{1}{2}\gamma_{20}a_2)\sin\delta_2 - \frac{1}{2}w\lambda_{20}\epsilon_1\Lambda\sin\delta_1 &= 0, \\ -w_2(a_2' + \frac{1}{2}\gamma_{20}a_2)\cos\delta_2 + w_2 b_2' a_2 \sin\delta_2 + \frac{1}{2}w\lambda_{20}\epsilon_1\Lambda\cos\delta_1 - \frac{1}{2}\lambda_{20}a_1 &= 0, \end{aligned} \tag{2.42}$$

  where $\delta_1 = \sigma_1 T_2 - b_1$ and $\delta_2 = \sigma_2 T_2 + b_2 - b_1$. For the steady-state responses, we must have $a_i' = 0$ and $\delta_i' = 0$. Thus $b_1' = \sigma_1$ and $b_2' = \sigma_1 - \sigma_2$. Eliminating δ_i from equations (2.42), we obtain the following set of nonlinear equations:

$$\begin{aligned} &\frac{9}{16}\beta^2 Z^2[M^2 + \lambda_{10}^2\lambda_{20}^2\epsilon_1^2 w^2\Lambda^2\gamma_{20}^2]a_1^6 + \frac{3}{2}\beta Z[\lambda_{10}\lambda_{20}\epsilon_1 w\Lambda\gamma_{20}N_o - MM_o]a_1^4 \\ &+(M_o^2 + N_o^2)a_1^2 - (M^2 + \lambda_{10}^2\lambda_{20}^2\epsilon_1^2 w^2\Lambda^2\gamma_{20}^2)^2 = 0, \\ &a_2^2 = \frac{[M_1 a_1^3 + N_1 a_1]^2 + [M_2 a_1^3 + N_2 a_1]^2}{Z^2 w_2^2[M^2 + \lambda_{10}^2\lambda_{20}^2\epsilon_1^2 w^2\Lambda^2\gamma_{20}^2]^2}, \end{aligned} \tag{2.43}$$

  where

$$\begin{aligned} Z &= 4(\sigma_1 - \sigma_2)^2 + \gamma_2^2, \\ M &= 2\Lambda^3\beta Z + 2\lambda_{10}\lambda_{20}w\epsilon_1\Lambda(\sigma_1 - \sigma_2), \\ N &= 2\lambda_{10}\lambda_{20}w_1(\sigma_1 - \sigma_2) - Z(6\Lambda^2 - 2w_1\sigma_1), \\ M_o &= NM + \lambda_{10}\lambda_{20}w\epsilon_1\Lambda\gamma_{20}(\lambda_{10}\lambda_{20}\gamma_{20} - \gamma_{10}Z), \\ N_o &= M(\lambda_{10}\lambda_{20}\gamma_{20} - \gamma_{10}Z) - \lambda_{10}\lambda_{20}w\epsilon_1\Lambda\gamma_{20}N, \\ M_1 &= \frac{3}{2}\beta Z\lambda_{10}\lambda_{20}^2\epsilon_1^2 w^2\Lambda^2\gamma_{20}(\sigma_1 - \sigma_2) - \frac{3}{4}\beta ZM\gamma_{20}w\lambda_{20}\epsilon_1\Lambda, \\ N_1 &= 2w\lambda_{20}\epsilon_1\Lambda N_o(\sigma_1 - \sigma_2) + \gamma_{20}w\lambda_{20}\epsilon_1\Lambda M_o \\ &\quad -\lambda_{20}\gamma_{20}[M^2 + \lambda_{10}^2\lambda_{20}^2\epsilon_1^2 w^2\Lambda^2\gamma_{20}^2], \\ M_2 &= \frac{3}{2}\beta ZMw\lambda_{20}\epsilon_1\Lambda(\sigma_1 - \sigma_2) + \frac{3}{4}\beta Z\lambda_{10}\lambda_{20}^2\epsilon_1^2 w^2\Lambda^2\gamma_{20}^2, \\ N_2 &= 2\lambda_{20}(\sigma_1 - \sigma_2)[M^2 + \lambda_{10}^2\lambda_{20}^2\epsilon_1^2 w^2\Lambda^2\gamma_{20}^2] \\ &\quad +N_o w\lambda_{20}\epsilon_1\Lambda\gamma_{20} - 2w\lambda_{20}\epsilon_1 M_o(\sigma_1 - \sigma_2). \end{aligned}$$

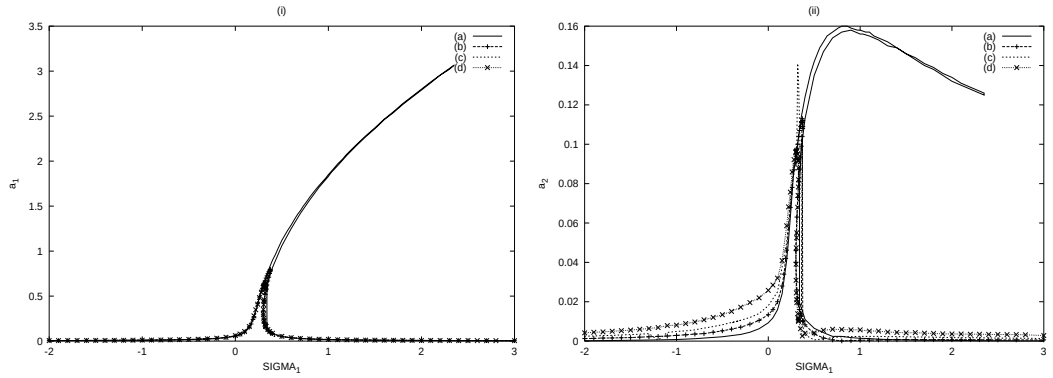

Figure 2.31: *Effet of the amplitude ϵ_1 on the superharmonic frequency-response curves. (i) corresponding for $a_1(\sigma_1)$ and (ii) for $a_2(\sigma_1)$ with the parameters $E = 0.5, \gamma_{10} = 0.01$, $\lambda_{10} = 0.12, \lambda_{20} = 0.2, \beta = 0.6; \gamma_{20} = 1.2; \sigma_2 = 0$ and (a): $\epsilon_1 = 0.0$;(b): $\epsilon_2 = 0.25$, (c): $\epsilon_1 = 0.5$, (d): $\epsilon_1 = 0.9$.*

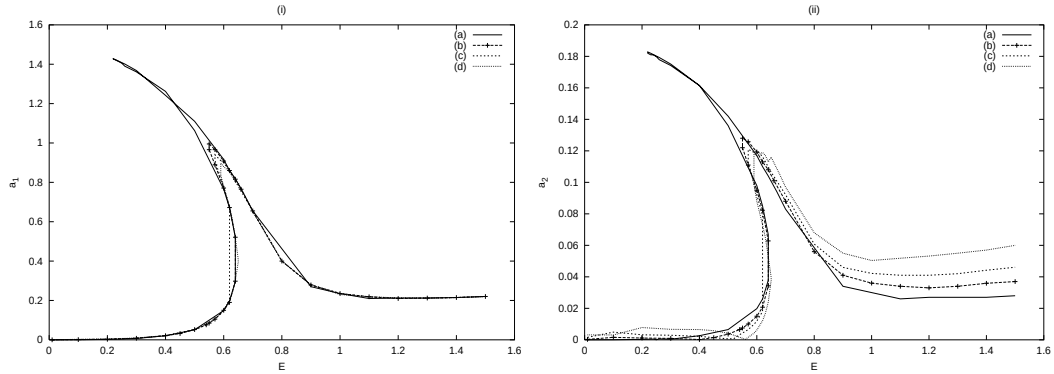

Figure 2.32: *Effect of the amplitude ϵ_1 on the superharmonic amplitude-response curves. (i) corresponding for $a_1(E)$ and (ii) for $a_2(E)$ with the parameters of Figure 2.31, $\sigma_1 = 0.5$ and (a): $\epsilon_1 = 0.0$; (b): $\epsilon_2 = 0.25$, (c): $\epsilon_1 = 0.5$, (d): $\epsilon_1 = 0.9$.*

Thus, in the case of superharmonic resonances, the motion of the two oscillators are coupled and described by equations (2.22). We find the amplitudes a_1 and a_2 when the detuning parameter σ_1 is varied. In the exact internal resonances ($\sigma_2 = 0$), the superharmonic frequency-response curves obtained for a given set of parameters are provided in Figure 2.31(i) for $a_1(\sigma_1)$ and in Figure 2.31(ii) for $a_2(\sigma_1)$. The behavior of the frequency-response curves in the superharmonic resonances show the well-known hysteresis phenomena. In Figure 2.32, we provide the superharmonic amplitude-response curves $a_i(E)$ (i=1,2) and the curves of Figure 2.32 shows the jump phenomena. The effect of the amplitude ϵ_1 of the parametric modulation on the behavior of the model in the superharmonic resonances is analyzed and it appears that the curves also show the hysteresis and jump phenomena for several values of the amplitude ϵ_1.

- **Subharmonic resonances.**
  It follows from equations (2.40) that secular terms are eleminated from x_3 and y_3 if

$$\begin{aligned} 2jA_1' + (j\gamma_{10} + 6\Lambda^2)A_1 + 3\beta A_1^2 \bar{A}_1 + \\ jw_2\lambda_{10}A_2 \exp(j\sigma_2 T_2) + 3\Lambda\beta\bar{A}_1^2 \exp(j\sigma_o T_2) = 0, \\ -w_2(2A_2' + \gamma_{20}A_2)\exp(j\sigma_2 T_2) + \lambda_{20}A_1 = 0. \end{aligned} \tag{2.44}$$

  Again, introducing the polar notations (2.19) for $A_i (i = 1, 2)$ and separating real and imaginary parts yields after some algebraic manipulations the following first order of

differential equations:

$$\begin{aligned}
\frac{3}{8}\beta a_1^3 - a_1 b_1' + 3\Lambda^2 a_1 + \frac{3}{4}\beta\Lambda a_1^2\cos\delta_4 - \frac{1}{2}w_2\lambda_{10}a_2\sin\delta_2 &= 0,\\
\frac{1}{2}\gamma_{10}a_1 + a_1' + \frac{3}{4}\beta\Lambda a_1^2\sin\delta_4 + \frac{1}{2}w_2\lambda_{10}a_2\cos\delta_2 &= 0,\\
a_2 b_2'\cos\delta_2 + w_2(a_2' + \frac{1}{2}\gamma_{20}a_2)\sin\delta_2 &= 0,\\
w_2(a_2' + \frac{1}{2}\gamma_{20}a_2)\cos\delta_2 - w_2 b_2' a_2\sin\delta_2 - \frac{1}{2}\lambda_{20}a_1 &= 0, \qquad (2.45)
\end{aligned}$$

where $\delta_4 = \sigma_o - 3b_1$, and $\delta_2 = \sigma_2 T_2 + b_2 - b_1$. For the steady-state responses, we must have $a_i' = 0$ and $\delta_i' = 0$. Thus $b_1' = \frac{\sigma_o}{3}$ and $b_2' = \frac{\sigma_o}{3} - \sigma_2$. Eliminating δ_i from equations (2.45), we obtain the following set of nonlinear equations:

$$\begin{aligned}
&\frac{9}{64}\beta^2 a_1^6 + \frac{3}{4}P_1 a_1^4 + Q_1 a_1^2 = 0,\\
&a_2 = \frac{\lambda_{o2}a_1}{w_2\sqrt{M}}, \qquad (2.46)
\end{aligned}$$

where

$$\begin{aligned}
M &= \gamma_{o2}^2 + 4(\frac{\sigma_o}{3} - \sigma_2)^2,\\
P_1 &= 3\Lambda^2 - \frac{\sigma_o}{3} - \frac{3}{2}\beta\Lambda^2 + \frac{\lambda_{o1}\lambda_{o2}(\frac{\sigma_o}{3} - \sigma_2)}{\gamma_{o2}^2 + 4(\frac{\sigma_o}{3} - \sigma_2)^2},\\
Q_1 &= \frac{1}{4}\left\{\gamma_{o1} + \frac{\lambda_{o1}\lambda_{o2}\gamma_{o2}}{\gamma_{o2}^2 + 4(\frac{\sigma_o}{3} - \sigma_2)^2}\right\}^2 + P_1^2.
\end{aligned}$$

We note that the behavior of the parametrical model in the subharmonic resonance is not depending for the amplitude ϵ_1 of the parametric modulation. The subharmonic frequency-response curves obtained for a given set of parameters are provided in Figure 2.14(i) for $a_1(\sigma_o)$ and in Figure 2.14(ii) for $a_2(\sigma_o)$. The amplitude-response curves are reported in Figure 2.15 for different values of σ_o.

2.3.4 Transitions to chaos

The aim of this subsection is to find some bifurcation sequences and how chaos arises in our parametric model as the parameters of the system evolve. The control parameters are the amplitude E_0 of the external excitation and the damping coefficient. Our investigation shows that a bifurcation diagram and the variation of the corresponding **Lyapunov** exponent versus the amplitude E_0 for $\epsilon_1 = 0.5$ is not different qualitatively for that presents in Figure 2.16 for the case of constant coupling. The transitions to chaos are those presented in the case of constant coupling.

2.4 Conclusion

In this chapter, we have considered the dynamics of a forced and parametric nonlinear electromechanical system consisting of an electrical **Duffing** oscillator coupled magnetically to a linear mechanical oscillator. The amplitude and the stability boundaries of the harmonic behavior have been derived using respectively the harmonic balance method and the **Floquet**

theory. It appears that the behaviors of the model show various interesting phenomena (hysteresis, resonant and antiresonance phenomena) for some combinations of the system parameters. In order to analyze the behavior of the model when the frequency of the voltage source is very large or very small as compared to the values of the natural frequencies of the oscillators, we have derived the stability chart using numerical simulations of the equations of motion. Bifurcation diagrams showing the transitions from regular to chaotic motion have been drawn. The canonical feedback controllers have been used to drive the electromechanical device from a chaotic trajectory to a regular target orbit. The effects of the parametric coupling on the dynamics, stability boundary and bifurcation structures on the electromechanical system have also been analyzed.

Bibliography

[II1] **Nayfeh A. H.** and **Mook D. T.** , "Nonlinear oscillations", Wiley-Interscience,New York (1979).

[II2] **Chen G.** and **Dong X.**, IEEE transactions on circuits and systems-I: Fundamental theory and applications, **40**, 591 (1993).

[II3] **Korenev B. G.** and **Reznikov L. M.,** "Dynamics vibration absorbers", John-wiley, new york (1997).

[II4] **Hayashi C.**, "Nonlinear Oscillations in Physical Systems," Mc-Graw-Hill, New-York (1964).

[II5] **Hayashi C.**, J. Appl. Phys; **24** 521 (1953).

[II6] **Stocker J. J.,** "Nonlinear vibration", Interscience publishers, New York (1950).

[II7] **Parlitz U.** and **Lauterborn W.**, Phys. Let. A**107**, 351 (1985).

[II8] **Pezeshki C.** and **Dowell E. H.**, Physica D **32**, 194 (1988).

[II9] **Ottino,** in "Kinematics of Mixing: Stretching, Chaos and Transport". Cambridge University press, Cambridge (1989).

[II10] **Pecora L. M.** and **Carrols T. L.,** Phys. Rev. Lett. **64**, 821 (1990)
Hayes S., Grebogi C. and **Mark A.,** Phys. Rev. Lett. **73**, 1781 (1994).
Cuomo K. M. and **Oppenheim A. V.,** Phys. Rev. Lett. **71**, 65 (1993).
Perez G. and **Cerdeira H. A.,** Phys. Rev. Lett. **44**, 1970 (1995).
Boccaletti S., Farini A and **Arechi, F. T.,** Phys. Rev. E**55**, 4979 (1997).
Woafo P., Phys. Lett. A **267**, 31 (2000).

[II11] **Chembo Kouomou Y.** and **Woafo P.**, Physica Scripta **62**, 255 (2000).

[II12] **Pezeschki C.** and **Dowell E. H.**, Physica D **32**, 194 (1988).

[II13] **Cheng A. H. D., C. Yang V., Kackl K.** and **Chajes M. J.**, Int. J. Non-linear Mech. **28**, 549 (1993).

Chapter 3 :
Dynamics of electromechanical systems with multiple functions

Chapter 3

Dynamics of electromechanical systems with multiple functions

3.1 Introduction

In the previous Chapter, we have considered the dynamics of an electromechanical transducer with one function and discussed in detail the effects of the amplitude of the parametric modulation on the behaviors of the model. In this Chapter, we consider electromechanical systems with multiple fonctions. Before dealing with such a model, we note that this extension can be obtained in two ways. Firstly, we can coupled in series or in parallel an electrical part to a mechanical part consisting of a large number of linear mechanical oscillators. Secondly, we can use two or a large number of electromechanical devices coupled unidirectionally through the feedback coupling, so that the problem of synchronization process of such model is very important for its technological exploitations in electromechanical engineering (considered in the next chapter). In this Chapter, the first way will be considered.

Considering the dynamics of an electromechanical transducer with multiple functions coupled in series and in parallel, two main points are considered. We first concentrate on the dynamics of the model with double and a large number of functions in series. The second point is the dynamics of such model with double functions in parallel. After the presentation of the model and the resulting equations of motion, we derive in section 3.2 the amplitudes of the harmonic oscillations and time delay using the harmonic balance method. The presence of hysteresis branches is used to derive the stability boundary of the harmonic oscillations. The stability chart is presented using the numerical simulations of the equations of motion. We derive the characteristics of sub- and superharmonic oscillatory states of the electromechanical model. In section 3.3, we extend our investigations by considering the electromechanical transducer with a large number of function in series. The effects of the number of a linear mechanical oscillator on the behavior of the model are discussed and it appears that for some set of physical parameters, the undesired behavior disappears with the increase of the number of the linear mechanical oscillators. We consider in section 3.4 the dynamics of the model with double functions in parallel. After describing the model and giving the resulting equations of motion, we derived the amplitudes of the harmonic oscillations and time delay. Section 3.5 is devoted to the conclusion of this Chapter.

3.2 Electromechanical transducer with double functions in series

3.2.1 Model and equations of motion

The electromechanical transducer with double functions in series is shown in Figure 3.1. It is composed of an electrical part (**Duffing** oscillator) coupled magnetically and in series to a mechanical part governed by two linear mechanical oscillators. The electrical part of the system is that presented before in the first chapter. The mechanical part is now composed of two mobile beams which can move respectively along the $\vec{y}$ and $\vec{z}$ axis on both sides. The rods T and T' are bound to mobile beams with springs of constants k and k'. The motion of the entire system is governed by the following nondimensional coupled differential equations

$$\begin{aligned} \ddot{x} + \gamma\dot{x} + x + \beta x^3 + \lambda_1\dot{x}_1 + \lambda_2\dot{x}_2 &= E_o \cos wt, \\ \ddot{x}_1 + \gamma_1\dot{x}_1 + w_1^2 x_1 - \lambda_{11}\dot{x} &= 0, \\ \ddot{x}_2 + \gamma_2\dot{x}_2 + w_2^2 x_2 - \lambda_{21}\dot{x} &= 0. \end{aligned} \tag{3.1}$$

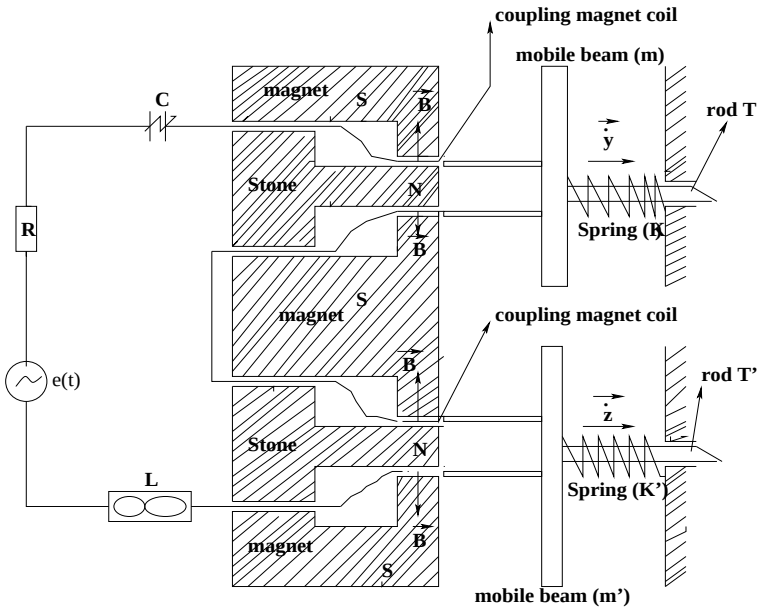

Figure 3.1: *Electromechanical transducer with double functions in series.*

The electrical part is represented by the variable x while x_1 and x_2 stand for the mechanical part (the two linear oscillators). x denotes the instantaneous electrical charge of the condenser, x_1 and x_2 the displacements of the two mobile beams. γ and γ_i are respectively the damping coefficients of the **Duffing** oscillator and the linear oscillators. The quantities λ_i and λ_{i1} are the coupling coefficients, β the nonlinear coefficient, w_1 and w_2 are the natural frequencies. E_o and w are respectively the amplitude and frequency of the external excitation (sinusoidal voltage source), while t is the non-dimensional time.

3.2.2 Amplitudes of the harmonic oscillations and time delay

In this subsection, we aim to derive the amplitude of the harmonic oscillations of equations (3.1). We use the harmonic balance method [III1]. For this purpose, we express x, x_1

and x_2 in the form

$$\begin{aligned} x &= a_1 \cos wt + a_2 \sin wt, \\ x_1 &= b_1 \cos wt + b_2 \sin wt, \\ x_2 &= c_1 \cos wt + c_2 \sin wt. \end{aligned} \tag{3.2}$$

Inserting equations (3.2) in equations (3.1) and equating the coefficients of $coswt$ and $sinwt$ separately to zero (assuming that the terms due to higher frequencies can be neglected), it comes after some algebraic manipulations that the amplitudes A, A_1 and A_2 satisfy the following nonlinear equations

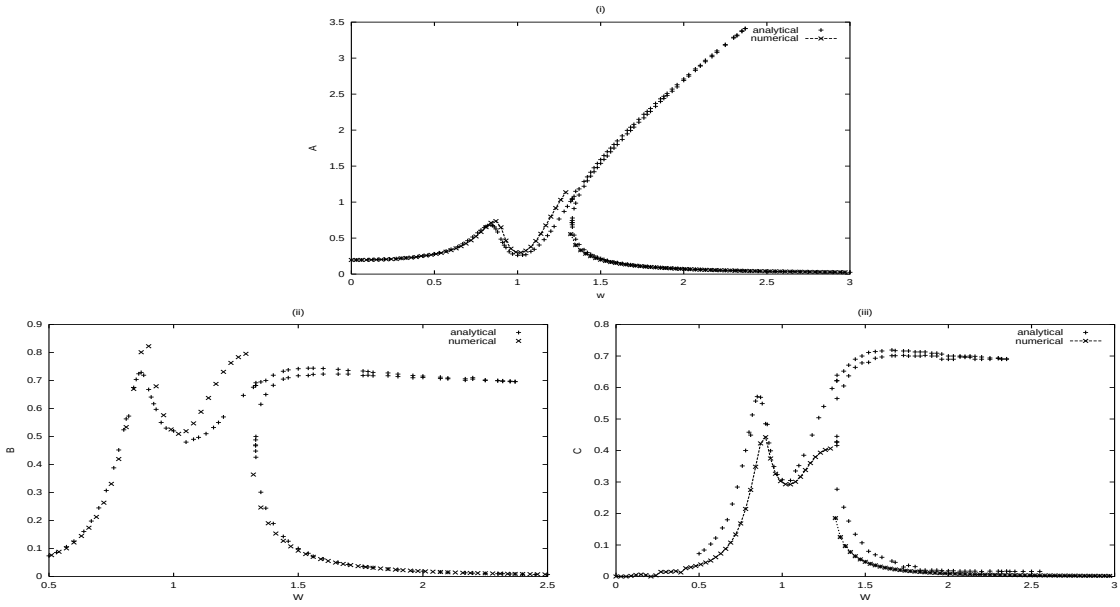

Figure 3.2: *Analytical and numerical frequency-response curves. (i) corresponding for $A(w)$, (ii) for $A_1(w)$ and (iii) for $A_2(w)$ with $E_0 = 0.2, \beta = 0.5, \gamma = 0.01, \gamma_1 = 0.2, \gamma_2 = 0.23$, $\lambda_1 = 0.4, \lambda_2 = 0.15, \lambda_{11} = 0.2, \lambda_{21} = 0.4, w_1 = w_2 = 1.0, E_0 = 0.2$.*

$$\begin{aligned} &\frac{9}{16}\beta^2 A^6 + \frac{3}{2}\beta F_2 A^4 + (F_2^2 + G_2^2)A^2 - E_0^2 = 0, \\ &A_1 = \frac{\lambda_{11} w}{\sqrt{D_1}} A, \\ &A_2 = \frac{\lambda_{21} w}{\sqrt{D_2}} A, \end{aligned} \tag{3.3}$$

where

$$\begin{aligned} A^2 &= a_1^2 + a_2^2, \qquad A_1^2 = b_1^2 + b_2^2, \qquad A_2^2 = c_1^2 + c_2^2, \\ D_2 &= (w_2^2 - w^2)^2 + w^2\gamma_2^2, \\ D_1 &= (w_1^2 - w^2)^2 + w^2\gamma_1^2, \\ F_2 &= 1 - w^2 - \frac{\lambda_1\lambda_{11} w^2(w_1^2 - w^2)}{D_1} - \frac{\lambda_2\lambda_{21} w^2(w_2^2 - w^2)}{D_2}, \\ G_2 &= \gamma w + \frac{\lambda_1\lambda_{11}\gamma_1 w^3}{D_1} + \frac{\lambda_2\lambda_{21}\gamma_2 w^3}{D_2}. \end{aligned}$$

In the linear case ($\beta = 0$), the frequency-response curves of the linear electromechanical system show antiresonance and resonance peaks as we have shown in the previous Chapter

with the set of physical parameters defined in Figure 3.2. In the nonlinear case ($\beta \neq 0$), the frequency-response curves show antiresonnance and resonance peaks, and the well-known hysteresis and jump phenomena as its appears in Figure 3.2.

In view of practical purpose, it is important to analyze the time delay between the two linear mechanical oscillators. From the above analysis, the phases ϕ_1 and ϕ_2 of the mechanical oscillators are given by

$$\begin{aligned}\tan\phi_1 = \frac{b_2}{b_1} &= \frac{-(w_1^2 - w^2)(F_2 + \frac{3}{4}\beta A^2) + w\gamma_1 G_2}{G_2(w_1^2 - w^2) + w\gamma_1(F_2 + \frac{3}{4}\beta A^2)}, \\ \tan\phi_2 = \frac{c_2}{c_1} &= \frac{-(w_2^2 - w^2)(F_2 + \frac{3}{4}\beta A^2) + w\gamma_2 G_2}{G_2(w_2^2 - w^2) + w\gamma_2(F_2 + \frac{3}{4}\beta A^2)}.\end{aligned} \tag{3.4}$$

The time delay is then defined as

$$\Theta_{1,2} = \frac{\phi_1 - \phi_2}{w}. \tag{3.5}$$

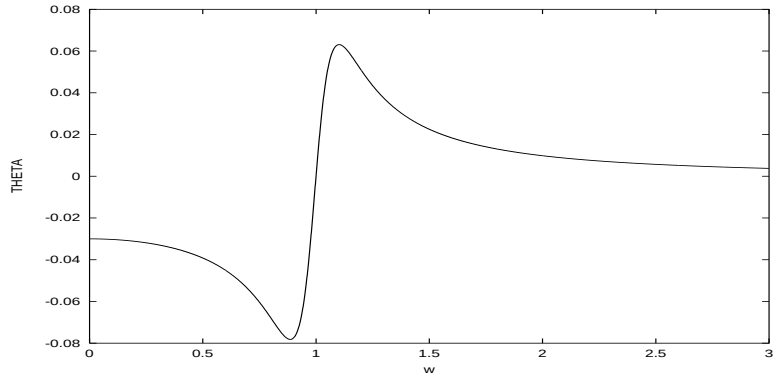

Figure 3.3: *Phase displacement curves between the two mechanical oscillators versus w with the parameters of Figure 3.2.*

This time delay is represented in Figure 3.3 when the frequency of the external excitation is varied. In the case of an exact resonance between the three oscillators (electrical and mechanical oscillators: $w_1 = w_2 = 1$) and for a fixed frequency w, $\Theta_{1,2}$ remains constant as the parameters of the system vary. In the particular case for $w_1 = w_2 = w$, both mechanical oscillators vibrate in phase. We note that the time delay changes very shortly with the variation of the nonlinearity coefficient β.

3.2.3 Stability of the harmonic states and stability chart

The harmonic oscillatory states defined by equations (3.3) are not always realized, but are actually able to exist only so long as they are stable. To study the stability of the harmonic oscillations, one considers the first nonlinear equations given by equation (3.3) rewritten as follows

$$E_0^2 = \frac{9}{16}\beta^2 A^6 + \frac{3}{2}\beta F_2 A^4 + (F_2^2 + G_2^2)A^2. \tag{3.6}$$

The appropriate analytical tool to investigate the stability conditions of the harmonic oscillatory states is the **Floquet** theory [III1], but it is difficult here to develop a **Floquet**

approach for equations (3.1). Due to the presence of hysteresis branches, we know that the turning points correspond to $\frac{dE_0^2}{dA^2} = 0$ and the stability condition can be written as $\frac{dE_0^2}{dA^2} > 0$. This shows that the periodic solutions are stable under such conditions that the amplitude A increases with the increase of the amplitude E_0 of the external excitation. From the physical point of view, this is a plausible conclusion. Differentiating E_0^2 with respect to A^2, it comes that the boundary curve between the stable and unstable regions is given by

$$\frac{27}{16}\beta^2 A_c^4 + 3\beta F_2 A_c^2 + F_2^2 + G_2^2 = 0, \tag{3.7}$$

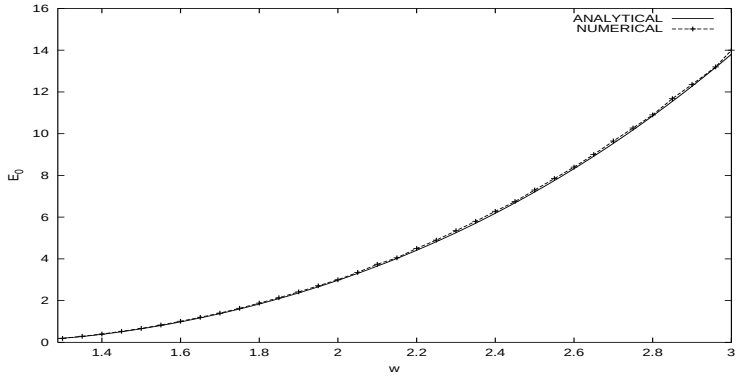

Figure 3.4: *Analytical and numerical stability boundaries in the (w, E_0) plane with the parameters of Figure 3.2.*

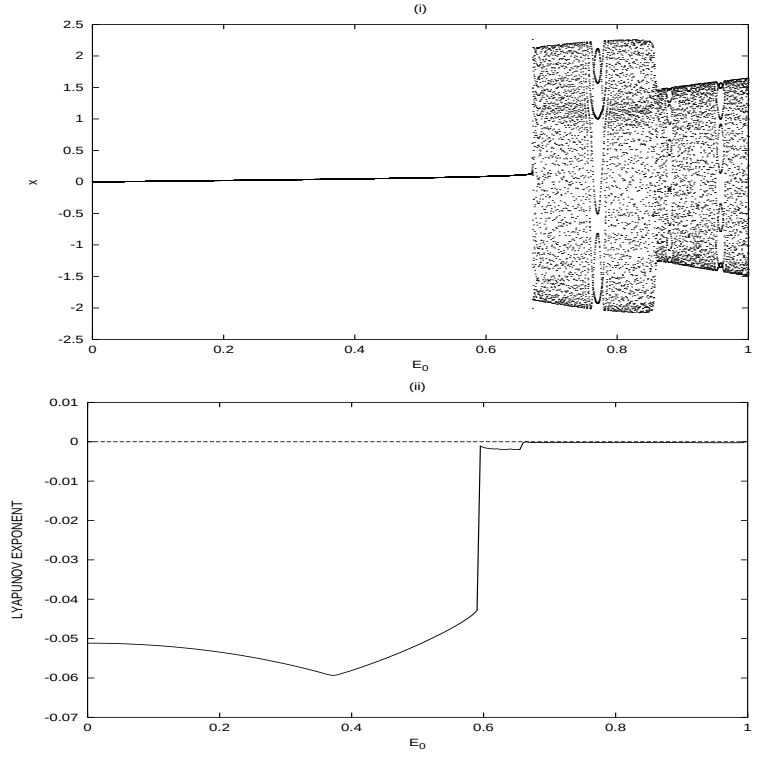

Figure 3.5: *Transition from the stability domain to the instability domain. The other parameters are those in Figure 3.2 and $w = 1.5$. (i) Bifurcation diagram showing the coordinate x versus E_0. (ii) The variation of the corresponding Lyapunov exponent.*

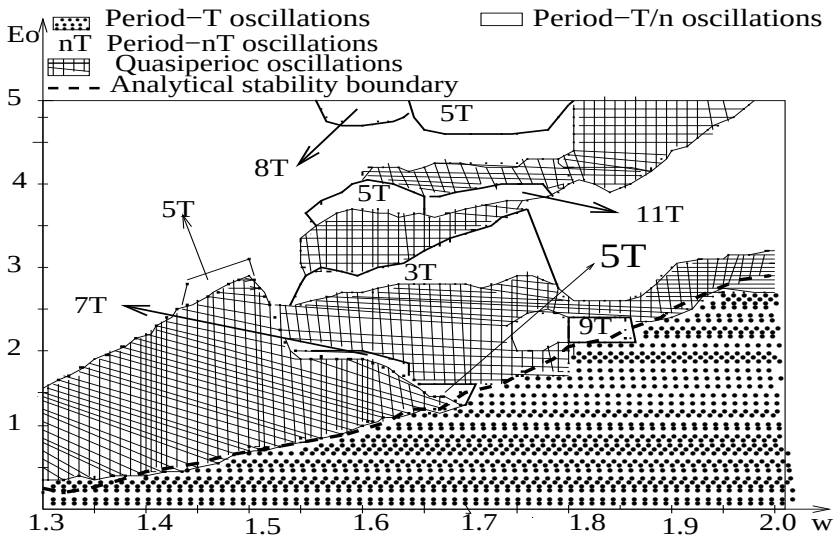

Figure 3.6: *Stability chart in the (w, E_0) plane with the parameters of Figure 3.2*

Extracting A^2 from this equation and inserting in equation (3.6), it comes that the stability boundary in the parameters space are given by the following relations:

$$E_{0\pm}^2 = \frac{9}{16}\beta^2 A_{c\pm}^6 + \frac{3}{2}\beta F_2 A_{c\pm}^4 + (F_2^2 + G_2^2)A_{c\pm}^2, \tag{3.8}$$

where

$$A_{c\pm}^2 = \frac{-8F_2 \pm \sqrt{F_2^2 - 3G_2^2}}{9\beta}.$$

In Figure 3.4, we have drawn the stability boundary of the harmonic oscillations in the (w, E_0) plane with the parameters of Figure 3.2. The domain of stability is the region below the curves where $\frac{dE_0^2}{dA^2}$ is positive. Our analytical results are confirmed by the direct numerical simulations of equations (3.1). For instance, with $w = 1.4$, the analytical treatment shows that the harmonic oscillations are stable for $E_0 < 0.39$ while from the numerical simulation we obtain $E_0 < 0.40$. Before the critical value of E_0, the system shows the periodic oscillations while after this critical value of E_0, the system exhibits a quasiperiodic behavior and period-T/n (where n being the integer) oscillations. To look the types of behaviors the electromechanical model exhibits in the instability domains, we have drawn a bifurcation diagram and the variation of the corresponding **Lyapunov** exponent as E_0 varies for $w = 1.5$ with the parameters of Figure 3.2. Our results are reported in Figure 3.5 and the following results are observed. As the amplitude E_0 increases, a period-T oscillations exist until $E_0 = 0.67$ (critical value corresponding to the limit value of E_0 for the stability of the harmonic oscillations) where a transition from period-T oscillations to a quasiperiodic behavior appears.

In Figure 3.6, we derive the stability chart using the numerical simulations of the equations of motion (3.1). The resulting phase diagram in the (w, E_0) plane is traced out by using the bifurcation diagram when the amplitude E_0 varies for a fixed frequency w. The following results are observed. One observes that as the amplitude E_0 increases, the system exhibits quasiperiodic oscillations, period-T/n and period-nT oscillations, within a rang of the frequency w. For example for $w = 1.6$, we have period-T oscillations for

$E_0 \in [0.0; 1.0]$, quasiperiodic oscillations for $E_0 \in [1.0; 1.8] \cup [1.9; 2.6] \cup [3.0; 3.7]$, period-7T oscillations for $E_0 \in [1.8; 1.9]$, period-3T oscillations for $E_0 \in [2.6; 3.0]$, period-5T oscillations for $E_0 \in [3.7; 4.0]$, etc..

3.2.4 Sub- and superharmonic oscillations

As we have explained before when E_0 is large, higher or superharmonic and subharmonic oscillations can be generated. To deal with such oscillations in our model, we use the multiple time scales method which is more indicated to find and establish the amplitudes of various orders of resonant states [III1]. For this method, we seek an asymptotic expansion of equations (3.1) in the form

$$\begin{aligned} x &= \epsilon x_{01}(T_o, T_2) + \epsilon^3 x_{03}(T_o, T_2) + ... \\ x_1 &= \epsilon x_{11}(T_o, T_2) + \epsilon^3 x_{13}(T_o, T_2) + ... \\ x_2 &= \epsilon x_{21}(T_o, T_2) + \epsilon^3 x_{23}(T_o, T_2) + ... \end{aligned} \tag{3.9}$$

To examine such resonances, we set $\gamma_i = \epsilon^2 \gamma_{oi}$, $\gamma = \epsilon^2 \gamma_o$, $\lambda_i = \epsilon^2 \lambda_{oi}$ and $\lambda_{ik} = \epsilon^2 \lambda_{oik}$ (with i,k=1,2), so that in the case of sub- and superharmonic resonances the effects of the damping, nonlinearity, and coupling coefficients appear in the same perturbation equations. Then the amplitude E_o is taken at the order $E_0 = \epsilon E$. Inserting these expansions in equations (3.1) and equating coefficients of like powers of ϵ, we obtain
Order ϵ,

$$\begin{aligned} &D_o^2 x_{01} + x_{01} = E \cos w T_o, \\ &D_o^2 x_{11} + w_1^2 x_{11} = 0, \\ &D_o^2 x_{21} + w_2^2 x_{21} = 0, \end{aligned} \tag{3.10}$$

Order ϵ^3,

$$\begin{aligned} D_o^2 x_{03} + x_{03} &= -2D_o D_2 x_{01} - \gamma_o D_o x_{01} - \beta x_{01}^3 - \lambda_{o1} D_o x_{11} - \lambda_{o2} D_o x_{21}, \\ D_o^2 x_{13} + w_1^2 x_{13} &= -2D_o D_2 x_{11} - \gamma_{o1} D_o x_{11} + \lambda_{o11} D_o x_{01}, \\ D_o^2 x_{23} + w_2^2 x_{23} &= -2D_o D_2 x_{21} - \gamma_{o2} D_o x_{21} + \lambda_{o21} D_o x_{01}. \end{aligned} \tag{3.11}$$

The solutions of equations (3.10) can be expressed in the form

$$\begin{aligned} x_{01} &= A_1(T_2) \exp(jT_o) + \Lambda \exp(jwT_o) + \bar{A}_1(T_2) \exp(-jT_o) + \Lambda \exp(-jwT_o), \\ x_{11} &= A_2(T_2) \exp(jw_1 T_o) + \bar{A}_2(T_2) \exp(-jw_1 T_o), \\ x_{21} &= A_3(T_2) \exp(jw_2 T_o) + \bar{A}_3(T_2) \exp(-jw_2 T_o), \end{aligned} \tag{3.12}$$

where

$$\Lambda = \frac{1}{2} \frac{E}{1 - w^2},$$

Substituting x_{01}, x_{11} and x_{21} into equations (3.11), we obtain

$$\begin{aligned} D_o^2 x_{03} + x_{03} &= -(2jA_1' + j\gamma_o A_1 + 3\beta A_1^2 \bar{A}_1 + 6\Lambda^2 A_1) \exp(jT_o) \\ &+ (j\gamma_o w\Lambda + 4\beta\Lambda A_1 \bar{A}_1 + 3\Lambda^3 \beta) \exp(jwT_o) - \beta A_1^3 \exp(3jT_o) \\ &- 3\beta A_1^2 \Lambda \exp(j(2+w)T_o) - 3\beta A_1 \Lambda^2 \exp(j(2w+1)T_o) \\ &- 3\beta \Lambda^2 A_1 \exp(j(1-2w)T_o) - 3\beta \Lambda A_1^2 \exp(j(2-w)T_o) \\ &- \Lambda^3 \beta \exp(3jwT_o) - jw_1 \lambda_{o1} A_2 \exp(jw_1 T_o) \end{aligned}$$

$$
\begin{aligned}
& -jw_2\lambda_{o2}A_3\exp(jw_2T_o) + C.C, \\
D_o^2x_{13} + w_1^2x_{13} &= -jw_1(2A_2' + \gamma_{o1}A_2)\exp(jw_1T_o) + j\lambda_{o11}A_1\exp(jT_o) \\
& +jw\lambda_{o11}\Lambda\exp(jwT_o) + C.C, \\
D_o^2x_{23} + w_2^2x_{23} &= -jw_2(2A_3' + \gamma_{o2}A_3)\exp(jw_2T_o) + j\lambda_{o21}A_1\exp(jT_o) \\
& +jw\lambda_{o21}\Lambda\exp(jwT_o) + C.C. \qquad (3.13)
\end{aligned}
$$

From equations (3.13), it comes two interesting resonant structures. The first one is the superharmonic state $w_1 = w_2 = 1$ and $3w = 1$, and the second one corresponds to the subharmonic state $w = 3$ with $w_1 = w_2 = 1$. Therefore we restrict our attention in this subsection to the case of sub- and superharmonic resonances.

• Superharmonic resonances

We consider the case where the nonlinear oscillator enters in superharmonic resonances with the external excitation, that is $3w = 1 + \epsilon^2\sigma$. We also assume that

$$
\begin{aligned}
w_1 &= 1 + \epsilon^2\sigma_1, \\
w_2 &= 1 + \epsilon^2\sigma_2, \qquad (3.14)
\end{aligned}
$$

where σ_1, σ_2 and σ are the detuning parameters indicating the accuracy of the resonances. The secular producing terms in the equations (3.13) must be eliminated. Hence, the solvability conditions are

$$
\begin{aligned}
2jA_1' + j\gamma_oA_1 + 6\Lambda^2A_1 + jw_1\lambda_{o1}A_2\exp(j\sigma_1T_2) & \\
3\beta A_1^2\bar{A}_1 + jw_2\lambda_{o2}A_3\exp(j\sigma_2T_2) - \Lambda^3\beta\exp(j\sigma T_2) = 0, & \\
-w_1(2A_2' + \gamma_{o1}A_2)\exp(j\sigma_1T_2) + \lambda_{o11}A_1 = 0, & \\
-w_2(2A_3' + \gamma_{o2}A_3)\exp(j\sigma_2T_2) + \lambda_{o21}A_1 = 0. & \qquad (3.15)
\end{aligned}
$$

The polar notation $A_i(T_2) = \frac{1}{2}a_i(T_2)\exp(jb_i(T_2))$ can be used to show that the amplitudes and phases of both oscillators are described by the following set of first order differential equations

$$
\begin{aligned}
\frac{3}{8}\beta a_1^3 - a_1b_1' + 3\Lambda^2a_1 + \beta\Lambda^3\cos\delta - \frac{1}{2}w_1\lambda_{o1}a_2\sin\delta_1 - \frac{1}{2}w_2\lambda_{o2}a_3\sin\delta_2 &= 0, \\
\frac{1}{2}\gamma_oa_1 + a_1' + \beta\Lambda^3\sin\delta + \frac{1}{2}w_1\lambda_{o1}a_2\cos\delta_1 + \frac{1}{2}w_2\lambda_{o2}a_3\cos\delta_3 &= 0, \\
w_1a_2b_2'\cos\delta_1 + w_1(a_2' + \frac{1}{2}\gamma_{o1}a_2)\sin\delta_1 &= 0, \\
w_1(a_2' + \frac{1}{2}\gamma_{o1}a_2)\cos\delta_1 - w_1b_2'a_2\sin\delta_1 - \frac{1}{2}\lambda_{o11}a_1 &= 0, \\
w_2a_3b_3'\cos\delta_2 + w_2(a_3' + \frac{1}{2}\gamma_{o2}a_3)\sin\delta_2 &= 0, \\
w_2(a_3' + \frac{1}{2}\gamma_{o2}a_3)\cos\delta_2 - w_2b_3'a_3\sin\delta_2 - \frac{1}{2}\lambda_{o21}a_1 &= 0, \qquad (3.16)
\end{aligned}
$$

where $\delta = \sigma T_2 - b_1, \delta_1 = \sigma_1T_2 + b_2 - b_1$ and $\delta_2 = \sigma_2T_2 + b_3 - b_1$. For the steady-state responses, we must have $a_i' = 0$ and $\delta_i' = 0$. Thus $b_1' = \sigma, b_2' = \sigma - \sigma_1$ and $b_3' = \sigma - \sigma_2$. Eliminating δ_i from equations (3.16), we obtain the following set of nonlinear equations

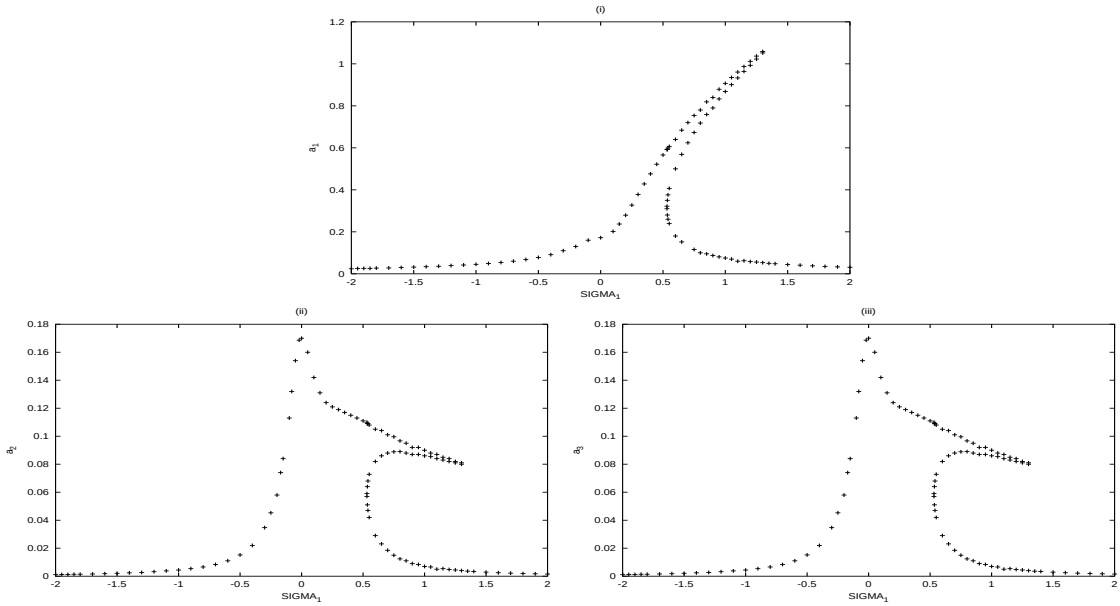

Figure 3.7: *Superharmonic frequency-response curves. (i) corresponding for* $a_1(\sigma_1)$ *, (ii) for* $a_2(\sigma_1)$ *and (iii) for* $a_3(\sigma_1)$ *with the parameters* $E = 0.5, \gamma_o = 0.1, \gamma_{o2} = 0.4, \lambda_{o1} = 0.12, \lambda_{o11} = 0.2, \lambda_{o21} = 0.2; \beta = 2.5; \lambda_{o2} = 0.3, \gamma_{o1} = 0.2; \sigma_2 = \sigma_3 = 0.$

$$\begin{aligned}
&\frac{9}{64}\beta^2 a_1^6 + \frac{3}{4}\beta M_2 a_1^4 + N_2 a_1^2 - \beta^2\Lambda^6 = 0,\\
&a_3^2 = \frac{\lambda_{o21}^2 a_1^2}{w_2^2(\gamma_{o2}^2 + 4(\sigma-\sigma_2)^2)},\\
&a_2^2 = \frac{\lambda_{o11}^2 a_1^2}{w_1^2(\gamma_{o1}^2 + 4(\sigma-\sigma_1)^2)},
\end{aligned} \tag{3.17}$$

where

$$\begin{aligned}
M_2 &= 3\Lambda^2 - \sigma + \frac{\lambda_{o1}\lambda_{o11}(\sigma-\sigma_1)}{4(\sigma-\sigma_1)^2+\gamma_{o1}^2} + \frac{\lambda_{o2}\lambda_{o21}(\sigma-\sigma_2)}{4(\sigma-\sigma_2)^2+\gamma_{o2}^2},\\
N_2 &= \frac{1}{4}\left\{\gamma_o + \frac{\lambda_{o1}\lambda_{o11}\gamma_{o1}}{4(\sigma-\sigma_1)^2+\gamma_{o1}^2} + \frac{\lambda_{o2}\lambda_{o21}\gamma_{o2}}{4(\sigma-\sigma_2)^2+\gamma_{o2}^2}\right\}^2 + M_2^2.
\end{aligned}$$

Thus, in the case of superharmonic resonances, the motion of the three oscillators are coupled and described by

$$\begin{aligned}
x(t) &= \epsilon a_1 \cos(3wt + \delta_1) + \epsilon\Lambda\cos wt + 0(\epsilon^3),\\
x_1(t) &= \epsilon a_2 \cos(3wt + \delta_2 - \delta_1) + 0(\epsilon^3),\\
x_2(t) &= \epsilon a_3 \cos(3wt + \delta_3 - \delta_1) + 0(\epsilon^3).
\end{aligned} \tag{3.18}$$

Using the **Newton-Raphson** algorithm, we find the amplitudes a_1, a_2 and a_3 when the detuning parameter σ is varied. In the exact internal resonances ($\sigma_2 = \sigma_1 = 0$), the superharmonic frequency-response curves obtained for a given set of parameters are provided in Figure 3.7(i) for $a_1(\sigma)$, in Figure 3.7(ii) for $a_2(\sigma)$ and in Figure 3.7(iii) for $a_3(\sigma)$. The behavior of the frequency-response curves in the superharmonic resonance show the well-known

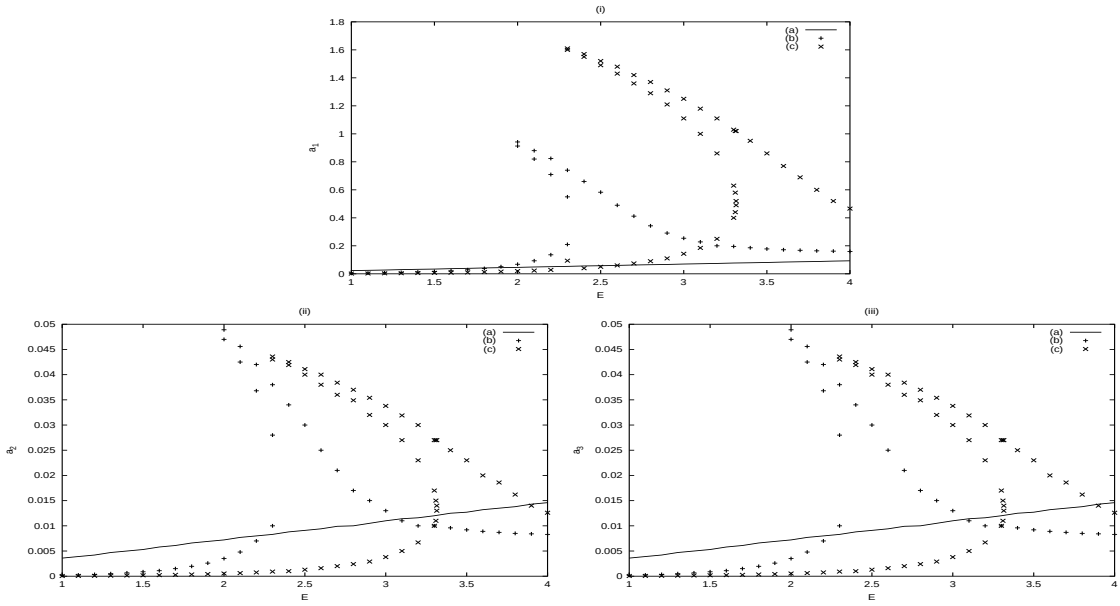

Figure 3.8: *Superharmonic amplitude-response curves. (i) corresponding for $a_1(E)$, (ii) for $a_2(E)$ and (iii) for $a_3(E)$ with the parameters of Figure 3.7 and (a): $\sigma_1 = 0.0$, (b): $\sigma_1 = 0.2$, (c): $\sigma_1 = 0.4$*

hysteresis phenomena. In Figure 3.8, we provide the superharmonic amplitude-response curves $a_i(E)$ (i=1,2,3) obtained for three fixed values of the detuning parameter σ. The curves of Figure 3.8 shows the jump phenomena for $\sigma = 1.5$ and $\sigma = 2.0$. It appears that for $\sigma = 1.2$, the hysteresis domain disappears. Our analysis show that, when $\sigma > 1.2$, the curves show the hysteresis phenomena and dissappears with decreasing of σ.

• Subharmonic resonances

To analyze these subharmonic resonances, we set $w = 3 + \epsilon^2\sigma_o$. σ_o is another detuning parameter indicating the accuracy of the subharmonic resonances. Eliminating the terms in equations (3.16) that produce secular terms in x_{03}, x_{13}, x_{23} and considering the expressions given by equations (3.14), we have

$$\begin{aligned} 2jA_1' + j\gamma_o A_1 + 6\Lambda^2 A_1 + jw_1\lambda_{o1}A_2\exp(j\sigma_1 T_2) \\ 3\beta A_1^2\bar{A}_1 + jw_2\lambda_{o2}A_3\exp(j\sigma_2 T_2) + 3\Lambda\beta\bar{A}_1^2\exp(j\sigma_o T_2) = 0, \\ -w_1(2A_2' + \gamma_{o1}A_2)\exp(j\sigma_1 T_2) + \lambda_{o11}A_1 = 0, \\ -w_2(2A_3' + \gamma_{o2}A_3)\exp(j\sigma_2 T_2) + \lambda_{o21}A_1 = 0. \end{aligned} \tag{3.19}$$

Again, introducing the polar notations for $A_i (i = 1, 2, 3)$ and separating real and imaginary parts yields

$$\begin{aligned} \frac{3}{8}\beta a_1^3 - a_1 b_1' + 3\Lambda^2 a_1 + \frac{3}{4}\beta\Lambda a_1^2\cos\delta_o - \frac{1}{2}w_1\lambda_{o1}a_2\sin\delta_1 - \frac{1}{2}w_2\lambda_{o2}a_3\sin\delta_2 &= 0, \\ \frac{1}{2}\gamma_{o1}a_1 + a_1' + \frac{3}{4}\beta\Lambda a_1^2\sin\delta_o + \frac{1}{2}w_1\lambda_{o1}a_2\cos\delta_1 + \frac{1}{2}w_2\lambda_{o2}a_3\cos\delta_2 &= 0, \\ a_2 b_2'\cos\delta_1 + (a_2' + \frac{1}{2}\gamma_{o1}a_2)\sin\delta_1 &= 0, \end{aligned}$$

$$
\begin{aligned}
w_1(a_2' + \frac{1}{2}\gamma_{o1}a_2)\cos\delta_1 - w_1 b_2' a_2 \sin\delta_1 - \frac{1}{2}\lambda_{o11}a_1 &= 0, \\
a_3 b_3' \cos\delta_2 + (a_3' + \frac{1}{2}\gamma_{o2}a_3)\sin\delta_2 &= 0, \\
w_2(a_3' + \frac{1}{2}\gamma_{o2}a_3)\cos\delta_2 - w_2 b_3' a_3 \sin\delta_2 - \frac{1}{2}\lambda_{o21}a_1 &= 0, \qquad (3.20)
\end{aligned}
$$

where $\delta_o = \sigma_o - 3b_1, \delta_1 = \sigma_1 T_2 + b_2 - b_1$ and $\delta_2 = \sigma_2 T_2 + b_3 - b_1$. For the steady-state responses, we must have $a_i' = 0$ and $\delta_i' = 0$. Thus $b_1' = \frac{\sigma_o}{3}, b_2' = \frac{\sigma_o}{3} - \sigma_1$ and $b_2' = \frac{\sigma_o}{3} - \sigma_2$. Eliminating δ_i from equations (3.20), we obtain the following set of nonlinear equations

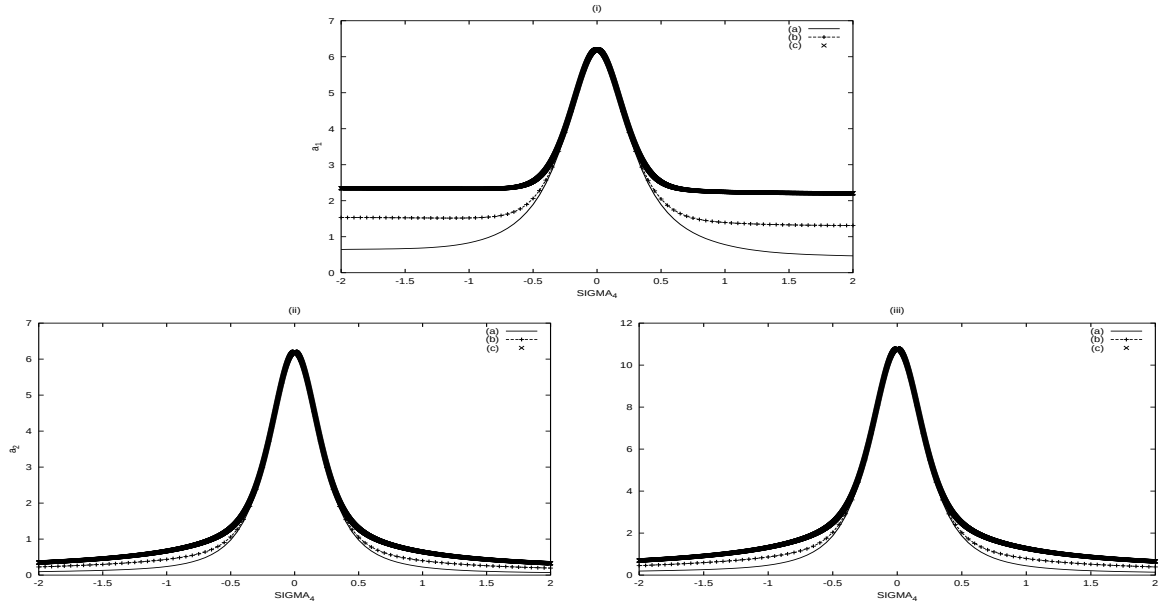

Figure 3.9: *Subharmonic frequency-response curves . (i) for $a_1(\sigma_4)$, (ii) for $a_2(\sigma_4)$ and (iii) for $a_3(\sigma_4)$ with the parameters $\gamma_o = 0.5, \gamma_{o2} = 0.23, \lambda_{o1} = 0.4, \lambda_{o11} = 0.2, \lambda_{o21} = 0.4; \beta = 0.5;$ $\sigma_2 = \sigma_3 = 0, \lambda_{o2} = 0.5, \gamma_{o1} = 0.2$ and $(a) : E = 1; (b) : E = 5, (c) : E = 8$.*

$$
\begin{aligned}
&\frac{9}{64}\beta^2 a_1^6 + \frac{3}{4}\beta P_2 a_1^4 + Q_2 a_1^2 = 0, \\
&a_3^2 = \frac{\lambda_{o21}^2 a_1^2}{w_2^2(\gamma_{o2}^2 + 4(\frac{\sigma_o}{3} - \sigma_2)^2)}, \\
&a_2^2 = \frac{\lambda_{o11}^2 a_1^2}{w_1^2(\gamma_{o1}^2 + 4(\frac{\sigma_o}{3} - \sigma_1)^2)}, \qquad (3.21)
\end{aligned}
$$

where

$$
\begin{aligned}
P_2 &= 3\Lambda^2 - \frac{\sigma_o}{3} - \frac{3}{4}\beta\Lambda^2 + \frac{\lambda_{o1}\lambda_{o11}(\frac{\sigma_o}{3} - \sigma_1)}{4(\frac{\sigma_o}{3} - \sigma_1)^2 + \gamma_{o1}^2} + \frac{\lambda_{o2}\lambda_{o21}(\frac{\sigma_o}{3} - \sigma_2)}{4(\frac{\sigma_o}{3} - \sigma_2)^2 + \gamma_{o2}^2}, \\
Q_2 &= \frac{1}{4}\left\{\gamma_o + \frac{\lambda_{o1}\lambda_{o11}\gamma_{o1}}{4(\frac{\sigma_o}{3} - \sigma_1)^2 + \gamma_{o1}^2} + \frac{\lambda_{o2}\lambda_{o21}\gamma_{o2}}{4(\frac{\sigma}{3} - \sigma_2)^2 + \gamma_{o2}^2}\right\}^2 + \left\{P_2 + \frac{3}{4}\beta\Lambda^2\right\}^2.
\end{aligned}
$$

Equations (3.21) show that either $a_1 = 0$ or

$$
\frac{9}{64}\beta^2 a_1^4 + \frac{3}{4}\beta P_2 a_1^2 + Q_2 = 0, \qquad (3.22)
$$

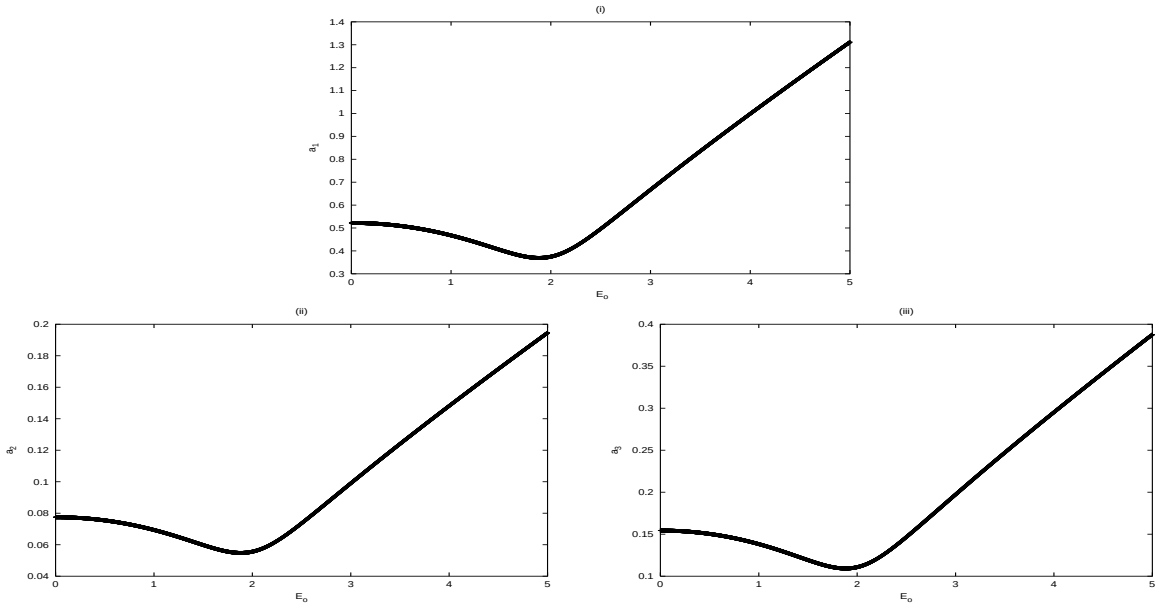

Figure 3.10: *Subharmonic amplitude-response curves. (i) for $a_1(E)$, (ii) for $a_2(E)$ and (iii) for $a_3(E)$ with the parameters of Figure 3.9 and $\sigma_o = 3$*

which is quadratic in a_1^2. Its solutions are

$$a_1^2 = p \pm \sqrt{p^2 - q}, \tag{3.23}$$

where

$$p = \frac{-8P_2}{3\beta}, \qquad\qquad q = \frac{64Q_2}{9\beta^2}.$$

It follows for the procedure use in the previous Chapter that, nontrivial solutions can exist only if

$$p_2 - \sqrt{p_2^2 + q_2} \leq \Lambda^2 \leq p_2 + \sqrt{p_2^2 + q_2},$$

with

$$p_2 = \frac{3\beta(U_2 - \frac{\sigma_4}{3})}{4[(3 - \frac{3}{4}\beta)^2 - 9]}, \qquad\qquad q_2 = \frac{(\gamma + V_2)^2}{4[(3 - \frac{3}{4}\beta)^2 - 9]},$$

$$\begin{aligned} U_2 &= \frac{\lambda_{o1}\lambda_{o11}(\frac{\sigma_o}{3} - \sigma_1)}{4(\frac{\sigma_o}{3} - \sigma_1) + \gamma_{o1}^2} + \frac{\lambda_{o2}\lambda_{o21}(\frac{\sigma_o}{3} - \sigma_2)}{4(\frac{\sigma_o}{3} - \sigma_2) + \gamma_{o2}^2}, \\ V_2 &= \frac{\lambda_{o1}\lambda_{o11}\gamma_{o1}}{4(\frac{\sigma_o}{3} - \sigma_1) + \gamma_{o1}^2} + \frac{\lambda_{o2}\lambda_{o21}\gamma_{o2}}{4(\frac{\sigma_o}{3} - \sigma_2) + \gamma_{o2}^2}. \end{aligned}$$

In the $\Lambda\sigma_o$-plane, the boundary of the region where nontrivial solutions can exist is given by

$$\Lambda_c^2 = p_2 \pm \sqrt{p_2^2 + q_2}.$$

In the subharmonic resonances, the motion of the two oscillators are described by

$$\begin{aligned} x(t) &= \epsilon a_1 \cos(\frac{1}{3}wt + \delta_o) + \epsilon\Lambda \cos wt + 0(\epsilon^3), \\ x_1(t) &= \epsilon a_2 \cos(\frac{1}{3}wt + \delta_1 - \delta_o) + 0(\epsilon^3), \\ x_2(t) &= \epsilon a_3 \cos(\frac{1}{3}wt + \delta_2 - \delta_o) + 0(\epsilon^3). \end{aligned}$$

We find the amplitudes a_1, a_2 and a_3 when the detuning parameter σ_o is varied. In the exact internal resonances ($\sigma_2 = \sigma_1 = 0$), the subharmonic frequency-response curves obtained for a given set of parameters are provided in Figure 3.9(i) for $a_1(\sigma_o)$, in Figure 3.9(ii) for $a_2(\sigma_o)$ and in Figure 3.9(iii) for $a_3(\sigma_o)$. We note that there is no jump phenomena in this case and the curves show the resonance peaks for different values of E. The amplitude-response curves are reported in Figure 3.10.

3.3 Extension to a large number of functions

3.3.1 Model and equations of motion

As in the previous section, we extend our analysis to the dynamical behavior of an electromechanical transducer with a large number of functions in series, shown in Figure 3.11. It is composed of an electrical part coupled magnetically and in series to a mechanical part governed by **n** linear mechanical oscillators. The mechanical part is now composed of **n** mobile beams which can move respectively along the $\vec{x}_i$ (i=1,,..,**n**) axis on both sides. The rods T_i are bound to mobile beams with springs of constants k_i. The motion of the entire system is now governed by the following **n**+1 nondimensional coupled nonlinear differential equations

$$\begin{aligned} \ddot{x} + \gamma\dot{x} + x + \beta x^3 + \sum_{i=1}^{\mathbf{n}} \lambda_i \dot{x}_i &= E_0 \cos wt, \\ \ddot{x}_1 + \gamma_1 \dot{x}_1 + w_1^2 x_1 - \lambda_{11}\dot{x} &= 0, \\ \vdots \qquad\qquad\qquad\qquad & \vdots \\ \ddot{x}_{\mathbf{n}} + \gamma_{\mathbf{n}} \dot{x}_{\mathbf{n}} + w_{\mathbf{n}}^2 x_{\mathbf{n}} - \lambda_{\mathbf{n}1}\dot{x} &= 0. \end{aligned} \tag{3.24}$$

The variable x denotes the instantaneous electrical charge of the condenser while x_i stand for the displacement of the **ith** mobile beams of the mechanical part. The quantities γ and γ_i are the damping coefficients while λ_i and λ_{i1} are the coupling coefficients. w_i are the natural frequencies and β the nonlinearity.

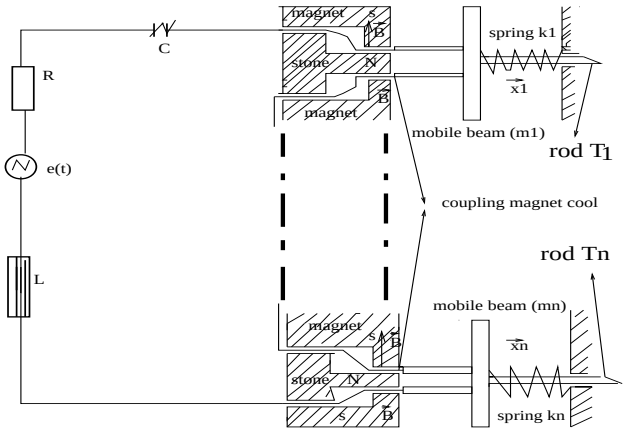

Figure 3.11: *Electromechanical transducer with a large number of functions in series*

3.3.2 Amplitudes of the harmonic oscillations and time delay

We derive the amplitudes of the harmonic oscillations of equations (3.24) by express x and x_i in the form

$$\begin{aligned} x &= a_1 \cos wt + a_2 \sin wt, \\ x_i &= b_{i1} \cos wt + b_{i2} \sin wt, \qquad (i = 1, ..., \mathbf{n}). \end{aligned} \tag{3.25}$$

Setting $A^2 = a_1^2 + a_2^2$ and $A_i^2 = b_{i1}^2 + b_{i2}^2$, inserting equations (3.25) into equations (3.24) and make use of the previous Section, it comes that the amplitudes A and A_i of the harmonic oscillations satisfy the following nonlinear equations

$$\begin{aligned} &\frac{9}{16}\beta^2 A^6 + \frac{3}{2}\beta F_n A^4 + (F_n^2 + G_n^2)A^2 - E_0^2 = 0, \\ &A_i = \frac{\lambda_{i1}}{w_i\sqrt{D_i}}A, \end{aligned} \tag{3.26}$$

where

$$\begin{aligned} D_i &= (w_i^2 - w^2)^2 + w^2\gamma_i^2, \\ F_n &= 1 - w^2 - \sum_{i=1}^{\mathbf{n}} \frac{\lambda_i \lambda_{i1} w^2 (w_i^2 - w^2)}{D_i}, \\ G_n &= \gamma w + \sum_{i=1}^{\mathbf{n}} \frac{\lambda_i \lambda_{i1} \gamma_i w^3}{D_i}. \end{aligned}$$

We note that when the $\mathbf{n}$ linear mechanical oscillators are identical, we obtain the following expressions of F_n and G_n

$$\begin{aligned} F_n &= 1 - w^2 - \frac{\mathbf{n}\lambda_1 \lambda_{11} w^2 (w_1^2 - w^2)}{D_1}, \\ G_n &= \gamma w + \frac{\mathbf{n}\lambda_1 \lambda_{11} \gamma_1 w^3}{D_1}. \end{aligned}$$

In the linear case ($\beta = 0$), the frequency-response curves of the linear electromechanical model with a large number of functions are represented in Figure 3.12 for three values of $\mathbf{n}$. The effects of a number of linear mechanical oscillators are observed and the curves also show one peak of antiresonances and two peaks of resonances. It is found that the points of resonance are moved when the number $\mathbf{n}$ of the linear mechanical oscillator increases while the amplitudes A and A_i decrease and vanish with a large value of $\mathbf{n}$.

In the nonlinear case, we use the **Newton-Raphson** algorithm to find the behavior of the frequency-response curves when the frequency of the external excitation w varies. The results are reported in Figure 3.13 where several frequency-response curves are shown. These Figures illustrate the effects of the number of the linear mechanical oscillators on the behavior of the electromechanical model. It appears the following comments. In the case of the exact internal and external resonances between the $\mathbf{n}$+1 oscillators ($w = w_i = 1$), the electromechanical model vibrates with a small value of the amplitude (antiresonance phenomenon) which decreases when the number of the linear mechanical oscillator increases. The model with a large number of functions in series can be used as an electromechanical vibration absorber [III2]. The domain of hysteresis phenomena decreases with the increase of the number $\mathbf{n}$ of the linear mechanical oscillators. Our investigation shows that the hysteresis phenomena disappears for large $\mathbf{n}$. For instance, with the parameters of Figure

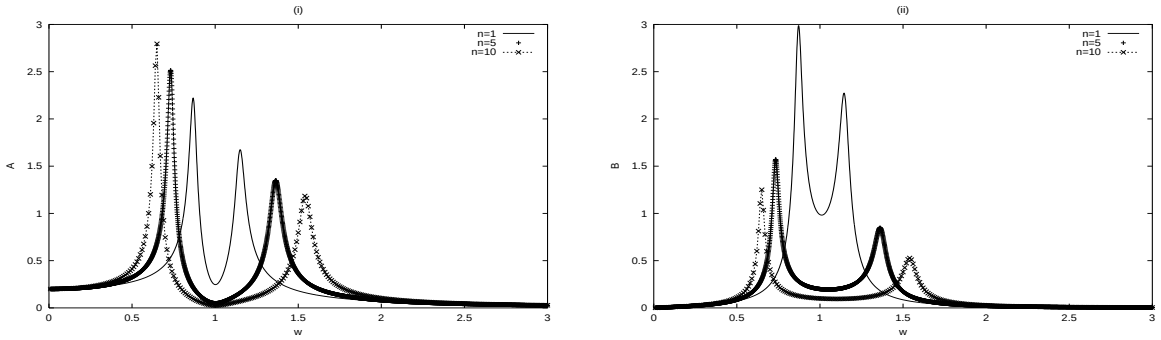

Figure 3.12: *Effects of the number of mechanical oscillators on the linear frequency-response curves with the parameters* $\gamma_1 = 0.1; \gamma = 0.01; \lambda_{11} = 0.4; \lambda_1 = 0.2; w_1 = 1.0; E_0 = 0.2$.

3.12 and $\beta = 0.95$, the disapearence of the hysteresis branches is obtained for $\mathbf{n} > 20$. In this case, the extension of the number of mechanical oscillators is using to absorb the hysteresis phenomena. In Figure 3.14, the effects of a number of linear mechanical oscillators on the amplitude-response curves are also presented and it is found that the jump phenomena disappears when the number **n** increases.

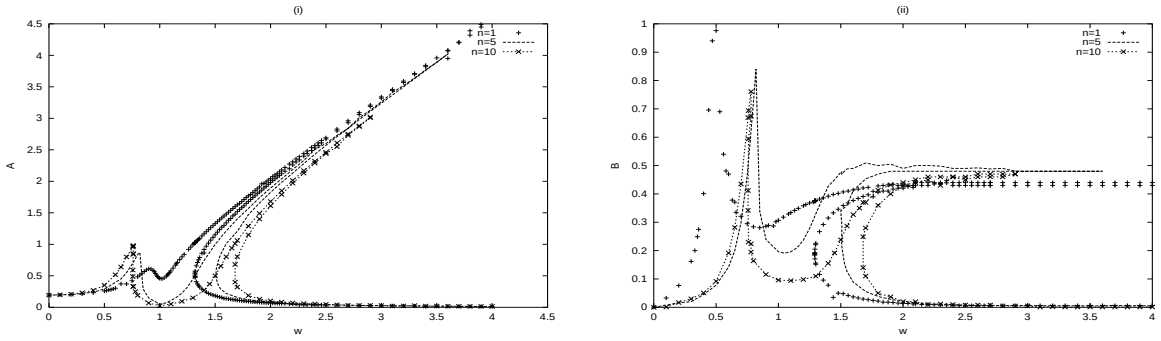

Figure 3.13: *Effects of the number of linear mechanical oscillators on the nonlinear frequency-response curves with the parameters of Figure 3.12 and* $\beta = 0.95$.

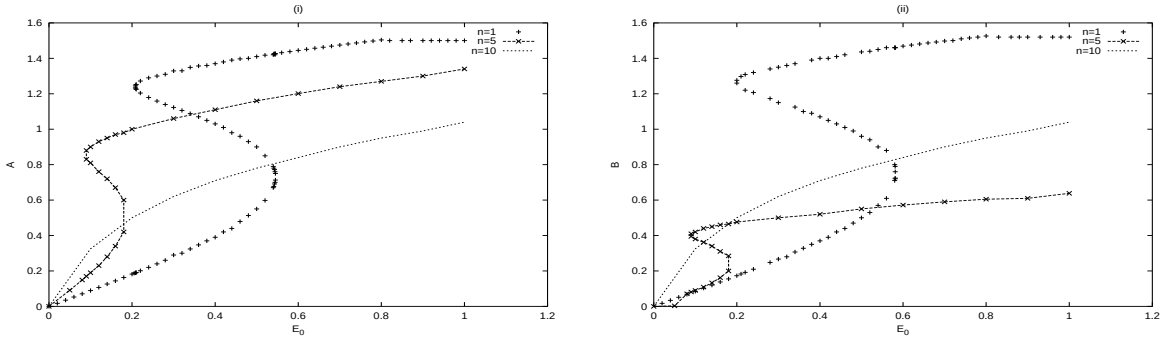

Figure 3.14: *Effects of the number of a linear mechanical oscillators on the amplitude-response curves with the parameters of Figure 3.12 and* $w = 1.5, \beta = 0.95$.

To determine the time delay between the **ith** and $(\mathbf{i+1})$**th** mechanical oscillators, let us express the corresponding phases ϕ_i and ϕ_{i+1} of any **ith** and **(i+1)th** mechanical oscillators as

$$\tan\phi_i \quad = \quad \frac{b_{i2}}{b_{i1}} = \frac{-(w_i^2 - w^2)(F_{i+1} + \frac{3}{4}\beta A^2) + w\gamma_i G_{i+1}}{G_{i+1}(w_i^2 - w^2) + w\gamma_i(F_{i+1} + \frac{3}{4}\beta A^2)},$$

$$\tan\phi_{i+1} = \frac{b_{(i+1)2}}{b_{(i+1)1}} = \frac{-(w_{i+1}^2 - w^2)(F_{i+1} + \frac{3}{4}\beta A^2) + w\gamma_{i+1}G_{i+1}}{G_{i+1}(w_{i+1}^2 - w^2) + w\gamma_{i+1}(F_{i+1} + \frac{3}{4}\beta A^2)}. \tag{3.27}$$

The time delay is then defined as:

$$\Theta_{i,i+1} = \frac{\phi_i - \phi_{i+1}}{w}. \tag{3.28}$$

The behavior of the time delay is not different from that presented in Figure 3.2. When the frequency of the external excitation is varied and it appears the following results. In the case of an exact resonance between the **n**+1 oscillators (electrical and **n** linear mechanical oscillators: $w_1 = w_2 = w_3 = ... = 1.0$) and for a fixed frequency w, $\Theta_{i,i+1}$ remains constant as the parameters of the system vary. In the particular case for $w_i = w$, all **ith** and **(i+1)th** linear mechanical oscillators vibrate in phase and we have

$$\tan\phi_i = \tan\phi_{i+1} = \frac{G_{i+1}}{F_{i+1} + \frac{3}{4}\beta A^2}.$$

We note that as in the case of electromechanical model with double functions, the time delay changes very shortly with the variation of the nonlinearity coefficient β.

3.3.3 Stability of the harmonic oscillations

We shall now determine the stability of the harmonic oscillations. By the procedure analogous for that of the model with double functions, we consider the first nonlinear equations given by equation (3.26) rewritten as follows

$$E_0^2 = \frac{9}{16}\beta^2 A^6 + \frac{3}{2}\beta F_n A^4 + (F_n^2 + G_n^2)A^2. \tag{3.29}$$

Due to the presence of hysteresis branches, we know that the turning points correspond to $\frac{dE_0^2}{dA^2} = 0$ and the stability condition can be written as $\frac{dE_0^2}{dA^2} > 0$. Differentiating E_0^2 with respect to A^2, it comes that the boundary curve between the stable and unstable regions is given by

$$\frac{27}{16}\beta^2 A_c^4 + 3\beta F_n A_c^2 + F_n^2 + G_n^2 = 0. \tag{3.30}$$

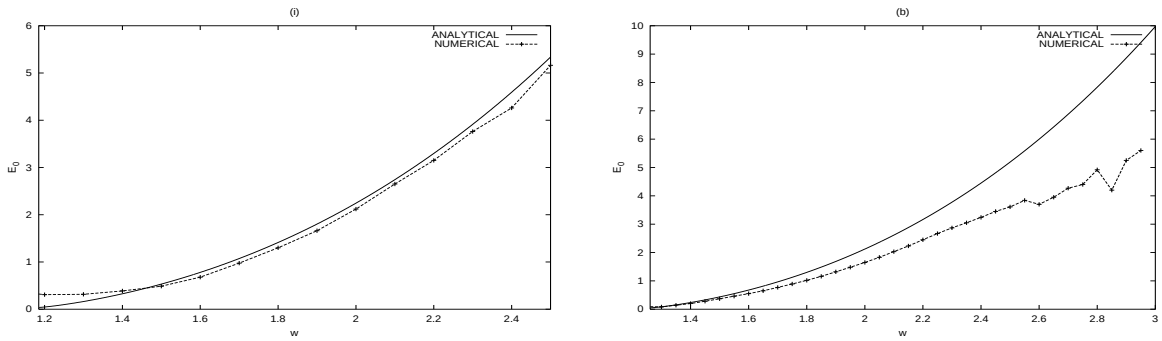

Figure 3.15: *Analytical and numerical stability boundaries in the (w, E_0) plane with the parameters of figure 3.13 (i):n=1 and (ii): n=2.*

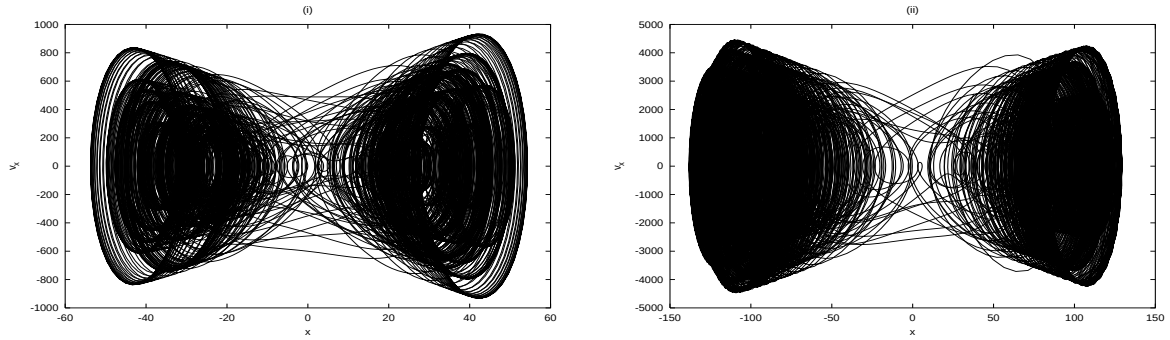

Figure 3.16: *Behavior of the model in the unstable domains with the parameters of figure 3.8 and n=2 (i):* $w = 1.4; E_0 = 0.5$ *and (ii):* $w = 1.6; E_0 = 0.8$.

Extracting A^2 from this equation and inserting in equation (3.29), it comes that the stability boundary in the parameters space are given by the following relations

$$E_{0\pm}^2 = \frac{9}{16}\beta^2 A_{c\pm}^6 + \frac{3}{2}\beta F_n A_{c\pm}^4 + (F_n^2 + G_n^2)A_{c\pm}^2, \tag{3.31}$$

where

$$A_{c\pm} = \frac{-8F_n \pm \sqrt{F_n^2 - 3G_n^2}}{9\beta}.$$

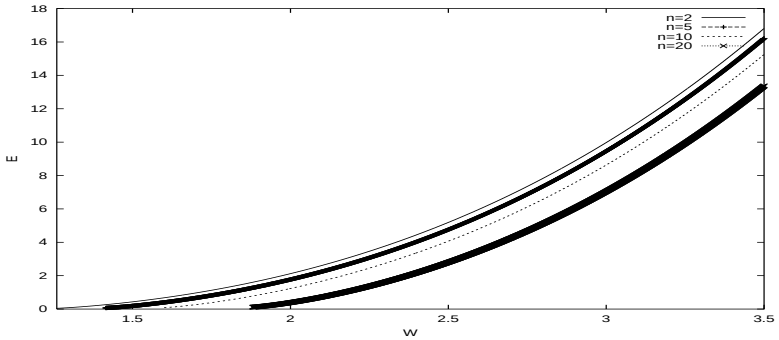

Figure 3.17: *Effect of the number of mechanical oscillators on the stability boundaries in the* (w, E_0) *plane with the parameters of Figure 3.13.*

In Figure 3.15, we have drawn the stability boundary of the harmonic oscillations in the (w, E_0) plane with the parameters of Figure 3.13 and n=1,2. The domain of stability is the region below the curves. Our analytical results are confirmed by the direct numerical simulations of equations (3.24). For instance, with $w = 1.4$ and $n = 2$, the analytical treatment shows that the harmonic oscillations are stable for $E_0 < 0.22$ while from the numerical simulations, we obtain $E_0 < 0.20$. Before the critical value of E_0, the system shows the periodic oscillations while just after this critical value of E_0, the system exhibits a quasiperiodic and a chaotic behavior. This type of behavior is shown in Figures 3.16(i) and 3.16(ii) respectively for $E_0 = 0.5; w = 1.4$ and $E_0 = 0.8; w = 1.6$. The effect of the number of mechanical oscillators on the stability boundaries is shown in Figure 3.17 with the set of physical parameters of Figure 3.13. In comparison with the stability boundaries obtained in the previous chapter following the **Floquet** theory, we have drawn in Figure 3.18 the stability boundaries curves obtained for the two analytical treatment for the case of the electromechanical transducer with one function. For low frequencies, it appears the

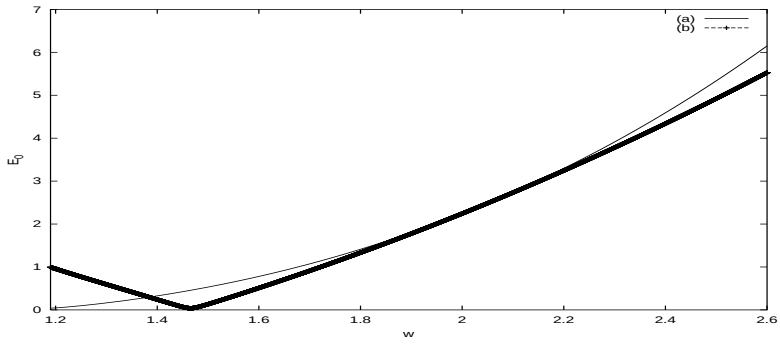

Figure 3.18: *Comparison between stability boundaries obtained follows Floquet theory and those from the hysteresis effect with the parameters of Figure 3.8 and n=1 (a): Hysteresis effect; (b): Floquet theory.*

difference between the two analytical curves. This can be explained by the fact that one of the two analytical methods is not more appropriate tool to derive stability boundaries of the harmonic oscillations on the electromechanical model.

Before closed with the above analysis, we can ressort the following comments about the two analytical methods using in this thesis to derive stability boundaries of the harmonic oscillations on electromechanical devices. Concerning the analytical method connected to the presence of hysteresis branches, we note that this method give us the stability condition and stability boundary of the periodic solutions which depending for the parameters of the electromechanical device and is physically realized. This analytical method is used in ref.[III3] to derive stability conditions of the harmonic oscillations with symmetrical and unsymmetrical non-linear characteristics. For the analytical method connected to the **Floquet** theory, we only obtained the stability boundary of the harmonic oscillations, which is not physically realized, because the resulting expressions of the **Hill** determinant is a complex number. For the physical point of view and the technological exploitation of the device, the analytical method connected to hysteresis branches is an appropriate analytical tool to investigate the stability conditions of the harmonic oscillatory states, this is a plausible conclusion.

3.3.4 Sub- and superharmonic oscillations

In the previous section, we have used the multiple time scale method [III1] to derive the amplitudes of sub- and superharmonic oscillations of the electromechanical device with double functions. We are now to extend our investigations to such device with a large number of functions. As we have briefly noted herebefore, we seek an asymptotic expansion of equations (3.24) in the following form

$$\begin{aligned} x &= \epsilon x_{01}(T_o, T_2) + \epsilon^3 x_{03}(T_o, T_2) + ... \\ x_i &= \epsilon x_{i1}(T_o, T_2) + \epsilon^3 x_{i3}(T_o, T_2) + ..., \qquad (n = 1, 2, 3, ...n). \end{aligned} \tag{3.32}$$

Inserting these expansions in equations (3.24) and equating coefficients of like powers of ϵ, we obtain
Order ϵ,

$$\begin{aligned} & D_o^2 x_{01} + x_{01} = E \cos wT_o, \\ & \vdots \qquad\qquad\qquad \vdots \\ & D_o^2 x_{i1} + w_1^2 x_{i1} = 0. \end{aligned} \tag{3.33}$$

Order ϵ^3,

$$
\begin{aligned}
&D_o^2 x_{03} + x_{03} = -2D_o D_2 x_{01} - \gamma_o D_o x_{01} - \beta x_{01}^3 - \lambda_{o1} D_o x_{11} - \sum_{i=1}^{n} \lambda_{oi} D_o x_{i1}, \\
&D_o^2 x_{13} + w_1^2 x_{13} = -2D_o D_2 x_{11} - \gamma_{o1} D_o x_{11} + \lambda_{o11} D_o x_{01}, \\
&\vdots \qquad\qquad\qquad\qquad \vdots \\
&D_o^2 x_{n3} + w_n^2 x_{n3} = -2D_o D_2 x_{n1} - \gamma_n D_o x_{n1} + \lambda_{on1} D_o x_{01}.
\end{aligned} \tag{3.34}
$$

The solutions of equations (3.33) can be expressed as

$$
\begin{aligned}
x_{01} &= A_1(T_2)\exp(jT_o) + \Lambda\exp(jwT_o) + \\
&\quad \bar{A}_1(T_2)\exp(-jT_o) + \Lambda\exp(-jwT_o), \\
x_{11} &= A_2(T_2)\exp(jw_2T_o) + \bar{A}_2(T_2)\exp(-jw_2T_o), \\
&\vdots \qquad\qquad\qquad\qquad \vdots \\
x_{i1} &= A_{i+1}(T_2)\exp(jw_+1_o) + \bar{A}_{i+1}(T_2)\exp(-jw_{i+1}T_o).
\end{aligned}
$$

Substituting x_{01} and x_{i1} into equations (3.35), we obtain

$$
\begin{aligned}
D_o^2 x_{03} + x_{03} &= -(2jA_1' + j\gamma_o A_1 + 3\beta A_1^2\bar{A}_1 + 6\Lambda^2 A_1)\exp(jT_o) \\
&\quad +(j\gamma_o w\Lambda + 4\beta\Lambda A_1\bar{A}_1 + 3\Lambda^3\beta)\exp(jwT_o) - \beta A_1^3\exp(3jT_o) \\
&\quad -3\beta A_1^2\Lambda\exp(j(2+w)T_o) - 3\beta A_1\Lambda^2\exp(j(2w+1)T_o) \\
&\quad -3\beta\Lambda^2 A_1\exp(j(1-2w)T_o) - 3\beta\Lambda A_1^2\exp(j(2-w)T_o) \\
&\quad -\Lambda^3\beta\exp(3jwT_o) - j\sum_{i=1}^{n} w_i\lambda_{oi}A_{i+1}\exp(jw_iT_o) + C.C, \\
D_o^2 x_{13} + w_1^2 x_{13} &= -jw_1(2A_2' + \gamma_{o1}A_2)\exp(jw_1T_o) + j\lambda_{o11}A_1\exp(jT_o) \\
&\quad +jw\lambda_{o11}\Lambda\exp(jwT_o) + C.C, \\
&\vdots \qquad\qquad\qquad\qquad \vdots \\
D_o^2 x_{n3} + w_n^2 x_{n3} &= -jw_n(2A_{n+1}' + \gamma_{on}A_{n+1})\exp(jw_nT_o) + j\lambda_{on1}A_1\exp(jT_o) \\
&\quad +jw\lambda_{on1}\Lambda\exp(jwT_o) + C.C.
\end{aligned} \tag{3.35}
$$

From equations (3.35), it comes two interesting resonant structures as we have seen here before. The first one is the superharmonic state $w_i = 1$ and $3w = 1$, and the second one corresponds to the subharmonic state $w = 3$ with $w_i = 1$.

• Superharmonic resonances

We consider the case where the nonlinear oscillator enters in superharmonic resonance with the external excitation, that is $3w = 1 + \epsilon^2\sigma$. We also assume that

$$
w_i = 1 + \epsilon^2\sigma_i, \tag{3.36}
$$

where σ_i and σ are the detuning parameters indicating the accuracy of the resonances. The secular producing terms in the equations (3.35) must be eliminated and the solvability conditions are

$$
2jA_1' + j\gamma_o A_1 + 6\Lambda^2 A_1 + 3\beta A_1^2\bar{A}_1
$$

$$
\begin{aligned}
+j\sum_{i=1}^{n} w_i\lambda_{oi}A_{i+1}\exp(j\sigma_i T_2) - \Lambda^3\beta\exp(j\sigma_o T_2) &= 0,\\
-w_1(2A_2' + \gamma_{o1}A_2)\exp(j\sigma_1 T_2) + \lambda_{o11}A_1 &= 0,\\
\vdots \qquad\qquad & \vdots\\
-w_n(2A_{n+1}' + \gamma_{on}A_{n+1})\exp(j\sigma_n T_2) + \lambda_{on1}A_1 &= 0.
\end{aligned} \tag{3.37}
$$

With the polar notation of $A_i = \frac{1}{2}a_i(T_2)\exp(jb_j(T_2))$, the amplitudes and phases of $\mathbf{n}$+1 oscillators are described by the following set of first order differential equations

$$
\begin{aligned}
\frac{3}{8}\beta a_1^3 - a_1 b_1' + 3\Lambda^2 a_1 + \beta\Lambda^3\cos\delta - \frac{1}{2}\sum_{i=1}^{n} w_i\lambda_{oi}a_{i+1}\sin\delta_i &= 0,\\
\frac{1}{2}\gamma_o a_1 + a_1' + \beta\Lambda^3\sin\delta + \frac{1}{2}\sum_{i=1}^{n} w_i\lambda_{oi}a_{i+1}\cos\delta_i &= 0,\\
a_2 b_2'\cos\delta_1 + (a_2' + \frac{1}{2}\gamma_{o1}a_2)\sin\delta_1 &= 0,\\
w_1(a_2' + \frac{1}{2}\gamma_{o1}a_2)\cos\delta_1 - w_1 b_2' a_2\sin\delta_1 - \frac{1}{2}\lambda_{o11}a_1 &= 0,\\
\vdots \qquad\qquad & \vdots\\
a_{n+1}b_{n+1}'\cos\delta_n + (a_{n+1}' + \frac{1}{2}\gamma_{on}a_{n+1})\sin\delta_n &= 0,\\
w_n(a_{n+1}' + \frac{1}{2}\gamma_{on}a_{n+1})\cos\delta_n - w_n b_{n+1}' a_{n+1}\sin\delta_n - \frac{1}{2}\lambda_{on1}a_1 &= 0.
\end{aligned} \tag{3.38}
$$

where $\delta = \sigma T_2 - b_1$ and $\delta_i = \sigma_i T_2 + b_{i+1} - b_1$. For the steady-state responses, $b_1' = \sigma$ and $b_{i+1}' = \sigma - \sigma_i$. Eliminating δ_i from equations (3.38), we obtain the following set of nonlinear equations

$$
\begin{aligned}
\frac{9}{64}\beta^2 a_1^6 + \frac{3}{4}\beta M_n a_1^4 + N_n a_1^2 - \beta^2\Lambda^6 &= 0,\\
a_{i+1}^2 &= \frac{\lambda_{oi1}^2 a_1^2}{w_i^2(\gamma_{oi}^2 + 4(\sigma-\sigma_i)^2)}.
\end{aligned} \tag{3.39}
$$

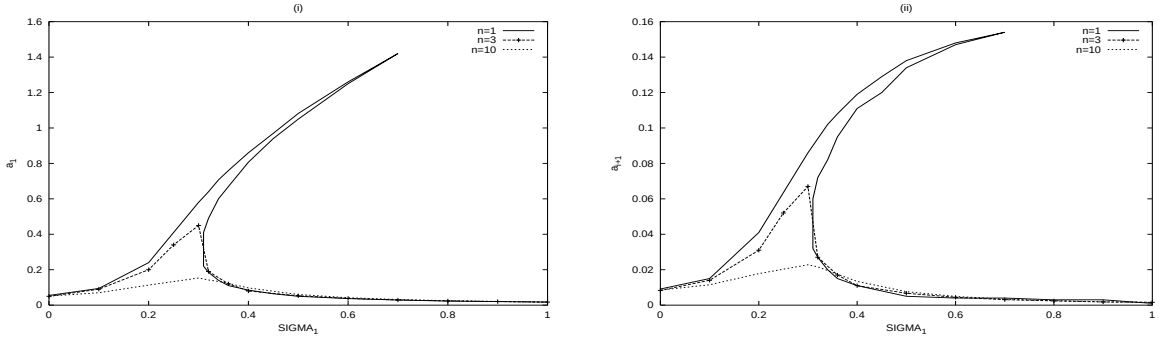

Figure 3.19: *Effects of the number of mechanical oscillators on the superharmonic frequency-response curves with the parameters* $E = 0.5, \gamma_o = 0.01; \gamma_{o1} = 1.2, \lambda_{o1} = 0.12, \lambda_{o11} = 0.2,$ $\beta = 0.6; \sigma_i = 0.$

where

$$
\begin{aligned}
M_n &= 3\Lambda^2 - \sigma + \sum_{i=1}^{n}\frac{\lambda_{oi}\lambda_{oi1}(\sigma-\sigma_i)}{4(\sigma-\sigma_i)^2 + \gamma_{oi}^2}.\\
N_n &= \frac{1}{4}\left\{\gamma_o + \sum_{i=1}^{n}\frac{\gamma_{oi}\lambda_{oi}\lambda_{oi1}}{4(\sigma-\sigma_{i+1})^2 + \gamma_{oi}^2}\right\}^2 + M_n^2.
\end{aligned}
$$

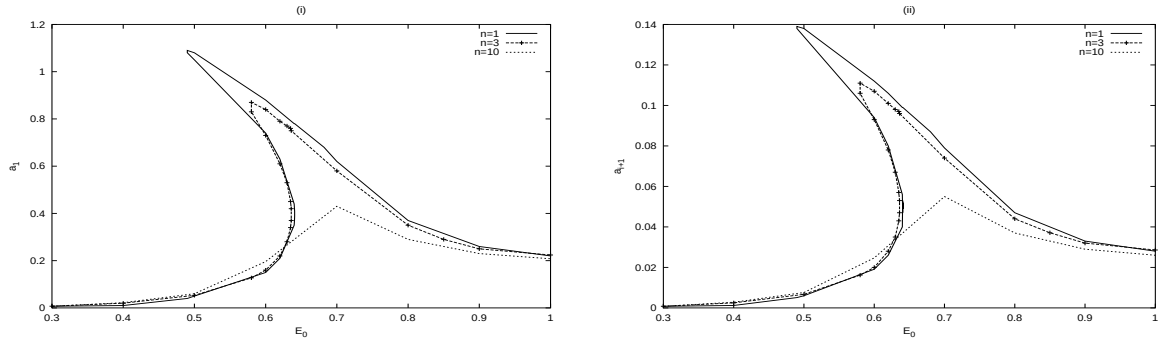

Figure 3.20: *Effects of the number of the linear mechanical oscillators on the superharmonic amplitude-response curves with the parameters of Figure 3.19 and* $\sigma_1 = 0.5$

When the linear mechanical oscillators are identical, M_n and N_n take the following expressions

$$\begin{aligned} M_n &= 3\Lambda^2 - \sigma_1 + \frac{n\lambda_{o1}\lambda_{o11}(\sigma-\sigma_1)}{4(\sigma-\sigma_1)^2+\gamma_{o1}^2}, \\ N_n &= \frac{1}{4}\left\{\gamma_o + \frac{n\gamma_{o1}\lambda_{o1}\lambda_{o11}}{4(\sigma-\sigma_1)^2+\gamma_{o1}^2}\right\}^2 + M_n^2. \end{aligned}$$

Figures 3.19 and 3.20 present the superharmonic frequency-response and amplitude-response curves respectively when the detuning parameter σ and the amplitude E are vary on the exact internal resonances ($\sigma_i = 0$). The effects of the number of the linear mechanical oscillators on the behavior of the model are observed and it appears that the hysteresis domain decreases with the increase of the number **n** of linear mechanical oscillator and disappears for large **n**.

• Subharmonic resonances

To analyze these subharmonic resonances, we set $w = 3 + \epsilon^2\sigma_o$. σ_o is the detuning parameter indicating the accuracy of the subharmonic resonances. Eliminating the terms in equations (3.35) that produce secular terms in x_{03} and x_{i3} considering the expressions given by equations (3.36), we have

$$\begin{aligned} 2jA_1' + j\gamma_o A_1 + 6\Lambda^2 A_1 + 3\beta A_1^2\bar{A}_1 + \\ j\sum_{i=1}^{n} w_i\lambda_{oi}A_{i+1}\exp(j\sigma_i T_2) + 3\Lambda\beta\bar{A}_1^2\exp(j\sigma_o T_2) = 0, \\ -w_1(2A_2' + \gamma_{o1}A_2)\exp(j\sigma_1 T_2) + \lambda_{o11}A_1 = 0, \\ \vdots \qquad\qquad \vdots \\ -w_n(2A_{n+1}' + \gamma_{on}A_{n+1})\exp(j\sigma_n T_2) + \lambda_{on1}A_1 = 0. \end{aligned} \tag{3.40}$$

Again, introducing the polar notations for A_i and separating real and imaginary parts, we obtain the following first order of differential equations

$$\begin{aligned} \frac{3}{8}\beta a_1^3 - a_1 b_1' + 3\Lambda^2 a_1 + \frac{3}{4}\beta\Lambda a_1^2\cos\delta_o - \frac{1}{2}\sum_{i=1}^{n} w_i\lambda_{oi}a_{i+1}\sin\delta_i &= 0, \\ \frac{1}{2}\gamma_o a_1 + a_1' + \frac{3}{4}\beta\Lambda a_1^2\sin\delta_o + \frac{1}{2}\sum_{i=1}^{n} w_i\lambda_{oi}a_{i+1}\cos\delta_i &= 0, \end{aligned}$$

$$
\begin{aligned}
a_2 b_2' \cos\delta_1 + w_1(a_2' + \frac{1}{2}\gamma_{o1} a_2)\sin\delta_1 &= 0, \\
w_1(a_2' + \frac{1}{2}\gamma_{o1} a_2)\cos\delta_1 - w_1 b_2' a_2 \sin\delta_1 - \frac{1}{2}\lambda_{o11} a_1 &= 0, \\
\vdots \qquad\qquad & \vdots \\
a_{n+1} b_{n+1}' \cos\delta_n + w_n(a_{n+1}' + \frac{1}{2}\gamma_{on} a_{n+1})\sin\delta_n &= 0, \\
w_n(a_{n+1}' + \frac{1}{2}\gamma_{on} a_{n+1})\cos\delta_n - w_n b_{n+1}' a_{n+1}\sin\delta_n - \frac{1}{2}\lambda_{on1} a_1 &= 0. \qquad (3.41)
\end{aligned}
$$

where $\delta_o = \sigma_o T_2 - 3b_1$ and $\delta_i = \sigma_i T_2 + b_{i+1} - b_1$. For the steady-state responses, we have $b_1' = \frac{\sigma_o}{3}$ and $b_{i+1}' = \frac{\sigma_o}{3} - \sigma_{i+1}$. Eliminating δ_i from equations (3.41), we obtain the following set of nonlinear equations

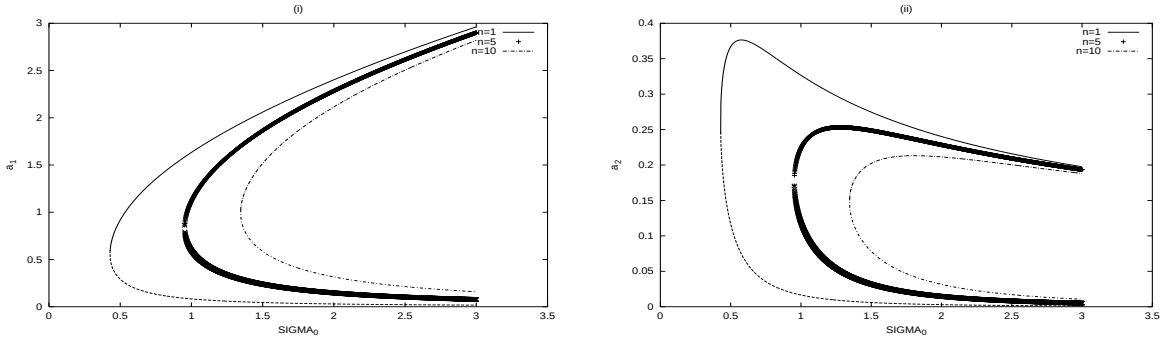

Figure 3.21: *Effects of the number of linear mechanical oscillators on the subharmonic frequency-response curves with the parameters* $\gamma_o = \gamma_{o1} = 0.01; \lambda_{o1} = 0.1; \lambda_{o11} = 0.4; \beta = 0.6; \sigma_2 = 0.$

$$
\begin{aligned}
&\frac{9}{64}\beta^2 a_1^6 + \frac{3}{4}\beta P_n a_1^4 + Q_n a_1^2 = 0, \\
&a_{i+1}^2 = \frac{\lambda_{oi1}^2 a_1^2}{w_i^2(\gamma_{oi}^2 + 4(\frac{\sigma_o}{3} - \sigma_i)^2)}, \qquad (3.42)
\end{aligned}
$$

where

$$
\begin{aligned}
P_n &= 3\Lambda^2 - \frac{\sigma_o}{3} - \frac{3}{4}\beta\Lambda^2 + \sum_{i=1}^{\mathbf{n}} \frac{\lambda_{oi}\lambda_{oi1}(\frac{\sigma_o}{3} - \sigma_i)}{4(\frac{\sigma_o}{3} - \sigma_i)^2 + \gamma_{oi}^2}, \\
Q_n &= \frac{1}{4}\left\{\gamma + \sum_{i=1}^{\mathbf{n}} \frac{\lambda_{oi}\lambda_{oi1}\gamma_i}{4(\frac{\sigma_o}{3} - \sigma_i)^2 + \gamma_{oi}^2}\right\}^2 + \left\{P_n + \frac{3}{4}\beta\Lambda^2\right\}^2.
\end{aligned}
$$

The solutions of equations (3.42) are $a_1^2 = 0$ or

$$
a_1^2 = p \pm \sqrt{p^2 - q}, \qquad (3.43)
$$

where

$$
p = \frac{-8P_n}{3\beta^2}, \qquad\qquad q = \frac{64Q_n}{9\beta^2}.
$$

Nontrivial solutions can exist only if

$$
p_n - \sqrt{p_n^2 + q_n} \le \Lambda^2 \le p_n + \sqrt{p_n^2 + q_n},
$$

with

$$p_n = \frac{3\beta(U_n - \frac{\sigma_o}{3})}{4[(3-\frac{3}{4}\beta)^2 - 9]}, \qquad q_n = \frac{(\gamma + V_n)^2}{4[(3-\frac{3}{4}\beta)^2 - 9]},$$

$$U_n = \sum_{i=1}^{n} \frac{\lambda_{oi}\lambda_{i1}(\frac{\sigma_o}{3} - \sigma_i)}{4(\frac{\sigma_o}{3} - \sigma_i) + \gamma_{oi}^2}, \qquad V_n = \sum_{i=1}^{n} \frac{\lambda_{oi}\lambda_{oi1}\gamma_i}{4(\frac{\sigma_o}{3} - \sigma_i) + \gamma_{oi}^2}.$$

The boundary of the region where nontrivial solutions can exist is given by

$$\Lambda_c^2 = p_n \pm \sqrt{p_n^2 + q_n}. \tag{3.44}$$

For the case of the identical linear mechanical oscillators, we have the following expressions

$$\begin{aligned}
P_n &= 3\Lambda^2 - \frac{\sigma_o}{3} - \frac{3}{4}\beta\Lambda^2 + \frac{\mathbf{n}\lambda_{oi}\lambda_{oi1}(\frac{\sigma_o}{3} - \sigma_1)}{4(\frac{\sigma_o}{3} - \sigma_1)^2 + \gamma_{oi}^2}, \\
Q_n &= \frac{1}{4}\left\{\gamma_o + \frac{\mathbf{n}\lambda_{o1}\lambda_{o11}\gamma_1}{4(\frac{\sigma_o}{3} - \sigma_1)^2 + \gamma_{o1}^2}\right\}^2 + \left\{P_n + \frac{3}{4}\beta\Lambda^2\right\}^2, \\
Un &= \frac{\mathbf{n}\lambda_1\lambda_{o2}(\frac{\sigma_o}{3} - \sigma_1)}{4(\frac{\sigma_o}{3} - \sigma_1) + \gamma_{o1}^2}, \\
V_n &= \frac{\mathbf{n}\lambda_{o1}\lambda_{o2}\gamma_{o2}}{4(\frac{\sigma_o}{3} - \sigma_1) + \gamma_1^2}.
\end{aligned}$$

In the exact internal resonances ($\sigma_i = 0$), we find the behaviors of the amplitudes a_i when the detuning parameter σ_o and the amplitude E_0 are vary. The effects of a number of the linear mechanical oscillators on the boundary of the region where nontrivial solutions can exist are observed. It is found that for $a_i(\sigma_o)$, this boundary increases when σ_o increases while for the case of $a_i(E_0)$, this boundary decreases for the increase of E_0. Our investigations show that when $n > 6$, the amplitude-response solutions could not exist in the $a_i - E_0$ plane. Before described and studied the dynamical behavior of another types of electromechanical device, let us make a following interesting remark for the electromechanical device with a large number of functions in series. Practically and during the functioning of such device, the engineer preoccupation is to known the response of the electromechanical device if the **ith** linear mechanical oscillator stops functioning, for some reasons tied to a deterioration of one or some of its components. In this situation, it is found that the mechanical part could not received faithfully electrical oscillations of the electrical part. Consequently, the electromechanical model stops to convert electrical oscillations to mechanical oscillations. This is one of limits and inconvenients of the electromechanical device with double or a large number of functions in series. Our purposes in the following section is to describ and study another electromechanical device in which any mechanical oscillator operates independently.

3.4 Electromechanical transducer with double functions in parallel

3.4.1 Model and equations of motion

We consider now an electromechanical transducer with double functions in parallel. As it is shown in Figure 3.23, the electrical part is now coupled in parallel with a mechanical part

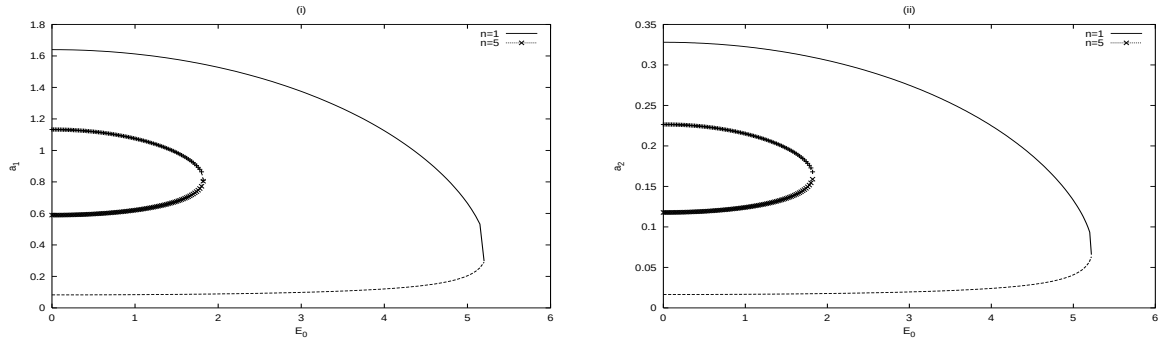

Figure 3.22: *Effects of the number of linear mechanical oscillators on the subharmonic amplitude-response curves with the parameters of Figure 3.21 and* $\sigma_o = 1.0$.

governing by two linear mechanical oscillators. Using again the electrical and mechanical laws, and taken into account the contributions of the **Laplace** force and the **Lenz** electromotive voltage, it is found that the system is described by the following nondimensional differential equations consisting of two electrical **Duffing** oscillators coupled to two linear mechanical oscillators as

$$\begin{aligned} \ddot{q} + \gamma\dot{q} + q + \beta q^3 + \lambda_1\dot{x} &= E_0 \cos wt, \\ \ddot{q} + \gamma\dot{q} + q + \beta q^3 + \lambda_2\dot{y} &= E_0 \cos wt, \\ \ddot{x} + \gamma_1\dot{x} + w_1^2 x - \lambda_3\dot{q}_1 &= 0, \\ \ddot{y} + \gamma_2\dot{y} + w_2^2 y - \lambda_4\dot{q}_2 &= 0, \\ \dot{q} = \dot{q}_1 + \dot{q}_2. & \end{aligned} \tag{3.45}$$

The electrical part is represented by the variable q while x and y stand for the mechanical parts. The quantities γ, γ_i and w_i are respectively the damping and the natural frequencies. β and λ_i are respectively the nonlinearity and damping coupling coefficients. We note that the particularity of this electromechanical device is that the two mechanical oscillators operate independently.

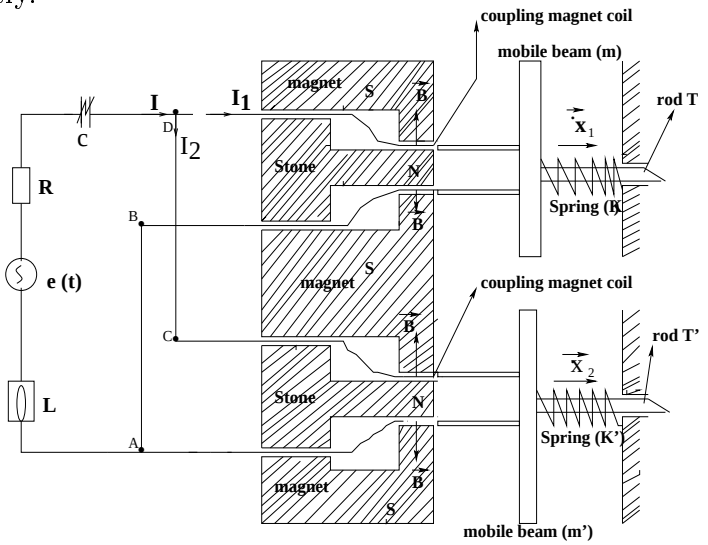

Figure 3.23: *Electromechanical transducer with double functions in parallel.*

3.4.2 Amplitudes of the harmonic oscillations and time delay

To derive the amplitudes of the harmonic oscillations, we express q, q_1, x and y in the form

$$\begin{aligned} q &= a_1 \cos wt + a_2 \sin wt, \\ q_1 &= b_1 \cos wt + b_2 \sin wt, \\ x &= c_1 \cos wt + c_2 \sin wt, \\ y &= d_1 \cos wt + d_2 \sin wt, \end{aligned} \tag{3.46}$$

Substituting equations (3.46) into equations (3.45) and equating the terms containing $\cos wt$ and $\sin wt$ to zero given us the following algebraic equations

$$\begin{aligned} (1 - w^2 + \frac{3}{4}\beta A^2)a_1 + w\gamma a_2 + w\lambda_1 c_2 &= E_0, \\ -w\gamma a_1 + (1 - w^2 + \frac{3}{4}\beta A^2)a_2 - w\lambda_1 c_1 &= 0, \\ (1 - w^2 + \frac{3}{4}\beta A^2)a_1 + w\gamma a_2 + w\lambda_2 d_2 &= E_0, \\ -w\gamma a_1 + (1 - w^2 + \frac{3}{4}\beta A^2)a_2 - w\lambda_2 d_1 &= 0, \\ (w_1^2 - w^2)c_1 + w\gamma_1 c_2 - w\lambda_3 b_2 &= 0, \\ -w\gamma_1 c_1 + (w_1^2 - w^2)c_2 + w\lambda_3 b_1 &= 0, \\ (w_2^2 - w^2)d_1 + w\gamma_2 d_2 - w\lambda_4 a_2 + w\lambda_4 b_2 &= 0, \\ -w\gamma_2 d_1 + (w_2^2 - w^2)d_2 + w\lambda_4 a_1 - w\lambda_4 b_1 &= 0. \end{aligned} \tag{3.47}$$

After some algebraic manipulations and setting $A^2 = a_1^2 + a_2^2$, $B^2 = b_1^2 + b_2^2$, $C^2 = c_1^2 + c_2^2$ and $D^2 = d_1^2 + d_2^2$, it comes that the amplitudes A, B, C and D satisfy the following nonlinear equations

$$\begin{aligned} &\frac{9}{16}\beta^2 A^6 + \frac{3}{2}\beta F A^4 + (F^2 + G^2)A^2 - E_0^2 = 0, \\ &B^2 = \frac{\lambda_2^2 \lambda_4^2 \Delta_o}{\lambda_1^2 \lambda_3^2 \Delta} A^2, \\ &C^2 = \frac{w^2 \lambda_2^2 \lambda_4^2}{\lambda_1^2 \Delta} A^2, \\ &D^2 = \frac{w^2 \lambda_4^2}{\Delta} A^2, \end{aligned} \tag{3.48}$$

where

$$\begin{aligned} \Delta &= [\lambda_3\lambda_1(w_2^2 - w^2) + \lambda_4\lambda_2(w_1^2 - w^2)]^2 + [w\lambda_3\lambda_1\gamma_2 + w\lambda_4\lambda_2\gamma_1]^2, \\ \Delta_o &= (w_1^2 - w^2)^2 + w^2\gamma_1^2, \\ F &= 1 - w^2 - \frac{\lambda_1\lambda_2\lambda_3\lambda_4 w^2(w_2^2 - w^2)}{\Delta} - \frac{\lambda_2^2\lambda_4^2 w^2(w_1^2 - w^2)}{\Delta}, \\ G &= \gamma w + \frac{\lambda_1\lambda_2\lambda_3\lambda_4\gamma_2 w^3}{\Delta} + \frac{\lambda_2^2\lambda_4^2\gamma_1 w^3}{\Delta}, \end{aligned}$$

With the following set of parameters $\lambda_1 = 0.2; \lambda_2 = 0.6; \lambda_3 = 0.19; \lambda_4 = 0.15; \gamma_1 = 0.13; \gamma_2 = 0.2; \gamma = 0.01; \beta = 0.5; w_1 = w_2 = 1.0; E_0 = 0.2$, the frequency-response curves of the linear

electromechanical system show one peak of antiresonance and two peaks of resonances as we have shown in the previous Chapter, while the nonlinear frequency-response and amplitude-response curves show respectively hysteresis and jump phenomena.

We analyze the time delay between the linear mechanical oscillators. From equations (3.47), we defined the phases ϕ_1 and ϕ_2 of the linear mechanical oscillators as

$$\begin{aligned} \tan\phi_1 &= \frac{d_2}{d_1} = \frac{r_2}{r_1}, \\ \tan\phi_2 &= \frac{c_2}{c_1} = \frac{d_2}{d_1}, \end{aligned} \tag{3.49}$$

where

$$\begin{aligned} r_2 &= -w\lambda_4(F + \frac{3}{4}\beta A^2)[\lambda_3\lambda_1(w_2^2 - w^2) + \lambda_4\lambda_2(w_1^2 - w^2)] \\ &\quad + w\lambda_4 G(w\gamma_2\lambda_3\lambda_1 + w\gamma_1\lambda_4\lambda_2), \\ r_1 &= w\lambda_4 G[\lambda_3\lambda_1(w_2^2 - w^2) + \lambda_4\lambda_2(w_1^2 - w^2)] \\ &\quad + w\lambda_4(F + \frac{3}{4}\beta A^2)(w\gamma_2\lambda_3\lambda_1 + w\gamma_1\lambda_4\lambda_2). \end{aligned}$$

The time delay is therefore defined as

$$\Theta_{1,2} = \frac{\phi_1 - \phi_2}{w} = \frac{k\pi}{w}. \qquad k = 1, 2, 3, ... \tag{3.50}$$

The time delay of the electromechanical system with double fonctions in parallel depends only of the frequency w of the external excitation and is independent of the mechanical device parameters as in the case of devices with **n** functions in series.

3.5 Conclusion

We have considered in this Chapter the dynamics of an electromechanical system with multiple functions, consisting of an electrical **Duffing** oscillator coupled magnetically in series and in parallel to two and **n** linear mechanical oscillators. The model with double functions have first been considered. We have derived the amplitude of the harmonic oscillations and time delay between the two linear mechanical oscillators using the harmonic balance method. It appears that the two linear mechanical oscillators vibrate in phase in the internal and external resonances. We have also derived the stability condition of the periodic solutions using the characteristics of the hysteresis branches. The extension of the model with a large number of functions in series have been considered. The influence of the number of mechanical oscillators have been analyzed on the behavior of the system. The electromechanical system with double functions in parallel has been also considered.

Bibliography

[III1] **Nayfeh A. H.** and **Mook D. T.** , "Nonlinear oscillations", Wiley-Interscience,New York (1979).

[III2] **Korenev B. G.** and **Reznikov L. M.,** "Dynamics vibration absorbers", John-wiley, new york (1997).

[III3] **Hayashi C.**, "Nonlinear Oscillations in Physical Systems," Mc-Graw-Hill, New-York (1964)

Chapter 4 : **Synchronization of electromechanical systems**

Chapter 4

Synchronization of electromechanical systems

4.1 Introduction

In recent years, the field of nonlinear science has seen a growing interest in the synchronization of nonlinear oscillators both in their regular and chaotic states [see ref.[IV1] and references therein]. The idea of synchronizing two chaotic oscillators was put on by **Pecora** and **Carrol** [IV2] by coupling both oscillators with a common drive signal. Latter on, **Kapitaniak** [IV3] shows that one can also synchronize two chaotic oscillators using the continuous feedback scheme developed by **Pyragas** [IV4]. The great interest devoted to such topic is due to the potential applications of synchronization in communications engineering (using chaos to mask the information bearing signals) [IV2,IV5-IV7], in biology and chemistry [IV8,IV9].

Another field where synchronization is of crucial importance is the automation engineering where one needs two or many devices to work in a synchronized manner both in their regular and chaotic regimes. In this field, electromechanical devices with natural and created (or introduced) nonlinearities are common and can lead the devices into various types of behavior [IV10-IV14].

From theoritical and experimental results already obtained, a great deal of effort is still required to find optimal parameters to shorten the synchronization time, define the synchronization threshold parameters [IV15] to avoid loss of synchronization [IV16], instability during the synchronization process. This problem is important in all the mentioned fields where synchronization finds or will find practical interest. For instance, in the communication engineering, the range of time during which the chaotic oscillators are not synchronized corresponds to the range of time during which the encoded message can unfortunately not be recovered or sent. More than a grave and irreversible loss of information, this is a catastrophe in digital communications since the first bits of standardized bit strings always contain the signalization data or identity card of the message.

In this Chapter, we consider the problem of synchronizing two electromechanical devices both in their regular and chaotic states with and without delay. The device is described by an electrical **Duffing** oscillator coupled magnetically to a linear mechanical oscillator. Our study uses the continuous feedback scheme of **Pyragas** [IV4]. We use the **Floquet** theory to derive the stability criteria and the optimal coupling strength of the synchronization process. This theory has been used recently to optimize and derive the duration time of the synchronization of two **Duffing** oscillators [IV17] as well as that of two **Van der Pol** oscillators [IV18].

The Chapter is organized as follows. After the statement of the problem in the next Section, we study analytically in Section 4.3 the stability of the synchronization process of two electromechanical devices in the regular states and give the behavior of the synchronization time. The delay is also taken into account. We derive the critical values K_{cr} under which, for a given precision, no synchonization is possible. In Section 4.4, we extend the investigation to the synchronization of two electromechanical devices in the chaotic states. Numerical simulations are used to complement our analytical results. Section 4.5 is devoted to conclusion.

4.2 Statement of the problem

As we have seen herebefore, the electromechanical device is described by two coupled differential equations (see equations (1.6)) consisting of an electrical **Duffing** oscillator coupled magnetically to a linear mechanical oscillator. Due to the presence of cubic nonlinearity, the electromechanical model presents the classical nonlinear resonance, antiresonance, hysteresis and jump phenomena, and when the amplitude E_0 is large enough, the model exhibits complex behaviors such as chaos. In this Chapter, we use the following set of parameters $\gamma_1 = 0.1; \gamma_2 = 0.30; \lambda_1 = 0.01; \lambda_2 = 0.06; w_2 = 1.2; w = 1.3$. Two values for β are used: $\beta = 0.1$ and $\beta = 1.32$. The values of E_0 are indicated when needed.

In the regular regime, for some sets of physical parameters and due to nonlinearity, the response of the system to the external excitation shows what is known as the multistability. In this case, the system presents the well-known hysteresis phenomena with two stable harmonic oscillations with different amplitudes. Each harmonic state has its own basin of attraction in the space of initial conditions. Consequently, if two systems are launched with different initial conditions belonging to different basins of attraction, they will finally circulate on different orbits. The objective of the synchronization in this case is to call one of the system (slave) from its orbit to that of the other system (master). Extension can be made to include a time delay between the slave and the master.

In the chaotic states, the essence is the high sensitivity to initial conditions. Indeed when the system is working in the chaotic regime, a very small difference in the initial conditions will lead to different time histories. The aim of the synchronization is to make so that two electromechanical devices with different initial conditions finally synchronize their time history.

As we note in the introduction, our aim is to study the stability and derive the characteristics of the synchronization of two of our electromechanical system. The master system is described by the components x and y while the slave system has the corresponding components u and v. The enslavement is carried out by coupling the slave to the master through the following scheme

$$\begin{aligned}
&\ddot{x} + \gamma_1\dot{x} + x + \beta x^3 + \lambda_1\dot{y} = E_0\cos wt,\\
&\ddot{y} + \gamma_2\dot{y} + w_2^2 y - \lambda_2\dot{x} = 0,\\
&\ddot{u} + \gamma_1\dot{u} + u + \beta u^3 + \lambda_1\dot{v} = E_0\cos wt - K(u(t) - x(t-\tau))H(t-T_0),\\
&\ddot{v} + \gamma_2\dot{v} + w_2^2 v - \lambda_2\dot{u} = 0,
\end{aligned} \tag{4.1}$$

where K is the feedback coupling or synchronization coefficient, τ is the time delay, T_0 the onset time of the synchronization and $H(x_1)$ is the Heaviside function defined by

$$H(x_1) = \begin{cases} 0 & \text{for } x_1 < 0,\\ 1 & \text{for } x_1 \geq 0. \end{cases}$$

Practically, the above coupling between the master system to the slave system can be realized as it shown in Figure 4.1. It can be noticed that, in the electrical part of the slave device, we have in serie a condenser C' and the resulting voltage $V_{C'} \equiv \frac{1}{C'}(u-x)$. So that, the equivalent of the feedback coefficient is $\frac{1}{C'}$. The resulting equations of motion of the unidirectionnally coupled electromechanical transducers is established in the Appendix Ap-2.

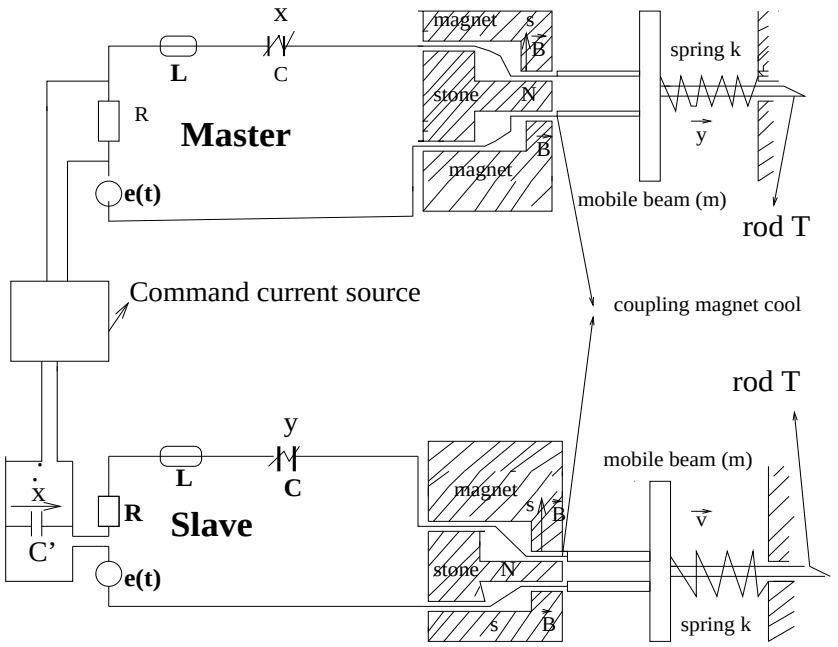

Figure 4.1: *Unidirectionnally coupled electromechanical transducers*

4.3 Synchronization of the regular states of two electromechanical systems

4.3.1 Stability and duration of the synchronization process without delay

Starting from $t = T_0$, the system changes its configuration and become physically interesting only so long as the dynamics of the slave device described by the components u and v is stable. We have to determine the range of K for which the synchronization process is achieve. The stability of the synchronization process is therefore strictly equivalent to the boundedness of ϵ_i defined as

$$\begin{aligned} \epsilon_1(t) &= u(t) - x(t), \\ \epsilon_2(t) &= v(t) - y(t). \end{aligned} \tag{4.2}$$

The new variables ϵ_i are the measure of the relative nearness of the slave to the master. From $t \geq T_0$, ϵ_i obey to

$$\begin{aligned} &\ddot{\epsilon}_1 + \gamma_1\dot{\epsilon}_1 + (1 + K + 3\beta x^2)\epsilon_1 + \lambda_1\dot{\epsilon}_2 = 0, \\ &\ddot{\epsilon}_2 + \gamma_2\dot{\epsilon}_2 + w_2^2\epsilon_2 - \lambda_2\dot{\epsilon}_1 = 0, \end{aligned} \tag{4.3}$$

assuming that they are small. The synchronization is achieved when ϵ_i goes to zero as t increases or is less than a given precision. The behavior of ϵ_i depends on K and on the form of the master (x, y). In the harmonic state, the master time evolution can be described by

$$\begin{aligned} x &= A\cos(wt-\phi), \\ y &= B\cos(wt-\psi), \end{aligned} \tag{4.4}$$

where A and B are the amplitudes while ϕ and ψ are the phases. Using the harmonic balance method [IV19], we insert equations (4.4) into the generating equations (1.6). Then by equating the coefficients of $\sin wt$ and $\cos wt$ separately (assuming that the terms due to higher frequencies can be neglected), it is found that A and ϕ are the solutions of the following equations

$$\begin{aligned} &\frac{9}{16}\beta^2 A^6 + \frac{3}{2}\beta F A^4 + (F^2+G^2)A^2 - E_o^2 = 0, \\ &\phi = \tan^{-1}\left\{\frac{G}{F+\frac{3}{4}\beta A^2}\right\}, \end{aligned} \tag{4.5}$$

where

$$\begin{aligned} D &= (w_2^2 - w^2)^2 + w^2\gamma_2^2, \\ F &= 1 - w^2 - \frac{\lambda_1\lambda_2 w^2(w_2^2-w^2)}{D}, \\ G &= \gamma_1 w + \frac{\lambda_1\lambda_2\gamma_2 w^3}{D}. \end{aligned}$$

Using the **Newton-Raphson** algorithm, one can hence find that the corresponding real positive solutions of equation (4.5) are

- for $\beta = 0.1$ with $E_0 = 0.5$

$$\begin{aligned} A_1 &= 2.74, & \phi_1 &= -1.05, \\ A_2 &= 0.76, & \phi_2 &= -0.21, \\ A_3 &= 3.21, & \phi_3 &= +1.59, \end{aligned}$$

- and for $\beta = 1.32$ with $E_0 = 0.2$

$$\begin{aligned} A_1 &= 0.64, & \phi_1 &= -0.47, \\ A_2 &= 0.34, & \phi_2 &= -0.23, \\ A_3 &= 0.94, & \phi_3 &= +1.48. \end{aligned}$$

Only the two last solutions of both sets are stable. With the form of the master given by equations (4.4), ϵ_i are now described by the following linear parametric equations

$$\begin{aligned} &\ddot{\epsilon}_1 + \gamma_1\dot{\epsilon}_1 + (\Omega_1^2 + \eta\cos(2wt-2\phi))\epsilon_1 + \lambda_1\dot{\epsilon}_2 = 0, \\ &\ddot{\epsilon}_2 + \gamma_2\dot{\epsilon}_2 + w_2^2\epsilon_2 - \lambda_2\dot{\epsilon}_1 = 0, \end{aligned} \tag{4.6}$$

where

$$\begin{aligned} \Omega_1^2 &= 1 + K + \eta, \\ \eta &= \frac{3}{2}\beta A^2. \end{aligned}$$

To discuss the stability of the synchronization process, we use the **Floquet** theory [IV19]. We set the following rescalings

$$\begin{aligned} \tau_1 &= wt, \\ u(\tau_1) &= \epsilon_1 \exp(\gamma_1 \tau_1 / 2w), \\ v(\tau_1) &= \epsilon_2 \exp(\gamma_2 \tau_1 / 2w), \end{aligned} \tag{4.7}$$

Equations (4.6) can be rewritten in the form

$$\begin{aligned} &\frac{d^2u}{d\tau_1^2} + [\delta_{11} + 2\epsilon_{11}\cos(4\tau_1 - 2\phi)]u + \delta_{12}\exp(-\epsilon\tau_1)v + c_1\frac{dv}{d\tau_1}\exp(-\epsilon\tau_1) = 0, \\ &\frac{d^2v}{d\tau_1^2} + \delta_{21}\exp(\epsilon\tau_1)u + \delta_{22}v + c_2\frac{du}{d\tau_1}\exp(\epsilon\tau_1) = 0, \end{aligned} \tag{4.8}$$

where the new parameters δ_{ij}, c_i and ϵ_{11} are given by

$$\begin{aligned} \delta_{11} &= (\Omega_1^2 - \frac{\gamma_1^2}{4})\frac{1}{w^2} = \frac{1}{w^2}\left\{1 + K + \eta - \frac{\gamma_1^2}{4}\right\}, \\ \delta_{22} &= \frac{1}{w^2}\left\{w_2^2 - \frac{\gamma_2^2}{4}\right\}, \qquad \epsilon_{11} = \frac{\eta}{w^2}, \\ \delta_{12} &= \frac{-\lambda_1\gamma_2}{2w}, \qquad \delta_{21} = \frac{\gamma_1\lambda_2}{2w}, \quad \epsilon = \frac{1}{2w}(\gamma_2 - \gamma_1), \\ c_1 &= \frac{\lambda_1}{2w}, \quad c_2 = \frac{-\lambda_2}{2w}, \end{aligned}$$

According to the **Floquet** theory [IV18], the solutions of equations (4.8) are

$$\begin{aligned} u(\tau_1) = \exp(\theta_1\tau_1)\alpha(\tau_1) = \sum_{n=-\infty}^{n=+\infty} \alpha_n \exp(a_n\tau_1), \\ v(\tau_1) = \exp(\theta_2\tau_1)\beta(\tau_1) = \sum_{n=-\infty}^{n=+\infty} \beta_n \exp(b_n\tau_1), \end{aligned} \tag{4.9}$$

where $a_n = \theta_1 + 2in, b_n = \theta_2 + 2in$, and the functions $\alpha(\tau_1) = \alpha(\tau_1 + \pi)$ and $\beta(\tau_1) = \beta(\tau_1 + \pi)$ replace the **Fourier** series. The quantities θ_1 and θ_2 are two complex numbers, while α_n and β_n are real constants.

Inserting equations (4.9) into equations (4.8) gives an infinite algebraic system, which may have solutions if and only if the associated **Hill's** determinant is set equal to zero. This condition defines the boundary dividing the parameters space in two domains: the stability and the instability ones. Limiting ourselves to a **Hill** determinant containing the sixth rows and sixth columns, we find that the boundary separating stability to instability domains are given by

$$\begin{aligned} \Delta(\theta_1,\theta_2) &= [(\delta_{11} + \theta_1^2)(\delta_{22} + \theta_2^2) - (\delta_{12} + c_1\theta_2)(\delta_{21} + c_2\theta_1)] \\ &\quad \{-(\delta_{21} + c_2(\theta_1 + 2i))(\delta_{12} + c_1(\theta_2 - 2i)) \\ &\quad \Big\{(\delta_{11} + (\theta_1 - 2i)^2)(\delta_{22} + (\theta_2 - 2i)^2) - \\ &\quad (\delta_{12} + c_1(\theta_2 - 2i))(\delta_{21} + c_2(\theta_1 + 2i))\Big\} \\ &\quad -(\delta_{22} + (\theta_2 + 2i)^2)(\delta_{11} + (\theta_1 + 2i)^2) \\ &\quad (\delta_{12} + c_1(\theta_2 - 2i))(\delta_{21} + c_2(\theta_1 + 2i)) + \\ &\quad (\delta_{22} + (\theta_2 - 2i)^2)(\delta_{22} + (\theta_2 + 2i)^2) \\ &\quad \Big\{(\delta_{11} + (\theta_1 - 2i)^2)(\delta_{11} + (\theta_1 + 2i)^2) - \epsilon_{11}^2\Big\}\Big\} \\ &= 0, \end{aligned} \tag{4.10}$$

with θ_1 and θ_2 given below.

Since, we have

$$\begin{aligned}\epsilon_1 &= \exp((\theta_1 - \frac{\gamma_1}{2w})\tau_1)\alpha(\tau_1),\\ \epsilon_2 &= \exp((\theta_2 - \frac{\gamma_2}{2w})\tau_1)\beta(\tau_1).\end{aligned}$$

Floquet theory states that the transition from stability to instability domains (π-periodic transitions) occurs at $\theta_1 = \frac{\gamma_1}{2w}$ and $\theta_2 = \frac{\gamma_2}{2w}$. Thus replacing θ_1 by $\frac{\gamma_1}{2w}$ and θ_2 by $\frac{\gamma_2}{2w}$ in equation (4.10), we obtain an equation which helps to determine the range of K in which the synchronization process is stable. Considering the case with $\beta = 0.1$, it is found from equation (4.10) that the stability is achieved for $K \in]-2.54; 0[\cup\,]0; 4.18[\cup]5.71; +\infty[$ if the slave comes from the orbit A_2 to follow the master at the orbit A_3. The results obtained from equation (4.10) are verified by a direct numerical simulation of equations (4.1) with the fourth order **Runge-Kutta** algorithm. The master and the slave are initially launched with the initial conditions $(x(0), \dot{x}(0), y(0), \dot{y}(0)) = (0.0, 0.01, 0.0, 0.02)$ and $(u(0), \dot{u}(0), v(0), \dot{v}(0)) = (2.0, 0.0, 0.1, 0.3)$ respectively. These sets of initial conditions lead respectively to periodic oscillations with amplitudes approximately equal to A_2 and A_3 respectively. Here the slave is forced to come from A_3 to A_2. For the case A_2 to A_3, we just have to inverse the initial conditions. For each set of initial conditions, the synchronization is launched at $T_0 = 200$ and K is varied until the synchronization is achieved. With this numerical procedure, we find that the slave transition from A_2 to A_3 requires at $K \in]0.0808; 4.25[\cup]4.38; +\infty[$. Despite the presence of a subdomain with $K < 0$ obtained from the analytical treatment (and which does not exist in the numerical results), we find that for $K > 0$, the agreement between the analytical and numerical results is quite good.

In the case $\beta = 1.32$, our analytical treatment gives that for the transition A_3 to A_2, we need $K \in]-1.2275; 0[\cup]0; +\infty[$. From the numerical simulation of the differential equations (with the initial conditions $(x(0), \dot{x}(0), y(0), \dot{y}(0)) = (0.0, 0.01, 0.0, 0.02)$ and $(u(0), \dot{u}(0), v(0), \dot{v}(0)) = (1.1, 0.01, 0.1, 0.3)$), it is found that the transition A_3 to A_2 occurs for $K > 0.5$. Here we find that the agreement between the analytical and numerical results is not as good as in the case $\beta = 0.1$. This can be understood by the increase of the nonlinearity effects for $\beta = 1.32$. Indeed, in this case, the single harmonic response (4.4) may be questionable. But despite this fact, the analytical treatment gives a good indication on the boundary of K for the synchronization to be achieved.

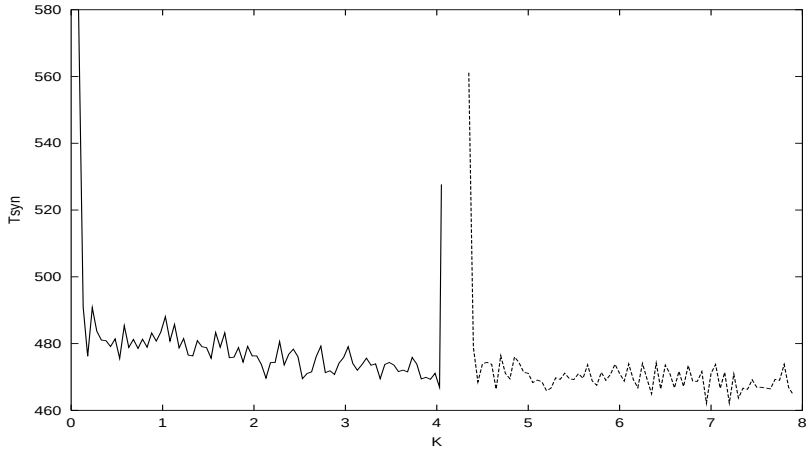

Figure 4.2: *Synchronization time T_{syn} versus the feedback coupling K coefficient for the transitions A_2 to A_3 for $\beta = 0.1, E_0 = 0.5$ and the precision $h = 10^{-10}$.*

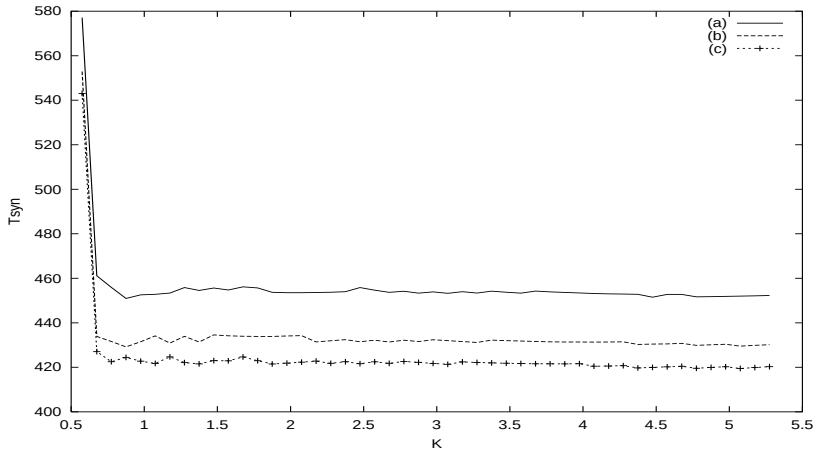

Figure 4.3: *Synchronization time T_{syn} versus K for the transitions A_3 to A_2 for $\beta = 1.32, E_0 = 0.2$ for different values of the precision h: (a): $h = 10^{-10}$, (b): $h = 3.10^{-10}$ and (c):$h = 5.10^{-10}$.*

The synchronization time is defined as

$$T_{syn} = t_{syn} - T_0, \tag{4.11}$$

where t_{syn} is the time instant at which the trajectories of the slave and the master are close enough to be considered as synchronized. Here, synchronization is achieved when the deviation ϵ_1 obeys to the following synchronization criterium

$$\epsilon_1 = |x - u| < h, \qquad \forall t > t_{syn}, \tag{4.12}$$

where h is the synchronization precision or tolerance. T_{syn} is plotted versus K in Figure 4.2 and Figure 4.3 for different values of the tolerance h. It is found that near the synchronization boundaries, T_{syn} is very large. But as K moves from the boundaries, T_{syn} decreases quickly and for large K, it attains a limiting small value depending on h.

4.3.2 Delayed synchronization ($\tau \neq 0$)

The purpose of delayed synchronization is to achieve the convergence of $u(t)$ and $v(t)$ towards $x(t-\tau)$ and $y(t-\tau)$ respectively. This is also an important goal to achieve in the field of electromechanical engineering. In this case ϵ_i rather obey to

$$\begin{aligned} &\ddot{\epsilon}_1 + \gamma_1\dot{\epsilon}_1 + [1 + K + 3\beta x_\tau^2]\epsilon_1 + \lambda_1\dot{\epsilon}_2 = -2E_0 \sin(w\tau/2)\sin(wt - w\tau/2), \\ &\ddot{\epsilon}_2 + \gamma_2\dot{\epsilon}_2 + w_2^2\epsilon_2 - \lambda_2\dot{\epsilon}_1 = 0, \end{aligned} \tag{4.13}$$

ϵ_i is now submitted to an external sinusoidal excitation whose amplitude depends on E_0 and τ. When $\tau = nT$ ($T = 2\pi/w$ is the period of the external excitation and n an integer), the external term vanishes and equations (4.13) is no more different to equations (4.6). Therefore, the whole analysis developed in the preceeding section remains valid. For $\tau \neq nT$, the stability domain remains that obtained herebefore but the external excitation induces steady state oscillations for ϵ_i and the amplitudes of ϵ_i can be very large depending on E_0 and τ. When K is varied, Ω_1 is modified, and resonances may occur with the external and parametric excitations. The method of multiple time scales demonstrates that Ω_1 should be far beyond w if we want to obtain small amplitudes for ϵ_i. We can therefore discard the linear parametric excitation and the variational equations (4.13) reduces to

$$\begin{aligned} &\ddot{\epsilon}_1 + \gamma_1\dot{\epsilon}_1 + \Omega_1^2\epsilon_1 + \lambda_1\dot{\epsilon}_2 = -2E_0 \sin(\frac{w\tau}{2})\sin(wt - \frac{w\tau}{2}), \\ &\ddot{\epsilon}_2 + \gamma_2\dot{\epsilon}_2 + w_2^2\epsilon_2 - \lambda_2\dot{\epsilon}_1 = 0, \end{aligned} \tag{4.14}$$

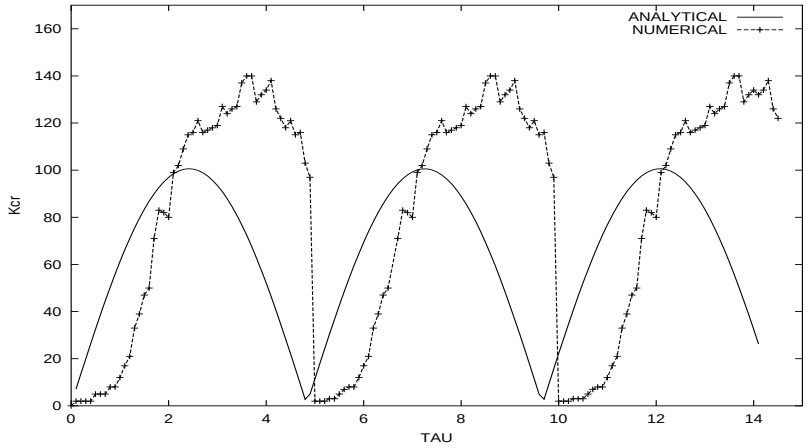

Figure 4.4: *Analytical and numerical K_{cr} versus τ for the slave transition from A_2 to A_3.*

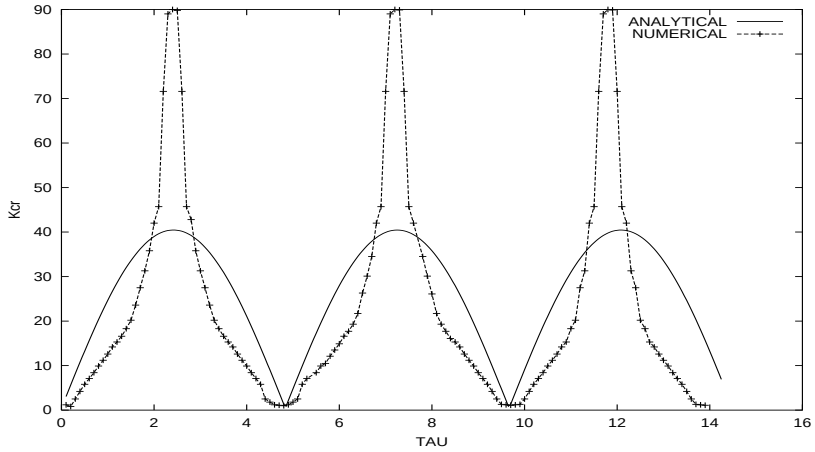

Figure 4.5: *Analytical and numerical K_{cr} versus τ for the slave transition from A_3 to A_2.*

Thus, far from the resonance peaks, the amplitudes of the steady state oscillations of ϵ_i are given by the following expressions

$$\begin{aligned}\epsilon_1(t) &= \frac{2D_1E_0\sin(w\tau/2)}{\sqrt{D_o}}\cos(wt - w\tau/2 - \psi_1),\\ \epsilon_2(t) &= \frac{2D_1E_0\lambda_2 w\sin(w\tau/2)}{\sqrt{D_1D_o}}\cos(wt - w\tau/2 - \psi_2),\end{aligned} \tag{4.15}$$

where

$$\begin{aligned}D_1 &= (w_2^2 - w^2)^2 + w^2\gamma_2^2,\\ D_o &= [(\Omega_1^2 - w^2)D_1 - \lambda_1\lambda_2 w^2(w_2^2 - w^2)]^2 + [\gamma_1 w D_1 + \lambda_1\lambda_2 w^3\gamma_2]^2,\end{aligned}$$

The analytical expressions of the critical values K_{cr} is precisely found by setting the equality between the amplitude of ϵ_1 and the precision h, so that $|\epsilon_1| < h$. This leads to

$$K > K_{cr} = \frac{Q + \sqrt{(\frac{2D_1E_0\sin w\tau/2}{h})^2 - (\gamma_1 w D_1 + \lambda_1\lambda_2\gamma_2 w^3)^2}}{D_1} - 1 - \eta, \tag{4.16}$$

where

$$Q = w^2 D_1 + \lambda_1 \lambda_2 w^2 (w_2^2 - w^2).$$

In Figure 4.4, we have plotted K_{cr} versus τ for the slave transition from A_2 to A_3 for $\beta = 0.1$ and $E_0 = 0.5$, and in Figure 4.5, the same is done for the slave transition from A_3 to A_2 for $\beta = 1.32$ and $E_0 = 0.2$. The synchronization tolerance used is $h = 10^{-2}$. The agreement between the analytical and numerical results is fairly good. The maximum value of K_{cr} occurs at $\tau = T/2$. Let us note that K_{cr} increases when the tolerance h decreases for a given set of parameters and time delay.

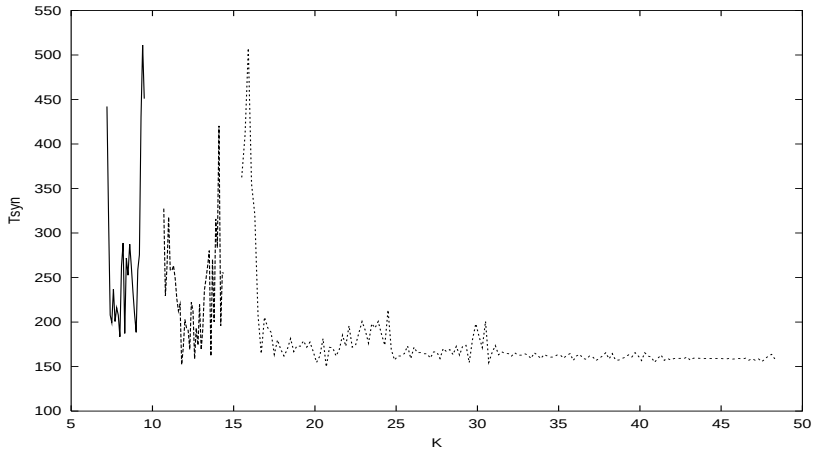

Figure 4.6: *Synchronization time T_{syn} versus K in the chaotic motion when $\tau = 0$. Initial conditions are as in Figure 4.3 and $h = 10^{-4}$.*

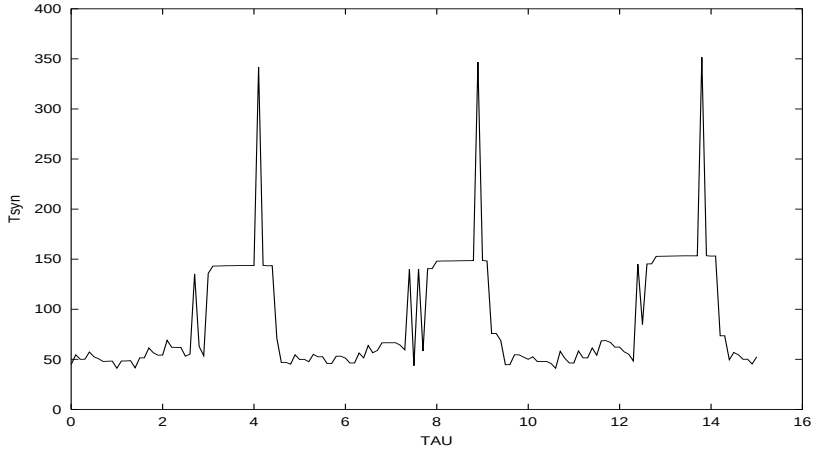

Figure 4.7: *Synchronization time T_{syn} versus the delay τ in the chaotic motion with the precision $h = 10^{-1}, K = 200$, and $E_0 = 22$.*

4.4 Synchronization of the chaotic states of two electromechanical systems

In this section, we extend the analysis of the synchronization process to chaotic states. The objective of this extension is to find if our analytical procedure can also help to derive the stability boundary of the synchronization of two chaotic electromechanical devices with and

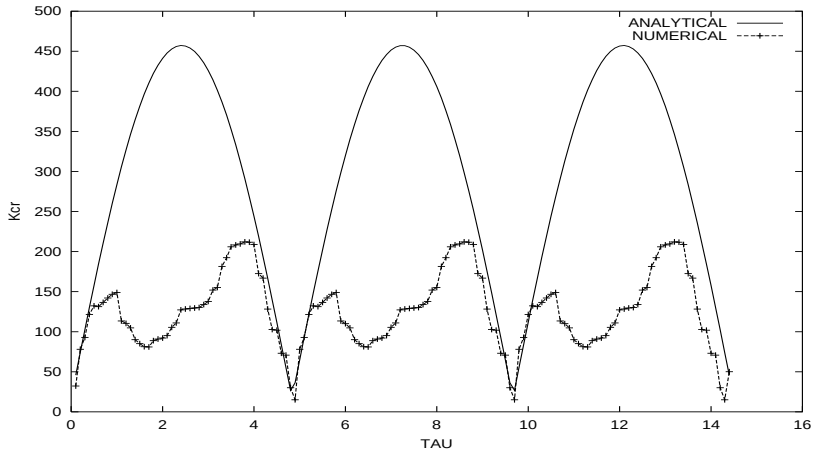

Figure 4.8: *Analytical and numerical K_{cr} versus τ in the chaotic motion. The initial conditions and the parameters are as in figure 2, with the precision $h = 10^{-1}$ and $E_0 = 22$.*

without delay. As it is known for the **Duffing** equation with a hard spring, chaos appears for high values of the external excitation amplitude E_0 [IV19]. This is also the case in our system. We find that with the set of parameters used in this Chapter, chaos appears around $E_0 = 22.0$. A chaotic phase portrait of the x component of the electromechanical system is shown in Figure 2.18. To use the analytical procedure (namely equations (4.10) and (4.16)), we need an approximate expression for the chaotic orbit. This is obviously not possible since a chaotic orbit is aperiodic and is composed of an infinite number of **Fourier** components. But we can however assumed that in the chaotic state, the virtual orbit is that obtained using the harmonic balance method. Thus, with equations (4.5), $\beta = 1.32$ and $E_0 = 22.0$, the virtual harmonic orbit has the amplitude $A = 2.89$. With this approximation, equations (4.10) gives that the two chaotic systems can be synchronized if $K > 5.75$. From the numerical simulation of equation (4.1), we find that the chaotic electromechanical systems are synchronized if $K \in [7.2; 9.8]U[10.8; 14.6]U]15.6; +\infty[$. Here we find that the difference between the analytical and the numerical results is large. But this is not due to the basic idea leading to the stability equation (4.10), but to the fact that with $\beta = 1.32$ and $E_0 = 22.0$, our virtual orbit with amplitude $A = 2.89$ is a very poor approximation and it is expected that by taking more harmonics, could be reduced the gap between the analytical and numerical results. Indeed, for other types of chaotic models where chaos does not need high nonlinear components to appear as the case of the soft **Duffing** oscillators, one finds good agreement between the analytical and the numerical results [IV15].

In Figure 4.6, we have plotted the variation of the synchronization time of two chaotic electromechanical systems with $h = 10^{-4}$. In Figure 4.7, T_{syn} versus τ is also reported while in Figure 4.8, K_{cr} versus τ, obtained from the analytical investigation and numerical simulation is also presented. For τ near nT, there is a good agreement between the analytical and numerical results.

Before conclude with this Chapter, we note that extension to a large number of electromechanical devices can be analyzed. In this case, the control strategy [IV4] can be implemented in two ways. In the first way, the master system controls directly the motion of the enslaved devices. Analytical investigations for this case are those presented here before. The second way consists of a series of cascading control. The master control the first slave which in its turn controls the second slave, etc... We assume that the slave devices are set in motion at the same time with different initial conditions and that the control is launched at the same time in the lattice. One also considers the synchronization of a network of electromechancal

devices in the chaotic states. In this case, the problem of the transitions from spatiotemporal chaos to complete synchronization states is a particular interest.

4.5 Conclusion

In this Chapter, we have considered the problem of synchronization without and with delay of two nonlinear electromechanical systems in their regular and chaotic states consists of a classical electrical **Duffing** oscillator coupled magnetically to a linear mechanical oscillator. The stability boundaries of the synchronization process has been obtained using the **Floquet** theory and numerical investigation. The influence of the synchronization precision has also be investigated. It has been found that the minimal feedback coefficient K_{cr} which enables the synchronization is a periodic function of the synchronization delay between the master and the slave devices. Some interesting agreements have been obtained between the analytical and the numerical results.

Bibliography

[IV1] **Kapitaniak T.,** "Controlling chaos", Academic press, London (1996).
Lakshamanan M. and **Murali K.,** "Chaos in Nonlinear Oscillators, Controlling and Synchronization" World Scientific, Singapore (1996).

[IV2] **Pecora L. M.** and **Caroll T. L.,** Phys. Rev. Lett. **64**, 821 (1990).

[IV3] **Kapitaniak T.,** (1994) Phys. Rev. E**50**, 1642 (1994).

[IV4] **Pyragas K.,** Phys. Lett, A**170**, 421 (1992).

[IV5] **Oppenheim A. V.**, **Wornell G. W.**, **Isabelle S. H.** , **Cuomo K.,** "Signal Processing in the context of chaotic signals"in: Proceedings of the International Conference on Acoustic, speech and signal Processing, IEEE, New York, Vol. **4**, 117 (1992).

[IV6] **Kocarev L. J., Halle K. S., Eckert K., Parlitz U., Chua L. O.,** Int. J. Bifurc. Chaos **2**, 709 (1992).

[IV7] **Perez G.** and **Cerdeira H. A.,** Phys. Rev. Lett. **74**, 1970 (1995).

[IV8] **Winfree A. T.,** "The Geometry of Biological Time," Springer-Verlag, New York, (1980).

[IV9] **Kuramuto Y.,** " Chemical oscillations, waves and Turbulence," Springer-Verlag, Berlin, (1980).

[IV10] **Jerrdlind J.** and **Stensson A.,** Chaos, Solitons and Fractals **11**, 2413 (2000).

[IV11] **Woafo P., Fotsin H. B., Chedjou J. C.,** Phys. Scripta **62**, 195 (1998).

[IV12] **Woafo P.,** Phys. Lett. A**267**, 31 (2000).

[IV13] **Kouomou Chembo Y., Woafo P.,** Phys. Scripta **62**, 255 (2000).

[IV14] **Chedjou J. C., Woafo P.** and **Domngang S.,** J. Vib. and Acoustics **123**, 170 (2001).

[IV15] **Pyragas K.**, Phys.Rev. E **58**, 3067 (1998).

[IV16] **Corron N. J.**,, Phys. Rev. E **63**, 055203 (2000).

[IV17] **Chembo Kouomou Y., Woafo P.,** Phys. Lett.A **298**, 18 (2002).

[IV18] **Woafo P.** and **Kraenkel R. A.,** Phys. Rev. E **65**, 036225 (2002).

[IV19] **Olson H. F.,** " Acoustical Engineering", Van Nostrand Princeton (1967).

[IV20] **Nayfeh A. H.** and **Mook D. T.,** "Nonlinear Oscillations", Wiley-Interscience, New York (1979).
Hayashi C., "Nonlinear Oscillations in Physical Systems", Mc-Graw-Hill, New-York (1964).

[IV21] **Parlitz U.** and **Lauterborn W.**, Phys. Lett. A**107**, 351 (1985).

General conclusions and perspectives

General conclusions and perspectives

1- Summary of the main results of this thesis

Before ending with this dissertation, let us give a summary of the main results. The aim purpose of this work has been to consider the dynamics and synchronization of electromechanical devices with a **Duffing** nonlinearity.

We have presented in the first Chapter the generalities on electromechanical systems and given some information for their interaction with electromechanical engineering. A description of the sources of nonlinearity and some electromechanical systems has been presented.

In chapter 2, we have analyzed analytically and numerically the behavior of forced and parametric electromechanical systems. We have found and analyzed the stability of harmonic oscillations using respectively the method of harmonic balance and the **Floquet** theory. Resonance, antiresonance and hysteresis phenomena have been observed. The amplitudes and the boundaries of the stability of the harmonic oscillations have been confirmed by a direct numerical simulation of the equations of motion. The characteristics of sub- and superharmonic oscillatory states in the electromechanical model have been derived using the multiple time scales method. The types of transitions from regular behavior to chaos have been analyzed using the numerical simulations of the equations of motion. We have used canonical feedback controllers algorithm to drive the electromechanical model from chaos to a regular target trajectory. We have analyzed the effects of the parametric coupling on the dynamics and stability boundary of the harmonic oscillations.

Chapter 3 has been devoted to the dynamics of an electromechanical device with multiple functions. We have first considered the model with double and a large number of functions in series. We have derived the amplitudes of the harmonic oscillations and time delay using analytical method. The effects of the number of linear mechanical oscillators on the behavior of the device has been analyzed and it appears that the points of resonance move when this number becomes large. The characteristics of sub- and superharmonic oscillations which occur in the model have been also derived. Secondly, the dynamics of the model with double functions in parallel are been considered, and the amplitudes of the harmonic oscillations and time delay have been also derived.

In Chapter 4, we have considered the problem of synchronizing electromechanical devices both in their regular and chaotic states with and without delay, using the continuous feedback scheme of **Pyragas**. We have used the **Floquet** theory to derive the stability criteria and the optimal coupling strength of the synchronization process. We have derived the critical values K_{cr} under which, for a given precision, no synchonization is possible. Numerical simulations have been used to complement our analytical results.

2- Perspectives

Despite the results obtained in this work, other points of interests will be solved in the future to complement and get a better understanding of this work.

• An interesting point to consider is to carry out the same study in self-sustained electromechanical devices. Here, the nonlinear component is a resistor whose $I-V$ curve contains a negative domain as described in chapter one. This will lead us to a system consisting of a **Duffing-Van der Pol** electrical oscillator coupled magnetically to a mechanical oscillator.

• When used in industries for cutting and drilling our devices could interact with medium possessing different elastic and damping coefficient. In this case, we face the problem of the dynamics of electromechanical devices with piece-wise like parameters. It is thus interesting to analyze such problem.

• Our study has focussed on the analytical and numerical study of the electromechanical system. To complement our knowledge in such devices, experimental studies should be carried out for eventual technological exploitation in micro and macroelectromechanical engineering.

These three points are currently under investigation and preliminary results have already been obtained.

APPENDIX

APPENDIX

Ap-1 Equations of motion of the controlled electromechanical system shown in Figure 2.22

We establish in this section the resulting equations of motion of the controlled electromechanical transducer. For this aim, we also apply the **Newton** second law of dynamics and the **Kirchhoff** law for the voltage in the controlled system. As it shown in figure 2.22; we have in the electrical part a new additional voltage $V_{C'} = \frac{1}{C'}(q - \bar{q}_o \cos \Omega t)$ and in the mechanical part a new external force $f_o = K'(z - z_o^o \cos \Omega t)$. Taken into account the **Laplace** force, the **Lenz** electromotive voltage, the new additional voltage $V_{C'}$ and force f_o, it is found that the controlled electromechanical system is described by the following set of differential equations:

$$\begin{aligned} L\ddot{q} + R\dot{q} + \frac{1}{C_o}q + a_3 q^3 + \frac{1}{C'}(q - \bar{q}_o^o \cos \Omega t) + lB_m\dot{z} &= v_o \cos \Omega t \\ m\ddot{z} + \lambda\dot{z} + Kz + K'(z - z_o \cos \Omega t) - lB_m\dot{q} &= 0 \end{aligned}$$

With the dimensionless variables defined in chapter one and

$$x_o = \frac{\bar{q}_o^o}{Qo}; \qquad y_o = \frac{\bar{z}_o}{l}; \qquad K_{21} = \frac{1}{LC'} \qquad K_{43} = \frac{K'LC_o}{m}$$

The above two differential equations is reduced to the following set of nondimensional differential equations:

$$\begin{aligned} \ddot{x} + \gamma_1\dot{x} + x + \beta x^3 + \lambda_1\dot{y} &= E_0 \cos wt - K_{21}(x - x_o \cos wt) \\ \ddot{y} + \gamma_2\dot{y} + w_2^2 y - \lambda_2\dot{x} &= -K_{43}(y - y_o \cos wt) \end{aligned}$$

Ap-2 Equations of motion of the unidirectionnally coupled electromechanical systems shown in Figure 4.1

As in the previous section, our aim in to establish the equations of motion of the slave when the synchronization process is launched, as its shown in figure 4.1. We have now in the electrical part a new additional voltage $V_{C'}$ in the capacitor C' connected in serie with the components of a RLC circuit and defined by the following expression:

$$V_{C'} = \frac{1}{C'}q' = \frac{1}{C'}(x - u)$$

With this expression of $V_{c'}$, it is found that the slave and the master are described by the following set of nondimensional differential equations:

$$\begin{aligned}
\ddot{x} + \gamma_1 \dot{x} + x + \beta x^3 + \lambda_1 \dot{y} &= E_0 \cos wt \\
\ddot{y} + \gamma_2 \dot{y} + w_2^2 y - \lambda_2 \dot{x} &= 0 \\
\ddot{u} + \gamma_1 \dot{u} + u + \beta u^3 + \lambda_1 \dot{v} &= E_0 \cos wt - K(x-u) \\
\ddot{v} + \gamma_2 \dot{v} + w_2^2 v - \lambda_2 \dot{u} &= O
\end{aligned}$$

with $K = \frac{1}{LC'}$.

List of publications

List of publications

1. **Harmonic oscillations, stability and chaos control in a nonlinear electromechanical system,**
   R. Yamapi, J. B. Chabi Orou and P. Woafo,
   Journal of Sound and Vibration **259**(5), *1253-1264* (2003).

2. **Harmonic dynamics and transitions to chaos in a nonlinear electromechanical system with parametric coupling,**
   R. Yamapi , J. B. Chabi Orou and P. Woafo,
   Physica Scripta **67**, 269-275 (2003).

3. **Synchronization of the regular and chaotic states of electromechanical devices with and without delay,**
   R. Yamapi, J. B. Chabi Orou and P. Woafo,
   International Journal of Bifurcation and Chaos, 2003 (In press).

4. **Dynamics of a nonlinear electromechanical system with multiple functions in series**
   P. Woafo, R. Yamapi, and J. B. Chabi Orou,
   Communication in Nonlinear Sciences and Numerical Simulations, 2003 (In press).

5. **Dynamics and synchronization of self-sustained electromechanical devices,**
   R. Yamapi, J. B. Chabi Orou and P. Woafo,
   Journal of Sound and Vibration 2003 (In press),

6. **Effects of discontinuity of elasticity and damping on the dynamics of an electromechanical transducer,**
   R. Yamapi, J. B. Chabi Orou and P. Woafo,
   Journal of Vibrations and Acoustics, 2003 (Submitted).

7. **Dynamics of an electromechanical vibrations absorber with magnetic coupling,** 2003 (To be submitted).